EVALUATION OF BELLED/TYPE PILES UPLIFT CAPACITY IN SANDY AND SOFT-ROCK GROUND

姜, 正求

https://doi.org/10.15017/4060143

出版情報：Kyushu University, 2019, 博士（工学）, 課程博士
バージョン：
権利関係：

EVALUATION OF BELLED-TYPE PILES UPLIFT CAPACITY IN SANDY AND SOFT-ROCK GROUND

KANG JUNGGOO

2020 MARCH

EVALUATION OF BELLED-TYPE PILES UPLIFT CAPACITY IN SANDY AND SOFT-ROCK GROUND

A THESIS SUBMITTED
IN PARTIAL FULFILLMENT OF THE REQUIREMENTS
FOR THE DEGREE OF
DOCTOR OF ENGINEERING

BY

KANG JUNGGOO

TO THE

DEPARTMENT OF CIVIL AND STRUCTURAL ENGINEERING
GRADUATE SCHOOL OF ENGINEERING
KYUSHU UNIVERSITY
FUKUOKA, JAPAN
2020

GEOTECHNICAL ENGINEERING LABORATORY
DEPARTMENT OF CIVIL AND STRUCTURAL ENGINEERING
GRADUATE SCHOOL OF ENGINEERING
KYUSHU UNIVERSITY
FUKUOKA, JAPAN

CERTIFICATE

*The undersigned hereby certify that they have read and recommended to the Graduate School of Engineering for the acceptance of this dissertation entitled, "**EVALUATION OF BELLED-TYPE PILES UPLIFT CAPACITY IN SANDY AND SOFT-ROCK GROUND**" by **KANG JUNGGOO** in partial fulfillment of the requirements for the degree of **DOCTOR OF ENGINEERING**.*

Dated: February 2020

Supervisor:

Professor, Noriyuki YASUFUKU, Dr. Eng

Examining committee:

Professor, Yasuhiro MITANI, Dr. Eng

Professor, Hideki SHIMADA, Dr. Eng

ACKNOWLEDGMENTS

The Ph.D. program at Kyushu University was a difficult challenge for me. Age and language problems always asked me if I could complete my Ph.D. as an international student. Even under challenging conditions, I finished my doctoral program safely with the help of many people. I want to thank my supervisor and colleagues for giving me a lot of advice and guidance in completing my Ph.D.

First, I would like to express my sincere gratitude to my supervisor Prof. Noriyuki YASUFUKU. I remember that my supervisor often cheered me when I was studying late. "Always challenge, create, and try!!" This cheer has always been a force for me. Also, the belief in me of my supervisor, Prof. Yasufuku Noriyuki guidance has been a significant force in tough Ph.D., and as a result, I was able to conduct creative and original research. Thank you very much for this teaching.

I would also like to address my thanks to Prof. Kenichi TOKIDA for introducing me to study at Kyushu University. During the research student period at Osaka University, I was able to learn the spirit, confidence, and effort of the researcher, and I was able to complete the doctoral program smoothly by introducing a good teacher.

Many thanks to Prof. Yasuhiro MITANI and Prof. Hideki SHIMADA for guiding the doctoral dissertation. The detailed reviews of the teachers helped me through my research and helped to improve the quality of the doctoral dissertation by commenting on the details.

I would like to express my sincere gratitude to Shinji ARAMAKI, Ph.D. a collaborator who has helped me a lot with friendly guidance and considerate communication for

international students. Also, I will never forget the passion of Mr. Michio NAKASHIMA, the laboratory technician. He has a lot of experience and can perform any difficult experiments. He is the best expert in the experiment and was able to overcome experimental difficulties during my Ph.D.

I would also like to thank Associate Professor Ryohei ISHIKURA, an associate professor who always takes care of all the students, even on a busy schedule. Assoc. Prof. Ryohei ISHIKURA has always been a positive teacher and helped me to study in a pleasant atmosphere.

I would also like to extend my sincere appreciation to other academic and technical staff in the geotechnical engineering laboratory, Mrs. Aki ITO.

The colleagues at the Kyushu University Geotechnical Engineering Laboratory were always the best. They are very kind, sincere, and cooperative. I will never forget the memories at the Kyushu University Geotechnical Engineering Laboratory. Thanks to all the lab colleagues.

Special thanks to the Cho-sun Scholarship Association for giving me the opportunity to focus my research on my Ph.D.

Finally, I would like to express my deepest gratitude to my favorite parents, who were delighted when they saw my doctoral dissertation.

KANG JUNGGOO

Fukuoka, March 2019

ABSTRACT

Pile foundations have been used to reliably support superstructures. In general, pile foundations are divided into end bearing piles, bearing piles, friction piles, and tension piles. In addition, depending on the type of pile, there are ready-made piles, prestressed concrete piles, and steel piles, where depending on the purpose in-situ, pile system to be used is selected. The structure and geometry of these piles makes them very vulnerable to various forces applied in the horizontal direction. Horizontal loads are applied to structures such as transmission towers, coastal structures, and high chimneys. In addition, Natural disasters such as heavy rainfall events, typhoons, earthquakes, and tsunamis induce horizontal loads on structures. The horizontal load on the structure simultaneously induces both compressive and tensile forces at the foundation of the pile. The previous researchers have proposed various uplift resistance structure systems to effectively cope with the compressive load and uplift load generated at the foundation of the piles, where those systems are currently applied to various structures.

Among the various uplift resistance foundation systems, the belled-type pile is a construction method that has an expanded pile tip similar to the shape of a bell. This pile is effective against horizontal loading due to its shape and is considered as a reliable method not only for the compressive loading but also for the uplift loading due to the bell-shaped tip. In addition, this method generally utilizes cast-in-place concrete. Consequently, the size, length, and shape of the pile are less restrictive in comparison to the ready-made piles. Therefore, various construction cases have adopted this system for large structures. Moreover, due to the development of the construction technology, the applicability becomes

higher, where it can be applied to soft-rock ground with an N value of 50. However, a robust model that considers the pile shape, penetration depth, ground conditions, and the complexity of the piles shape to evaluate the uplift resistance of the pile is still lacking. Therefore, in this study, aiming at facilitating the effective construction and design of belled-type piles, the uplift resistance characteristics and the soil behavior of the belled-type piles were investigated using a model test. In addition, based on the results of the model test, an evaluation equation considering the pile tip inclination angle of the belled-type pile was proposed. The evaluation equation proposed in this study can be used as basic data for the design of shallow sand foundation, deep sand foundation, and soft-rock foundation. The dissertation is divided into 7 chapters:

Chapter 1 discusses the research trends on the uplift resistance of belled-type piles, the specific objectives of this study, and the approach of research.

Chapter 2 provides a review of the literature on the proposed evaluation formulas and test methods. This chapter is divided into three sections. The first section examined the uplift resistance mechanisms and basic theory uplift resistance to the previous conventional pile. The remaining two sections introduce in detail the research method and the proposed model of the uplift resistance structure system.

Chapter 3 introduces the test scope and test methods of model tests. Standard of model soil, scale of model ground, method of constructing sand ground according to unit density, method of constructing soft-rock ground using soil-cement, basic characteristics of sand used in model ground, and soil-cement performed on soft-rock ground that introduces in detail the general part of the model test such as the characteristics of the model and the measuring equipment used during the model test.

Chapter 4 explains the results of model tests of conventional piles and belled-type piles performed on sandy ground. Model tests were performed on the sand ground for unit weight, pile penetration depth, and pile tip inclination angle of belled-type piles. In addition, image analysis was conducted using half-circular model tests and the shape of the failure surface of the target ground was clearly observed. Based on the result, the characteristics of the uplift resistance and the soil behavior on the unit weight of sand were confirmed, and the failure surface formation conditions of belled-type piles and the applicability of the ground on the unit weight were verified.

Chapter 5 summarizes the results of the belled-type pile model tests on the strength of the soft-rock ground, the shape of the tip of the pile and the penetration depth of the pile. Based on the results of the model test, the uplift resistance of the soft-rock ground was clearly different from the previously studied sand and clay ground. In particular, the failure mechanism, displacement characteristics and the maximum uplift load trend on soft lock ground are clearly explained.

Chapter 6 proposes an uplift resistance model for sand ground and the soft-rock ground. In the uplift resistance model for sand ground, an uplift resistance model was proposed considering the pile tip inclination angle of the belled-type pile, penetration depth and unit weight of sand. In addition, the sand ground has been proposed in two types, divided into shallow ground and deep ground in consideration of the failure surface pattern. The uplift resistance model on soft ground was proposed using uniaxial compression tests, tensile tests, etc., which were obtained through preliminary tests. The uplift resistance model proposed in this section can predict the uplift resistance of belled-type piles with general soil parameters such as internal friction angle, unit density and shear stress of uniaxial compression test without considering the shape of the failure surface.

Chapter 7 summarizes the main findings of this dissertation and delineates the future work.

Table of Contents

CHAPTER VII

CONCLUSIONS AND FUTURE WORKS

List of Figures

List of Table

List of Notations

A_s	: Belled-type pile tip area
b_b	: Diameter of belled type pile tip
b_s	: Diameter of shaft
b_e	: Corrected diameter of pile tip
D_r	: Relative density
ε	: Percentage of error
$\theta_{\mathrm{E}}, \theta$	: Angle of the failure surface
θ_i	: Pile tip inclination angle
η	: Depth factor of failure surface shape
κ	: Coefficient of unit weight
K_0	: Earth pressure at rest
K_s	: Coefficient of lateral earth pressure
K_u	: Uplift factor
L	: Penetration depth of pile
LVDT	: Linear Variable Displacement Transducer
N_u	: Breakout factor
p_0'	: Effective vertical mean earth pressure
P_u	: Ultimate uplift capacity
$P_{u(net)}$	: Net ultimate uplift capacity
S_f	: Shear stress on failure surface

T : Shear stress at the failure surface

V : Volume in failure surface

W_s : Weight of soil-cement inside failure surface

W : Weight of the pile

γ_d : Unit weight of sand

γ_c : Unit weight of Soil-Cement.

φ : Internal friction angle

ψ : Dilatancy angle ($\psi = \varphi/2°$, $\psi = \varphi$-30°)

σ_a : Pressure in a cylinder

σ_c : Compressive stress

σ_t : Tensile stress

δ : Pile-soil friction

λ : Slendness ratio

CHAPTER I

INTRODUCTION

1.1 BACKGROUND

The pile foundations have been used in the decades to support the stability of superstructures. However, due to natural disasters such as heavy rainfall, typhoons, earthquakes, and tsunamis, the moment forces are generated on some structures. The moment forces will generate not only the uplift load but also the compressive load (Fig.1-1). The previous researchers have been proposed a various uplift resistance foundation system (anchor plate, belled-type pile, and helical pile) as an effective and to resist the compressive and uplift forces where are generated at the pile foundation.

Among the various uplift resistance foundation systems, the belled-type pile is a construction method that has an expanded pile tip, similar to a bell-shape. This pile is

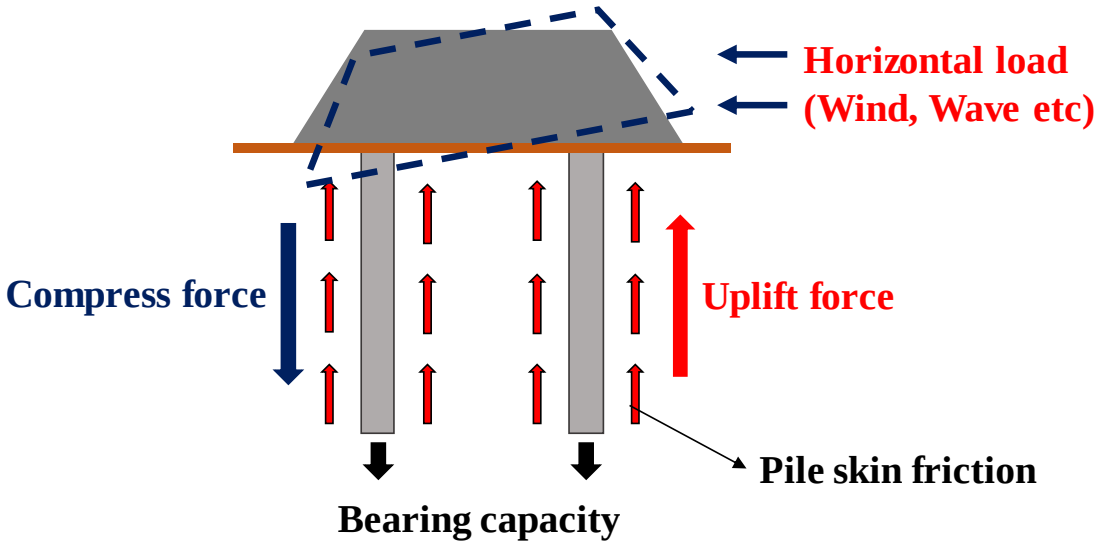

Fig.1-1 Influence of horizontal loads applied to the structure.

effective against horizontal load because it has a reliable method not only the compressive load but also for the uplift load due to the belled-type pile tip. In addition, this method generally utilizes cast-in-place concrete. Based on the result, the size, length, and shape of the pile are less restrictive than ready-made piles. Therefore, various construction cases have been using this method for large structures among civil structures. Moreover, due to the development of construction technology, the applicability is high because it can be applied to soft rock ground with an N value of 50. However, the lack of evaluation criteria quantified by pile shape, penetration depth, various ground conditions, and the complexity of shape characteristics compared to conventional piles, have not clarified the evaluation method for uplift resistance.

1.2 THE UPLIFT RESISTANCE OF BELLED-TYPE PILES

The study of the uplift resistance of conventional piles depends on the friction between the pile and the soil. The theory of limit friction was proposed by Meyerhof (1968) using model tests. In addition, Das (1976) improved the Meyerhof (1968) study taking into account the impact on penetration depth and critical penetration depth was proposed.

Chattopadhyay & Pise (1986) proposed an uplift capacity resistance prediction model for the conventional pile. This model assumed a force acting on the failure surface around the pile and the failure surface at the limit equilibrium.

Early studies on the uplift resistance of belled-type piles were conducted by Giffels et al (1960). It was studied to estimate the uplift resistance of anchor plates used in transmission towers. Other studies have been conducted by Ireland (1963) and Adams and Hayes (1967). In contrast, Majer (1955), Balla (1961), Downs and Chieurzzi (1966), Baker and Kondner (1966), Meyerhof and Adams (1968), Hanna and Carr (1971), Hanna and Sparks (1973),

Das and Seeley (1975a, b), Clemence and Veesaert (1977), Andreadis et al. (1981), Sutherland et al. (1982), Murray and Geddes (1987), Ghaly et al. Many researchers (1991 a, b) and others performed classical laboratory model tests in the study of uplift resistant structural systems and bell piles. In these studies, model tests under various conditions were carried out to analyze the behavior of pile and uplift resistive systems. Ovesen (1981), Tagaya et al. (1983, 1988), Dickin (1988), Dickin and Leung (1990, 1992), etc., used centrifugal model tests to perform full-scale tests on stress levels. The obtained results more accurate than the conventional test. In these studies, various characteristics regarding the uplift resistance of belled-type pile and uplift resistive structures were found. However, despite the research results of various researchers, it is difficult to predict the accurate uplift resistance until now due to the various ground and pile shapes.

1.3 OBJECTIVES AND SCOPES

The main objective of this study is to observe the uplift resistance characteristics of soil behavior, tip shape of pile, penetration depth and various conditions of the ground. According to this objective, circular chamber model tests, and half-circular chamber model tests. It was performed under conditions of sand ground and soft-rock ground. In particular, the tests were performed in consideration of the pile tip shape and the pile penetration depth. The specific objective is mentioned as follows:

1. To evaluate the uplift resistance characteristics of belled-type piles based on the geotechnical point of view. Based on the relative density of sand and the strength of the soft-rock ground, the model base is constructed to conduct a circle chamber test of the uplift resistance of belled-type piles. Based on the test results, the uplift resistance characteristics according to the ground conditions of the belled-type piles will be verified.

2. To investigate the failure pattern behavior of soil on the belled-type pile in various ground conditions. A video camera with high resolution was used during the test in the half-circular model. Image analysis is performed on the recorded results to analyze failure surface patterns.

3. To propose the improved evaluation uplift resistance capacity model on the belled-type pile. The proposed model is improved by modifying the model test results and the previous conventional piles model.

1.4 FRAMEWORK AND OUTLINES

In order to achieve the objective of this research, this paper is organized into seven chapters with a framework, as shown in Fig.1-2. The outline of each chapter is described as follow:

CHAPTER 1 describes the background of this research, introduction to uplift resistance of belled-type piles.

CHAPTER 2 summarizes previous research on the uplift resistance of piles, belled-type pile and uplift resistance structure systems. It reviews the following aspects: Basic uplift resistance mechanisms of conventional piles, previous research on the uplift resistance behavior of belled-type piles, failure mechanisms. In addition, improvements from the previous models are summarized.

CHAPTER 3 describes in model tests performed in the laboratory. It explains in the characteristics of the ground materials used in the test, the method of constructing the ground, and the properties of model soil and model pile used in the model test. In addition, model

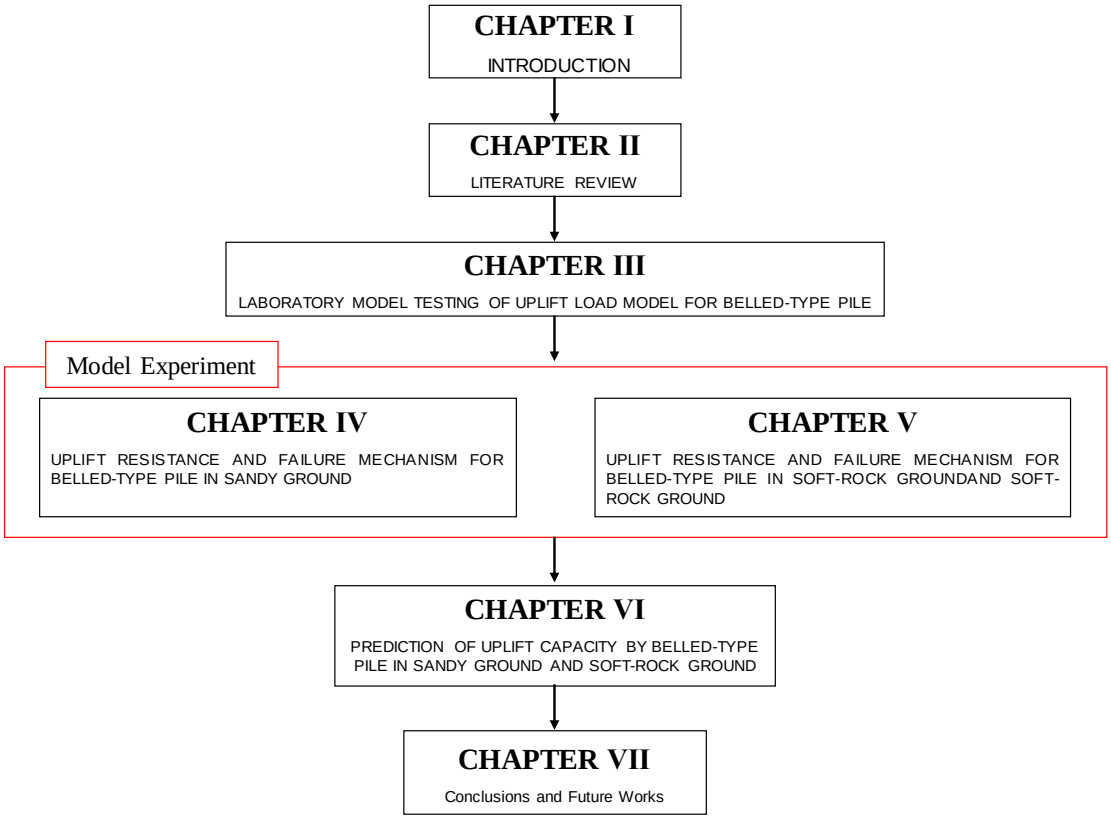

Fig.1-2 Flowchart of the research.

tests describe the test setup, measurement methods, scale factors, and test procedures used in detail.

CHAPTER 4 reports the results of an uplift resistance model test of belled-type piles on the sandy ground. Model tests are performed on the sandy ground in 5 steps according to relative density. Penetration depth is performed under three conditions, assuming shallow and deep ground conditions. In addition, the circular model test examined the characteristics of the uplift load, and in the half-circular test of the soil behavior under the applied uplift load is observed.

CHAPTER 5 reports the results of an uplift resistance model test of belled-type piles on the soft-rock ground. Soft-rock ground model tests are performed at the 2-type strength and 2-type penetration depth conditions of the soft-rock ground.

CHAPTER 6 proposes an uplift resistance prediction model for the belled-type piles by improving the previous model. The improved model suggests a model that can be applied to the belled-type pile, taking into account the limit equilibrium model of the conventional piles proposed in the previous research. In addition, the reliability of the improved prediction equation is verified by performing comparative analysis with the calculated values of the proposed model, the results of model tests, and the improved prediction model proposed in this study.

CHAPTER 7 shows the summaries, conclusions, main outcomes of the research, and recommendations of the future work.

1.5 ORIGINAL CONTRIBUTION

In this study, model tests and image analysis methods are used to investigate the uplift resistance and soil behavior characteristics of the belled-type pile under various conditions. In addition, the objective of this study is to propose an uplift resistance model of belled-type piles using model test results and literature studies.

Some new finding is obtained to which are considered as the originality of this research. As follows:

1. The uplift resistance characteristics and failure surface formation conditions for the relative density of the applied sandy ground of the belled-type pile were confirmed in the model test. Similarly, in the model tests performed on soft-rock ground, the uplift resistance characteristics according to the ground strength and the extent and shape of the failure surface according to the strength of the soft-rock ground were clearly identified.

2. The previous belled-type piles were researched using anchor plates and helical piles. Therefore, there was a difficulty in applying the tip shape of the belled-type pile and the pile-soil friction. In this study, the test was carried out considering the pile tip inclination angle, penetration depth and ground condition of the belled-type pile.

3. Utilizing the limit equilibrium model proposed in the conventional pile has proposed an improved model that can be applied to the belled-type pile. An improved model is proposed, taking into account the pile tip inclination angle of the belled-type pile, the soil-pile friction and the failure surface identified in the model test.

REFERENCES

Das, B. M., Moreno, R and Dallo, K. F. (1985). Ultimate pullout capacity of shallow vertical anchors in clay. *Soil and Foundations*, 25(2), 148-152.

Meyerhof, G. G., and Adams, J. I. (1968). The ultimate uplift capacity of foundations. *Canadian Geotechnical Journal*, 5(4), 225-244.

Meyerhof, G. G., and Adams, J. I. (1973). Uplift resistance of inclined anchors and piles. *Proceedings of the 8th ICSMFE*, 2, 167-172.

Ilamparuthi, K. and Dickin, E. A. (2001). The influence of soil reinforcement on the uplift behaviour of belled piles embedded in sand. *Geotextiles and Geomembranes*, 19(1), 1-22.

Lin, J. G., Hsu, S. Y. and Lin, S. S. (2015). The new method to evaluate the uplift capacity of belled piles in sandy soil. *Journal of Marine Science and Technology*, 23(4), 523-533.

CHAPTER II

LITERATURE REVIEW

2.1 INTRODUCTION

The belled-type pile is a method of increasing the uplift resistance by extending the tip of the pile.

In the previous study, the uplift resistance of piles was investigated by model tests considering the pile-soil frictional and the deformation of the surrounding soils. Based on the results, various evaluation models were proposed. Additionally, many uplift resistance structure systems including belled-type piles were proposed using similar test results as conventional pile research methods.

This section introduces the uplift resistance mechanism and typical models of the conventional piles that were previously studied. In addition, the research trends, basic models, analysis methods, limitations of belled-type piles, and uplift resistance structure systems studied are described in detail.

2.2 UPLIFT RESISTANCE MECHANISM OF CONVENTIONAL PILES

2.2.1 Limit Friction Theory

Meyerhof (1973) proposed an evaluation model for the uplift resistance of conventional piles considering friction between piles and soil by model tests. Based on the result, the limit friction theory generated between the pile and soil was proposed.

The uplift resistance capacity of the conventional pile proposed by Meyerhof (1973) is shown in Eq.2.1. Where the uplift coefficient (K_u) is proposed by using the results of the laboratory model test. Since sand does not consider pile-soil friction, it can be expressed as shown in Eq.2.2.

$$P_{un} = (c + p_0' K_u tan\delta) A_s \tag{2.1}$$

since sand is c = 0.

$$P_{un} = f_{av} \pi b_s L = \frac{\pi}{2} K_u b_s \gamma_d L^2 tan\delta \tag{2.2}$$

Where, P_{un}: net ultimate uplift capacity (kgf), P_u: ultimate uplift capacity (kgf), A_s: surface area of the pile (cm^2), b_s: pile diameter (cm), p_0': effective vertical mean earth pressure (kgf/cm^2), δ: soil-pile friction angle (º), L: penetration depth of pile (cm), K_u: uplift factor, γ_d: unit weight of sand (g/cm^3), φ: internal friction angle (º).

The proposed uplift factor (K_u) increases linearly with increasing internal friction angle (φ) of sand and penetration depth of the pile. However, the uplift factor (K_u) is difficult to estimate due to the different characteristics of the ground.

To solve this problem, some researchers studied the relationship between the relative density of sand and the internal friction angle (φ) using a direct shear test, triaxial test, and model test. On the other hand, Meyerhof (1973) presented the relationship of $K_u = \varphi$ for the circular piles for clearer design.

2.2.2 Critical Embedment Ratio Theory

Das (1977) calculated the frictional force per unit area generated around piles up to a certain depth (z) from the ground surface uplift loading on piles (Eq.2.3).

$$f = K_u tan\delta\gamma z \tag{2.3}$$

In Eq.2.3, the uplift resistance up to the penetration depth (L) of the pile can be expressed as Eq.2.4.

$$P_u = \int_0^L p \cdot f dz \tag{2.4}$$

Where p is the perimeter of the pile.

Das (1983) used the model test results to show that the unit friction force (f) acting on the pile skin increases to a certain depth according to the slenderness ratio (λ) of the pile. However, at a depth above the limit, the unit friction force (f) reaches a constant value.

Das (1983) used this result to define the critical embedment depth for the uplift factor (K_u) of conventional piles and proposed it in Eq.2.8. The critical embedment ratio is dependent on the relative density (D_r) and expressed as

$$(L/b_s)_{cr} = 0.156Dr + 3.58 \text{ (For } Dr \leq 70\%) \tag{2.5}$$

and

$$(L/b_s)_{cr} = 14.5 \text{ (For } Dr > 70\%) \tag{2.6}$$

The net ultimate uplift capacity (P_{un}) of piles in the sand can be estimated as,

$$P_{un} = \frac{1}{2} p\gamma L^2 K_u tan\delta \qquad [If,\ L/b_s \leq (L/b_s)_{\text{cr}}\,] \tag{2.7}$$

$$P_{un} = \frac{1}{2} p\gamma L_{\text{cr}}^2 K_u tan\delta + p\gamma L_{\text{cr}} K_u tan\delta (L - L_{\text{cr}}) \qquad [If, L/b_s > (L/b_s)_{\text{cr}}\,] \tag{2.8}$$

Das (1977) uplift resistance model is basically based on the uplift resistance model and the uplift factor (K_u) suggested by Meyerhof (1967).

2.2.3 Limit Equilibrium Model

Chattopadhyay & Pise (1986) calculated the uplift resistance by considering the failure surface in the pile ground as a log curve considering the Limit equilibrium at the failure surface. Fig.2-1 shows the failure surface proposed by Chattopadhyay & Pise (1986).

Chattopadhyay & Pise (1986) introduced the following assumptions for theoretical calculations.

1. The transverse spreading of the failure surface depends on the slenderness ratio(λ), internal friction angle (φ) of the soil, and the pile-soil friction angle (δ). The maximum transverse value of the failure surface with constant penetration ratio is " pile-soil friction angle (δ) = internal friction angle (φ)" and decreases as the pile-soil friction angle (δ) decreases. If pile-soil friction angle (δ) = 0°, failure occurs at the interface between pile and ground.

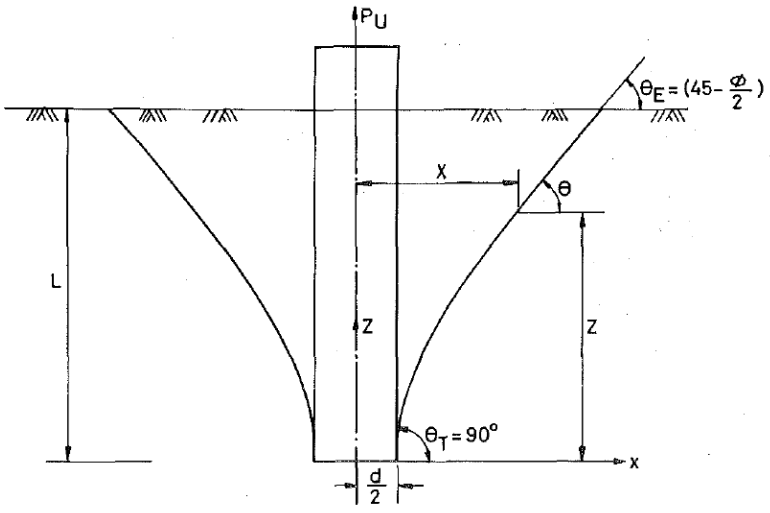

Fig.2-1 Pile and failure surface by Chattopadhyay & Pise (1986).

2. If $\delta \geq 0^{o}$, the failure surface gradually extends from the pile tip to the ground (Meyerhof & Adams, 1968).

3. The failure surface slope angle at the ground surface is $(45° - \varphi/2)$ when $\delta > 0^{o}$ and $\delta = 0^{o}$, it is 90^{o}.

Calculation of the slope angle of failure surface at point z from the pile tip, assuming the log curve from the pile tip, is given by Eq.2.9.

$$\frac{dz}{dx} = \tan\left(45° - \frac{\varphi}{2}\right)\frac{H}{z}e^{\beta\left(1-\frac{z}{L}\right)} \tag{2.9}$$

where, $\beta = \lambda(50° - \varphi)/2\delta$, β assumes that the internal friction angle (φ) value does not exceed 50^{o}.

If the condition in Eq.2.9 is satisfied, then at the pile tip ($z = 0$), $\theta = 90^{o}$; and at the soil surface ($z = L$), $\theta = (45° - \varphi/2)$. Integrating Eq.2.9 produces a logarithmic failure surface as shown in Eq.2.10(a).

$$x = \frac{Le^{-\beta\left(1-\frac{Z}{L}\right)}}{\beta\tan\left(45°-\frac{\phi}{2}\right)}\left(\frac{Z}{L} - \frac{1}{\beta}\right) + C \tag{2.10-a}$$

$$\text{Hence, } C = \frac{b_b}{2} + \frac{L}{\beta^2\tan\left(45°-\frac{\phi}{2}\right)}\exp(-\beta) \tag{2.10-b}$$

Therefore, the distance x from the center of the pile to the failure surface for a given depth can be expressed as Eq.2.11.

$$x = \frac{b_b}{2} + \frac{L}{\beta^2\tan\left(45°-\frac{\varphi}{2}\right)}\exp(-\beta) + \frac{Le^{-\beta\left(1-\frac{Z}{L}\right)}}{\beta\tan\left(45°-\frac{\phi}{2}\right)}\left(\frac{Z}{L} - \frac{1}{\beta}\right) \tag{2.11}$$

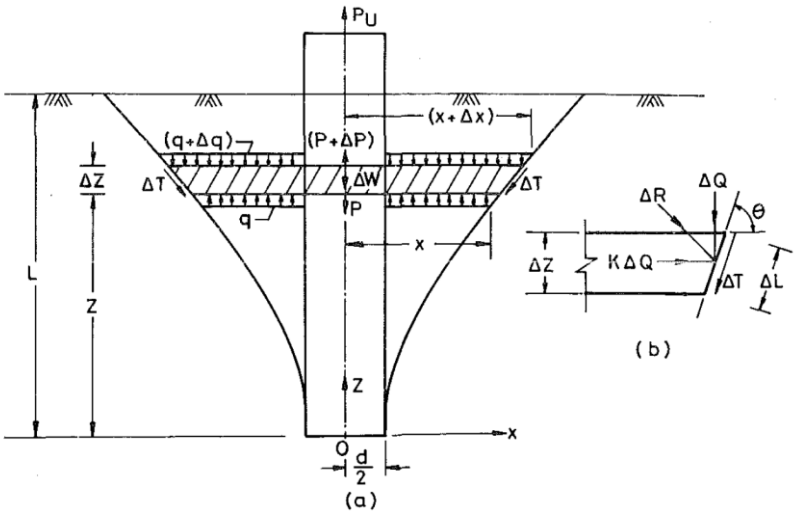

Fig.2-2 Free body diagram of circular disc wedge proposed by Chattopadhyay & Pise (1986).

On the other hand, since $z = L$ at the ground surface, the distance (X_G) from the center of the pile to the failure surface can be expressed as Eq.2.12.

$$\frac{X_G}{b_b} = \frac{1}{2} + \frac{\lambda \exp(-\beta)}{\beta^2 \tan\left(45° - \frac{\varphi}{2}\right)} + \frac{\lambda}{\beta \tan\left(45° - \frac{\varphi}{2}\right)}\left(1 - \frac{1}{\beta}\right) \tag{2.12}$$

Substituting $\beta = \lambda(50° - \varphi)/2\delta$ in this equation can be expressed as Eq.2.13.

$$\frac{X_G}{b_b} = \left(\frac{1}{2} + \frac{2\delta}{(50° - \varphi)\tan\left(45° - \frac{\varphi}{2}\right)}\right) + \frac{1}{\lambda}\left(\frac{2\delta}{50° - \varphi}\right)^2 + \frac{1}{\tan\left(45° - \frac{\varphi}{2}\right)}\left\{exp\left[\frac{-\lambda(50° - \varphi)}{2\delta}\right] - 1\right\} \tag{2.13}$$

Fig.2-2 shows a free body diagram of the circular disc wedge proposed by Chattopadhyay & Pise (1986). The model is calculated from the weight of soil inside the failure surface and the shear strength of the failure surface.

The shear resistance ΔT equation acting on the failure surface of length Δz is

$$\Delta T = \Delta R tan\varphi \tag{2.14}$$

Where ΔR is a force acting perpendicular to the shear plane. It represents the element of force in the shear plane as follows.

$$\Delta R = \Delta Q(cos\theta + Ksin\theta) \quad (2.15\text{-a})$$

$$\Delta\, Q = \gamma_S(H - z - \tfrac{\Delta z}{2})\Delta L \quad (2\text{-}15\text{-b})$$

At this time, if $K = (1 - sin\varphi)$, $(tan\delta/tan\varphi)$, the lateral earth pressure coefficient acting on the shear surface is the static earth pressure coefficient $K = K_0 = (1 - sin\varphi)$ when the friction angle between the pile and soil is equal to the internal friction angle (φ).

Therefore, the uplift resistance capacity is derived as follows.

$$\Delta R = \gamma_d \left(L - z - \tfrac{\Delta z}{2}\right)(cos\theta + Ksin\theta)\Delta L \quad (2.16\text{-a})$$

And

$$\Delta T = \gamma_d \left(L - z - \tfrac{\Delta z}{2}\right)(cos\theta + Ksin\theta)\tfrac{\Delta z tan\varphi}{sin\theta} \quad (2.16\text{-b})$$

In extreme equilibrium, the sum of the normal forces for any element in the failure surface is zero.

$$(P + \Delta P) - P + q\pi x^2 - (q + \Delta q)\pi(x + \Delta x)^2 - \Delta W - 2\pi\left(x + \tfrac{\Delta x}{2}\right)\Delta T sin\theta = 0 \quad (2.17)$$

Where, after substituting Eq.2.17 and taking the limit value and substituting $q = \gamma_d(L - z)$, it can be written as Eq.2.18.

$$\frac{dP}{dz} = \gamma_d \pi dL\left\{\tfrac{2x}{2}\left(1 - \tfrac{z}{L}\right)[cot\theta + (cos\theta + Ksin\theta tan\varphi)tan\varphi]\right\} \quad (2.18)$$

Therefore, the total uplift resistance of the pile is given by Eq.2.19.

$$\therefore P_u = \gamma_d \pi dL \int_0^L \left\{ \frac{2x}{2} \left(1 - \frac{z}{L}\right) [cot\theta + (cos\theta + Ksin\theta tan\varphi) tan\varphi] \right\} dz \quad (2.19)$$

The uplift resistance model proposed by Chattopadhyay & Pise (1986) is derived from the limit equilibrium equation. This equation has a higher reliability than the previous evaluation equation but depends heavily on the beta value (β), which is the downside.

2.2.4 Modified Limit Equilibrium Model

K. Shanker (2007) simplified the proposed model by Chattopadhyay & Pise (1986). His proposed model presents the failure surface linearly using laboratory model tests and can be applied to the slenderness ratio (λ) of 20 or more.

The following describes the main points in the model presented by K. Shanker (2007).

1. The use of limit equilibrium equation, as defined by Chattopadhyay & Pise (1986).
2. The failure surface of K. Shanker (2007) is assumed to be linear, and the failure angle in contact with the ground utilizes a dilatancy angle (ψ).
3. If the slenderness ratio (λ) of the pile is 20 or more, the failure surface is assumed to be generated at $3L/4$ of the pile.

K. Shanker improved the model of Chattopadhyay & Pise (1986) and proposed an uplift resistance model for conventional piles. In particular, K. Shanker's (2007) model is relatively advantageous to Chattopadhyay & Pise (1986) model when calculating the uplift resistance since the failure surface is assumed to be linear.

2.3 UPLIFT BEHAVIOR OF BELLED-TYPE PILES AND UPLIFT RESISTANCE STRUCTURE SYSTEM

In the study of the uplift resistance of the belled-type pile and uplift resistance structure system, the influence on the soil behavior that generates uplift resistance is more important than that of the influence of the pile-soil friction. However, it is complicated to clearly define the soil behavior due to various ground conditions and the tip shape of the belled-type pile. Therefore, the previous researchers have conducted model tests considering various ground conditions and influences on the tip shape of foundation structures and have reported the results. This chapter describes the research trends and results that have been studied.

2.3.1 Previous Research of Belled-Type Pile and Uplift Resistance Structure System

Early research on the uplift resistance of pile and uplift resistance structural systems began with large-scale field tests of anchor plate foundation used in transmission towers (Giffels et al. (1960), Ireland (1963) and Adams and Hayes (1967)).

Majer (1955), Balla (1961), and Das and Seeley (1975 a, b) studied the uplift resistance characteristics of belled-type piles and the soil behavior characteristics using model tests. It is summarized by the uplift coefficient, limit penetration depth, and failure surface. Ovesen (1981), Tagaya et al (1983, 1988), Dickin (1988), Dickin and Leung (1990, 1992), and others performed tests on uplift resistance of anchor plates and belled-type piles based on centrifugal modeling techniques. Technological advances in model tests have led to higher reliability.

Theoretical analyses include basic expansion theory proposed by Vesic (1971), limit equilibrium analysis by Chattopadhyay and Pise (1986), and elasto-plastic finite element method analysis proposed by Rowe and Davis (1982), Saran et al. (1986). However, many

of these research methods presented various design methods. Therefore, it was difficult to exchange mutual research until now.

2.3.2 Uplift Resistance Analysis Model

The uplift resistance design theory of belled-type piles has been studied by researchers such as Majer (1955), Balla's (1961), Meyerhof and Adams (1968), Ovesen (1981), and Dickin and Leung (1990, 1992). Fig.2-1 shows a schematic diagram of the basic equation (Eq.2.1) of the uplift resistance basic system. Eq.2.20 is the most basic uplift resistance structure system proposed by the researchers. An important factor in the equation is the calculation of uplift resistance by the pile weight, the shear strength on the failure surface, and the weight of the soil inside the failure surface. The following is shown in Eq.2.20.

Description of the model briefly shown in terms of uplift resistance capacity:

$$P_u = \mathrm{W} + \gamma_d V + T \qquad \text{(2.20-a).}$$

Where, P_u: ultimate uplift capacity, W: the weight of the pile, γ_d: dry unit weight, V: volume in failure surface, T: shear stress at the failure surface.

The following shows the ultimate uplift resistance capacity by subtracting the weight of the pile from the uplift resistance to indicate net ultimate uplift resistance.

The net ultimate uplift resistance capacity of a pile:

$$P_{un} = P_u - W \qquad \text{(2.20-b)}$$

Where, P_{un}: net ultimate uplift capacity, P_u: ultimate uplift capacity, W: the weight of the pile.

Eq.2.20(a), proposed by previous researchers, is a comprehensive concept. In order to apply this equation effectively, the effects of failure surface shape and pile penetration depth must be considered.

2.3.3 Failure Mechanism of Belled-Type Pile

The failure surfaces of belled-type piles and uplift resistance structures system are proposed by analyzing the results of the model test. Fig.2-3 shows three basic failure surfaces arranged by Dickens (1988). In this result, the penetration depth (L) of the model tests is performed on the shallow foundation, and the ground material is sand.

The following describes the three basic forms of failure surface by Dickin (1988). Fig.2-3(a) is a vertical sliding surface model, which was assumed by Majer (1955), one of the earliest researchers. This model is based on the soil weight at the top of the anchor tip and the shear strength at the failure surface.

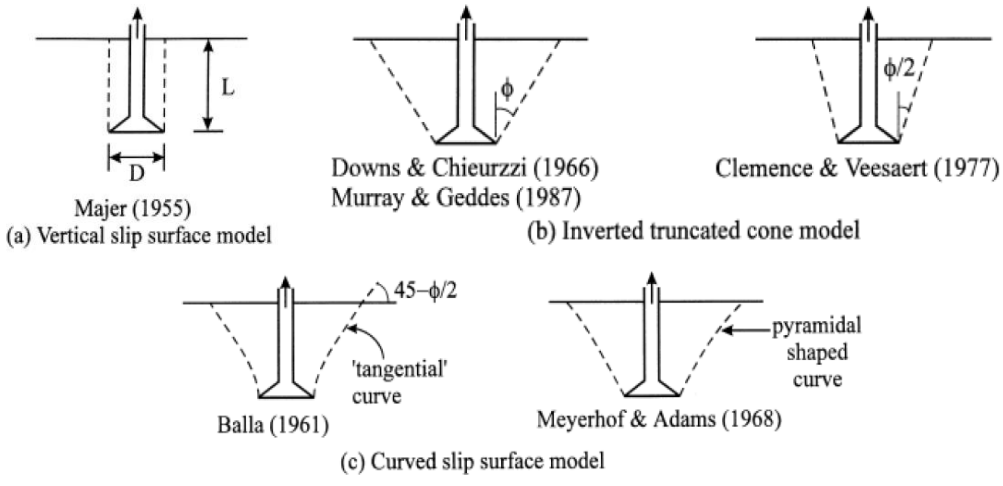

Fig.2-3 Three basic failure surfaces by belled-type piles Dickin (1988).

Fig.2-3(b) shows an invert truncated model. This model assumes that a failure surface with a failure angle at the tip of a belled-type pile appears as a linear line on the ground. The failure angle, which is an important parameter in this model, has been suggested to be 90º - φ and 90º - $\varphi/2$ according to previous studies. (Downs and Chieurzzi. 1966; Clemence and Veesaert.1977; Murray and Geddes.1987)

Fig.2-3(c) is a sliding curved surface model that is proposed by Bella's (1961) and Meyerhof & Adams (1986). This model is an inverted truncated cone model, which assumes a linear failure plane as a curve. The linearity of the failure surface is reported as a tangential curve and pyramid curve. According to Bella (1961), the failure surface of the foundation in dense sand is curved and the tangent of the surface in contact with the ground is about $45° - \varphi/2$ horizontal. Its theory of circular failure surface showed similar results as full-scale tests on shallow foundations. In addition, Meyerhof and Adams (1968) suggested a pyramidal slip surface on top of the anchors observed in laboratory model tests.

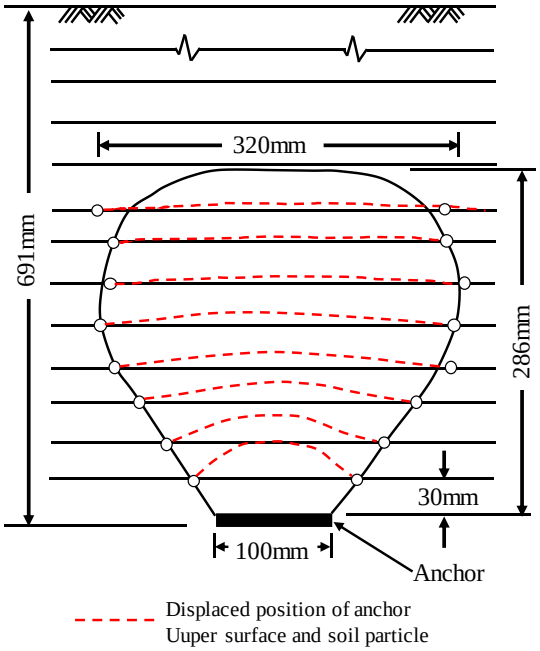

Fig.2-4 Delineation of rupture surface in half-cut model test on deep anchor in dense sand (Ilamparuthi. K et al. 2002).

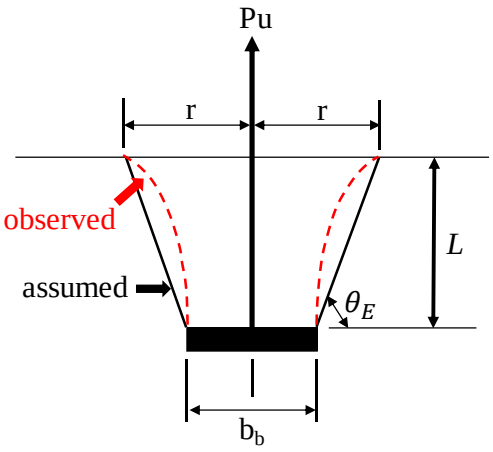

(a) Shallow foundation ($L/b_b < 3$)

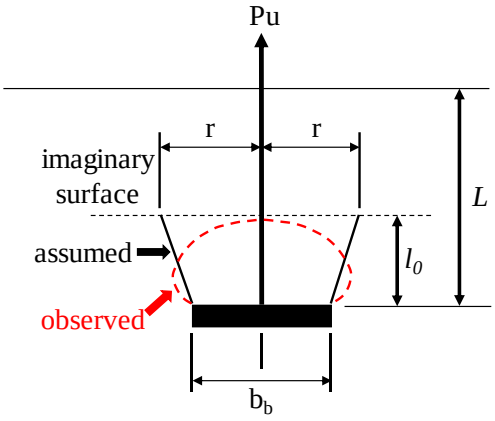

(b) Deep foundation ($L/b_b > 3$)

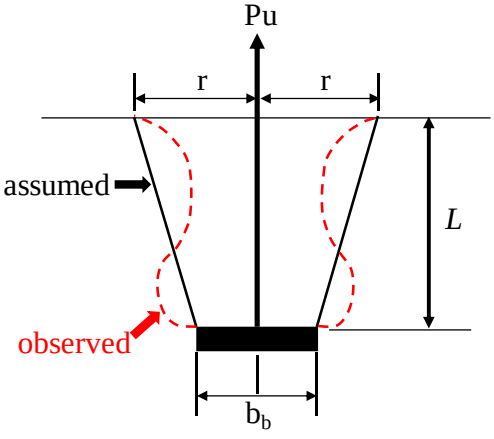

(c) Intermediate depth foundation ($L/b_b \simeq 3{\sim}4$)

Fig.2-5 Failure surface of screw anchor pile for penetration depth (Ghalys. 1991).

2.3.4 Failure Mechanism of Belled-Type Piles Considering Penetration Depth

Fig.2-4 and Fig.2-5 show the failure surfaces of the uplift resistance structure system studied on a deep foundation. The previous researchers considered the slenderness ratio ($\lambda = L/b_b$) of the pile tip diameter (b_b) and pile penetration depth (L). The uplift resistance system is classified into shallow and deep foundations based on slenderness ratio (λ) 3.

According to Ilamparuthi. K et al. (2002) and Ghalys (1991) the model test confirms that the failure surface of anchor-plate, belled-type piles, and screw piles changes in the case of deep foundations ($\lambda > 3$).

Failure surfaces of the uplift resistant structural system conducted in a deep foundation ($\lambda > 3$) based on the results of the model test are different from the shallow foundation.

In the tests of Ghalys (1991) the model, the model showed that the shape of the failure surface depends on the penetration depth of the screw piles. Therefore, the uplift resistance model must take into account the penetration depth.

2.3.5 Lateral Earth Pressure Coefficients

Due to various assumptions about the failure mechanism, the earth pressure coefficient applied to the ground has been modified and proposed. Different modified lateral earth pressure coefficients have been proposed to consider the factors, such as the internal friction angle of sand, the unit weight of sand, and penetration depth.

Table.2-1 shows the recommended modified earth pressure coefficients proposed by previous researchers.

2.3.6 Breakout Factor (N_u)

The previous researchers have proposed a breakout factor to simply compare the proposed uplift resistance capacity models of belled-type piles and uplift resistance structure systems.

Eq.2.21 represents Breakout Factor (N_u), which is a dimensionless coefficient. It is summarized as a coefficient for the uplift resistance of sand piles and is affected by the penetration depth of the pile, the area around the pile, and the unit weight of the soil.

Table.2-1 Assumption made in design methods summarized by Dickin (1988).

Source	Recommended Coefficient (K)	φ (°)	Value of K	Remarks
Meyerhof and Adams (1968),	K_u = 0.9	34.5 39.5 43	1.1~1.8 1.2~2.1 1.3~2.5	K varies linearly with L/b_b ratio
Clemence and Veesaert (1977)	K_0	34.5 39.5 43	0.43 0.36 0.32	K = 1 used in calculations
Surterland et al (1982)	K_0	34.5 39.5 43	0.43 0.36 0.32	-
Kulhawy (1985)	K_a to K_0 K_0 to 1 K_0 to K_0	Loose Medium Dense	- - -	Used stress modification factor to adjust for construction influences
Chattopadhyay & Pise (1986)	K_a	34.5 39.5 43	0.43 0.36 0.32	-
Bobbitt and Clemence (1987)	$S_f K_u$	34.5 39.5 43	0.66~1.1 0.72~1.3 0.78~1.5	60% of Meyerhof and Adams (1968) values
Ghaly (1991)	$K_u = \frac{(1+sin\delta)}{(1-sin\delta)}$	34.5 39.5 43	2.2 2.5 2.8	δ = 0.6~0.7 φ for shallow anchors

$$N_u = \frac{P_{u(net)}}{\gamma_d A_s L} \tag{2.21}$$

where, $P_{u(net)}$: net ultimate uplift capacity, L: depth of penetration, A_s: surface area of the pile (cm^2), γ_d: the unit weight of soil.

Formulation of the breakout factor (N_u) by many researchers has been summarized by Dickens and Lang (1992), as shown in Table.2-2. This table contains the failure mechanism used for the breakout factor (N_u) and the parameters used during the calculation.

To verify the breakout factor proposed by many researchers, Dickin's and Leung (1990) compared the calculations of the previous breakout factor by the penetration ratio under the conditions of 1m diameter and 40º sand internal friction angle. Table.2-3 is based on the comparison; the value of the Breakout factor (N_u) has changed under the influence of the penetration depth. Most of the previous studies have been designed for shallow foundations, hence there is a clear difference in the breakout factor (N_u) designed for deep foundations.

Table.2-2 Previous design methods summarized by Dickin and Leung (1990).

Researcher	Method of Analysis	Equation (N_u: Breakout factor)
Majer (1968),	Vertical slip surface	$N_u = 1 + 2K\left(\frac{L}{b_b}\right) tan\varphi$tan φ where K is the coefficient of lateral stress in soil
Balla's (1977)	Tangential-curve slip surface	$N_u = (F1 + F3)(\frac{4}{\pi})(\frac{L}{B_B})^2$ Where, F1 and F3 are depend on φ and γ_d and obtained from chart provided by author
Downs and Chieuzzi (1966)	Inverted cone slip surface; angle with vertical = φ	$N_u = 1 + 2\left(\frac{L}{B_B}\right) tan\varphi + \frac{4}{3}\left(\frac{H}{b_b}\right)^2 tan^2\varphi +$ $(\frac{b_s}{b_b})^2$
Meyerhof and Adams (1968)	Pyramidal-shaped slip surface	$N_u = 2\left(\frac{L}{b_b}\right) K'_u tan\varphi \left[m\left(\frac{L}{b_b}\right) + 1\right] + 1$ Where K'_u=0.9 for 30º < φ < 45º and m is the shape factor, dependent on φ

Table.2-2 (Continued)

Researcher	Method of Analysis	Equation (N_u: Breakout factor)
Clemence and Veesaert (1977)	Inverted cone slip surface; cone angle with vertical = $\varphi/2^{o}$	$N_u = \left[1 + \left(\frac{L}{b_b}\right) tan\left(\frac{\varphi}{2}\right)\right]^2 + 4K_0 tan\varphi \cos^2\left(\frac{\varphi}{2}\right)\left[\frac{1}{2}\left(\frac{L}{b_b}\right) + \frac{1}{2}\left(\frac{L}{b_b}\right)^2 tan\left(\frac{\varphi}{2}\right)\right]$ Where K_0 is the coefficient of lateral earth pressure.
Anadreadis and Harvey (1982)	Derived from model and field tests on anchors	Chart of N_u in terms of φ and L/b_b provided by anchors
Ovesen (1981)	Derived from centrifugal model tests on horizontal anchor plate	$N_u = 1 + (4.32tan\varphi - 1.58)\left(\frac{L}{b_e}\right)^{1.5}$ where, $b_e = \sqrt{(\pi b_b^2/4)}$
Rowe and Davis (1982)	Finite-element analysis giving uplift capacity of strip anchors	$N_u = F_\gamma F_\psi F_\kappa F_R$ where F_γ is a function of φ and L/b_b, F_ψ is a function of ψ and L/b_b, R_K and R_R may be taken as unity; charts are provided by the authors.
Surterland et al. (1982)	Inverted cone slip surface; cone angle is a function of φ	$N_u = \frac{8}{3}\left(\frac{L}{b_e}\right)^2 tan^2\alpha + 4\left(\frac{L}{b_e}\right) tan\alpha + 1$ where $\alpha = 0.25\left[I_D(1 + cos^2\varphi) + 1 + sin^2\varphi\right]\varphi$ $b_e = \sqrt{(\pi b_b^2/4)}$
Vermmer and Sutjiadi (1985)	Inverted cone slip surface; cone angle = ψ	$N_u = 1 + 2\left(\frac{L}{B_e}\right) tan\varphi cos\varphi_{cv}$ where φ_{cv} is the critical state friction angle
Murray and Geddes (1987)	Inverted cone slip surface; cone angle = φ	$N_u = 1 + \left(\frac{L}{B_e}\right)\tan\varphi\left[2 + \frac{\pi}{3}\left(\frac{L}{b_b}\right)^2 tan\varphi\right]$ where $b_e = \sqrt{(\pi b_b^2/4)}$

Where, $P_{u(net)}$: net uplift capacity of pile, φ: internal friction angle, L: penetration depth of pile, γ_d: unit weight of sand.

Table 2-3 Comparison between theoretical uplift breakout factor, N_u for piles in sand with belled-type pile diameter of 1m and with angle of friction of 40°.

Research source	L/b_b			Remarks
	1	2	3	
Majer (1955)	1.7	3	4.4	-
Balla (1961)	3.2	10.3	19.1	$K = K_0 = 0$
Downs and Chieurzzi (1966)	3.6	14.5	32.9	Assume F1+F3=0.6 For L/b_b = 5, 7
Meyerhof and Adams (1968)	3.0	10.3	21.8	K'_u = 0.9; m = 0.35
Clemence and Veesaert (1977)	2.6	7.5	14.5	K_0 = 4
Ovesen (1981)	3.5	13.7	28.4	b_e= 0.886m
Andreadis and Harvey (1981)	4.0	14.0	32.	Extropolated results for L/b_b=1
Rowe and Davis (1982)	2.7 F_γ=1.8 R_ψ=1.05 S_f =1.4	9.3 F_γ=3.2 R_ψ=1.16 S_f=2	18.7 F_γ=4.8 R_ψ=1.3 S_f =3	$R_K = R_R = 1$ $\psi = 17^o$ b_e= 0.886m
Surterland et al. (1982)	3.3	10.9	22.6	I_D=0.6
Vermeer and Sutjiadi (1985)	2.7	5.1	8.5	b_e= 0.886m φ_{cv}=25.6° ($\psi = 17^o$)
Murray and Geddes (1987)	3.8	15.1	34.0	b_e= 0.886m

2.4 SUMMARY

This chapter summarizes the results of previous studies and proposed models for conventional piles, belled-type piles, and uplift resistance structure systems. In addition, the basic theory of conventional piles is introduced in detail (limit friction theory, marginal penetration ratio theory, and the equilibrium's limit equilibrium analysis).

Based on the review, the various models presented in the previous study confirmed that the pile-soil frictional and the impact of failure surface resulting from soil behavior were the most important factors in calculating the uplift resistance capacity of piles. However, many studies so far do not have much improvement from previous research.

The following summarizes the improvements needed in the models presented in previous research.

1. Research on the failure mechanism on various grounds is necessary. In particular, since most of the models studied so far have been studied on clay and sandy ground, there is no proposed uplift resistance capacity model of soft-rock ground, which can be constructed nowadays.

2. Various uplift resistance structure systems have difficulty considering the pile-soil friction. Therefore, the pile-soil friction that can be generated in the belled-type pile cannot be taken into account.

3. Although many researchers have studied the penetration depth, the failure mechanism that occurs under deep ground conditions is not clearly identified.

Due to the above three effects, it is considered that the reliability of the uplift resistance capacity model of the belled-type piles proposed to date is low.

REFERENCES

Balla, A. (1961). The resistance to breaking out of mushroom foundations for pylons. *Proceedings of the 5th International Conference on Soil Mechanics and Foundation Engineering*, Paris, France, 1, 221-227.

Chattopadhyay, B. C., and Pise, P. J. (1986). Uplift capacity of piles in sand. *Journal of Geotechnical Engineering*, 112(9), 888-904.

Clemence, S. P, and Veesaert, C. J. (1977). Dynamic pullout resistance of anchors in sand. *Proceedings of International Symposium on Soil Structure Interaction*, Roorkee, India, 389-397.

Das, B. M., Seeley, G. R. and Pfelfle, T. W. (1977). Pullout resistance of rough rigid piles in granular soil. *Soils and Foundations*, 17(3), 72-77.

Das, B. M. (1983). A procedure for estimation of uplift capacity of rough piles. *Soil and Foundation*, 109(3), 122-126.

Das, B. M., and Seeley, G. R. (1975b). Uplift capacity of buried model pile in Sand. *Journal of the Geotechnical Engineering*, 101(20), 1091-1094.

Dickin, E. A., and Leung, C. F. (1990). Performance of pile with enlarge base subject to uplift force. *Canadian Geotechnical Journal*, 27, 546-556.

CHAPTER III

LABORATORY MODEL TESTING OF UPLIFT LOAD MODEL FOR BELLED-TYPE PILE

3.1 INTRODUCTION

This chapter introduces model tests for evaluating the uplift resistance of belled-type piles. The model test carried out in this study consists of a circular test and a half-circular test and was designed to confirm the uplift resistance characteristics and soil behavior. Moreover, the test setup, measurement equipment, scale and model ground setup and uplift loading mechanism methods used in this study are described in detail.

3.2 LABORATORY SIMULATION AND TEST CONDITIONS

The test model was performed to verify the uplift resistance characteristics of belled-type piles caused uplift loading and the behavior of the ground.

An outline of the test model in the laboratory is shown in Fig.3-1. The test model was carried out using five types of belled-type piles in soil conditions with the different relative density of sand, and strength of soil-cement. The laboratory model test consists of three aspects: (1) Circle chamber test, (2) Half- Circle chamber test, (3) Soil properties test and Cement content ratio test of soft-rock ground. The detailed test cases and the associated test conditions are represented in Table.3-1.

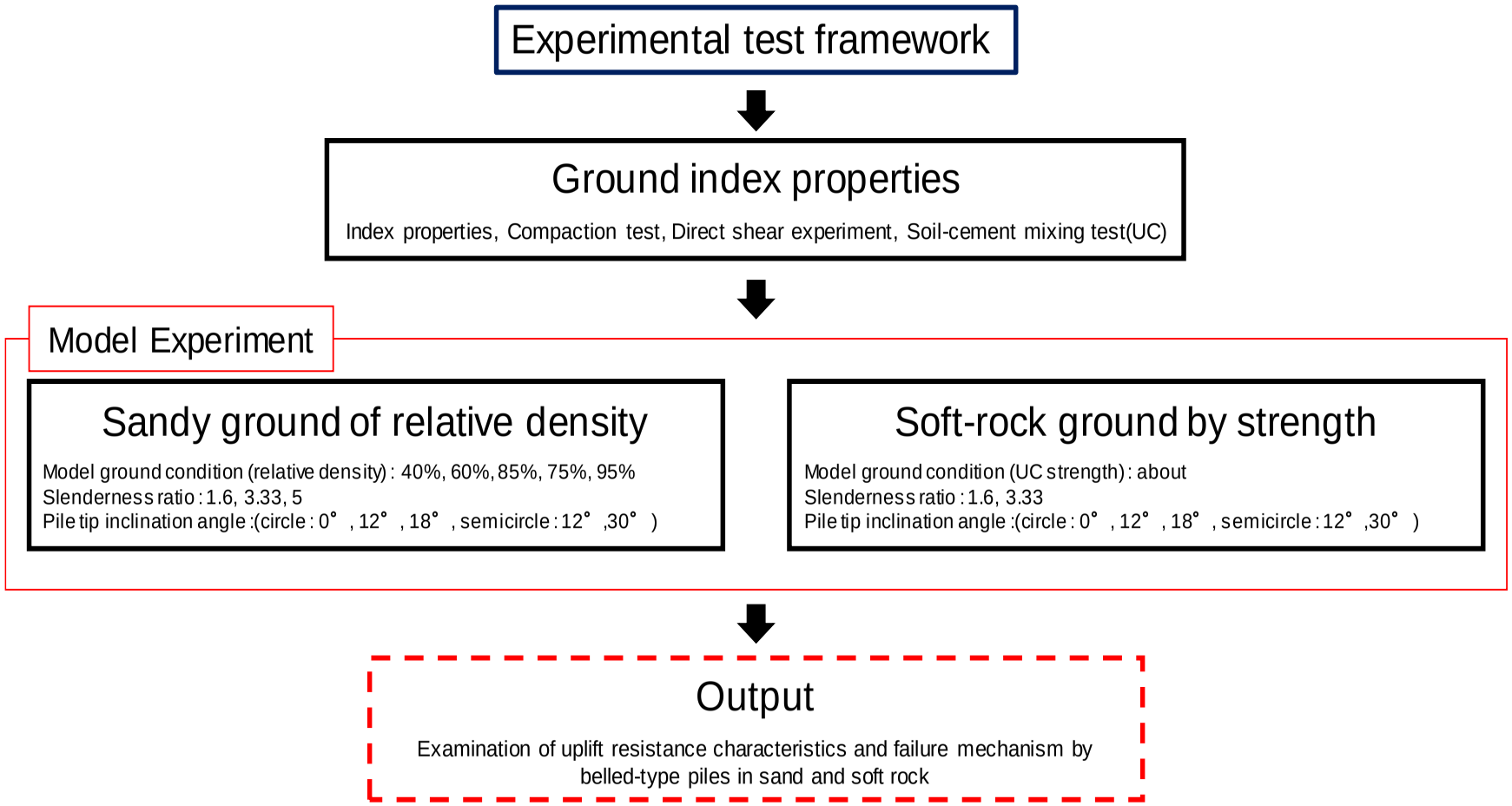

Fig.3-1 Experimental framework outline.

Table.3-1(a) Sandy ground experiment condition.

Chamber style	Relative density (%)	Pile tip inclination angle (θ_i) (º)	Slenderness ratio (λ)	Loading system
Circular	40, 60, 75, 85, 95	0, 12, 18	1.66, 3.33, 5	Screw-jack
Half-circular		12. 30	3.33, 5	

Table.3-1(b) Soft-rock ground experiment condition.

Chamber style	Uniaxial compressive strength (kN/m^2)	Pile tip inclination angle (θ_i) (º)	Slenderness ratio (λ)	Loading system
Circular	615	0	3.33	BF cylinder
	737	12	3.33	
	1001	12	1.66	
Half-circular	787	12	1.66	Screw-jack
	286	12	1.66	
	656	30	1.66	

※ Slenderness ratio (λ) = pile penetration depth pile (L) / pile tip diameter (b_b).

3.2.1 Model Chamber

Fig.3-2 shows the test model apparatus. The test apparatus consists of a model chamber, loading device, and measuring device (load-cell, LVDT, and HD video camera). The model chamber made of steel plate 500mm in height, 750mm in penetration ratio and diameter of the pile. The diameter of the model pile 30mm is made 300mm in length and designed to be able to test in the model chamber under 30cm. It was determined (Fig.3-2(b)). In addition, the Teflon coating inside the chamber is applied to reduce friction between walls and ground.

Fig.3-2(c) shows the half-circular chamber. The separation surface of the half-circular chamber has a structure that the acrylic plate can be installed. In order to observe the failure mechanism, the half-circular chamber has been used.

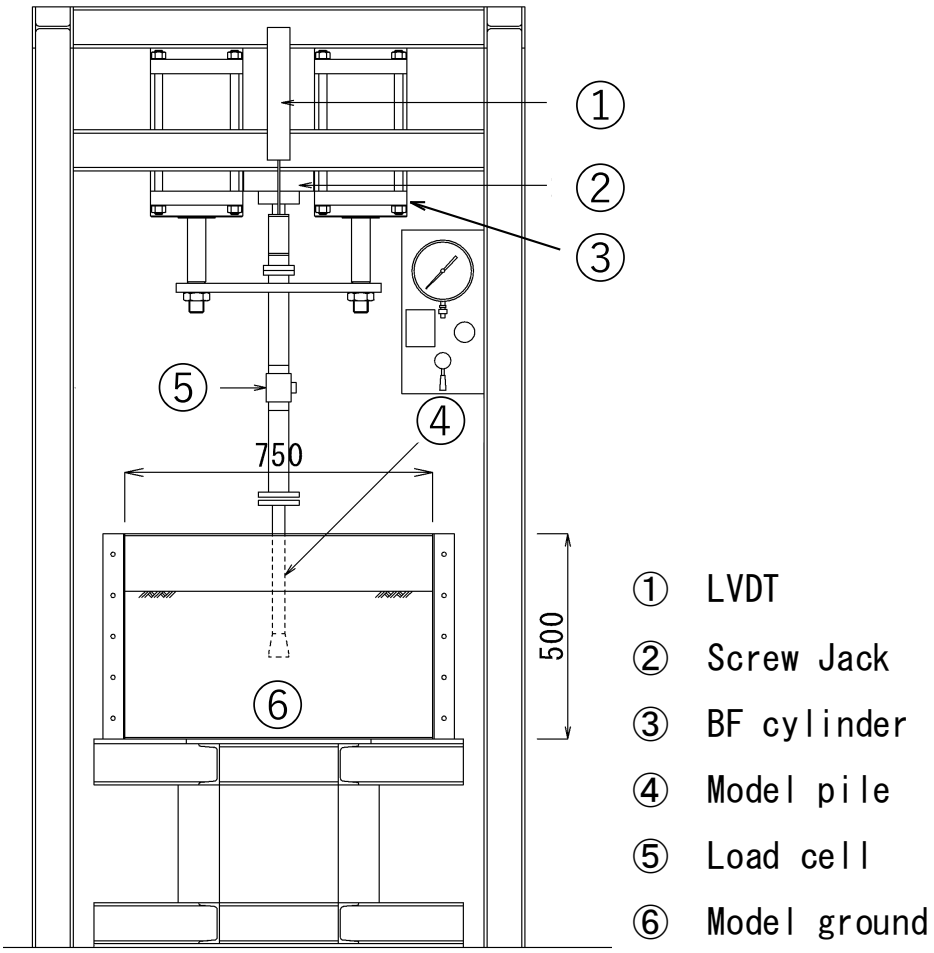

(a) Model apparatus

※ BF cylinder: Air cylinder of Bellofram, USA

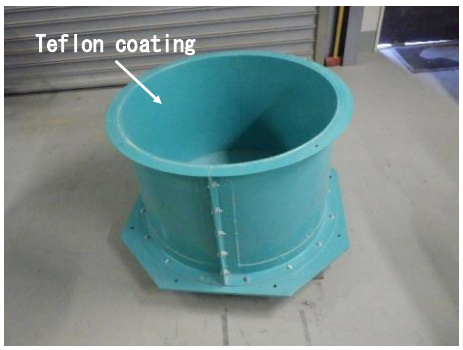

(b) Circular chamber (c) Half-circular chamber

Fig.3-2 Experimental model apparatus.

3.2.2 Loading System

The loading device consists of two types according to the test conditions. Fig.3-3(a) shows a screw-jack. Screw-jack was considered for the strain control test. The maximum load capacity of the screw-jack can be adjusted to 10kN.

Fig.3-3(b) shows the screw-jack operation panel. The relation between the scale of the Table.3-2 represent the average of the measured values for 1 minute. The speed of the screw-jack can be ± 20 cm in stroke, but it can be done at a stable loading speed if it is within ± 15 cm.

Fig.3-4 shows two BF cylinders at each end of a screw-jack. BF cylinder can adjust the load by air pressure. A total load of these two cylinders is about 35 kN and the BF cylinders were carried out in the tests beyond the range of screw-jack loads in this study. In addition, the BF cylinders were tested under stress control conditions and can be surcharge load using additional parts.

The relationship between the air pressure and the loading load of the BF cylinder is shown in Fig.3-4(b). The load is proportional to the pressure in the cylinder and the relation is as follows.

$$\text{Compression axis: } P = 2 \times 19.6 \times \sigma_a$$

$$\text{Uplift axis: } P = 2 \times 18.0 \times \sigma_a$$

Where, P: loading load by 2 BF cylinders (kN), σ_a: Pressure in a cylinder (MPa)

Table.3-2 Relation between screw-jack scale and loading speed.

	Scale	Compress speed (mm/min)		Uplift speed (mm/min)	
L02	2	3.86	3.84	-3.85	-3.87
L05	2.7	5.45	5.44	-5.48	-
L03	3	6.44	6.45	-6.51	-6.52
L04	4	9.06	9.08	-9.08	-9.09

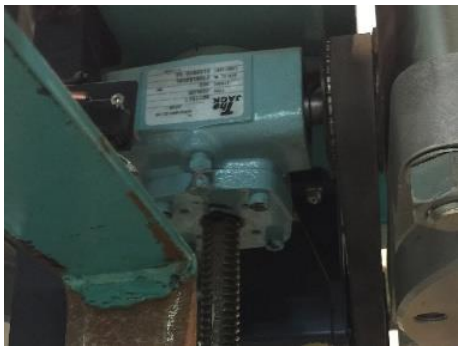

(a) Screw-jack apparatus

(b) Screw-jack operation panel

Fig.3-3 Screw-jack loading apparatus.

(a) BF cylinder

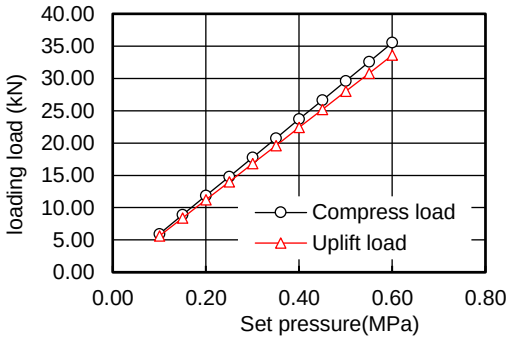

(b) BF cylinder calibration

Fig.3-4 BF cylinder loading apparatus.

3.2.3 Measuring System

Fig.3-5 shows the measuring apparatus. The measuring apparatus consists of a load-cell and an LVDT. The load-cell was determined to have a maximum capacity of 2t to minimize noise due to uplift loading. The LVDT has a range of 50cm and 200 times measurements were taken per minute to increase the accuracy of the test.

(a) LVDT (b) Load-cell

Fig.3-5 Measuring apparatus.

3.3 MODEL GROUND

3.3.1 Sand Ground

(a) Material Characteristics of Sand Model Ground

Kumamoto fine sand (K7) was used as the material for the composition of the sandy ground. Table.3-3 shows physical properties. Each property value was obtained using indoor tests. The test method of each physical property was carried out in accordance with the Japanese Geotechnical Society.

Fig.3-6 shows the distribution curve (JIS A 1204:2009). In addition, Fig.3-7 shows the relationship between the compaction test (JIS A 1210:2009) and Fig.3-8 shows the relationship between the relative density (D_r) of sand and the internal friction angle (φ). The internal friction angle (φ) of sand with respect to relative density (D_r) was used for direct shear test (JGS 0941-2009) results. The relation between relative density (D_r) and internal friction angle (φ) was found to be proportional, and the internal friction angle (φ) was identified to be between 35º and 43º according to the relative density (D_r).

(b) Sand Model Ground Production Method

Model tests using sand were produced with low relative density ($D_r = 40\%, 60\%$), and high relative density ($D_r = 75\%, 85\%, 95\%$). There are two ways to make the ground, depending on the relative density (D_r).

The low relative density ($D_r = 40\%, 60\%$) was performed by the air-drop method. Fig.3-9 shows the test instrument used in the air-drop method. In this study, the air-drop method drops to sand at a height of about 1m and controls the relative density (D_r) of the sand by adjusting the size of the hole installed at the bottom of the hopper suspension. Fig.3-10 shows the test results of the relative density (D_r) calibration.

The model ground of high relative density (D_r) was compacted to adjust the relative density (D_r). The ground production method of high relative density (D_r) model is based on a 5cm thickness of one layer and puts a sample considering the relative density (D_r) and uses a compacted rubber hammer.

The model ground production method of the half-circular chamber is similar to the model ground production of the circular chamber. However, since the length of the half-circular model pile is 10 cm shorter than that of the circular model pile, the thickness of the supporting layer is made 1 cm higher than that of the circular chamber. In addition, the silicone grease was used to prevent the inflow of sand between the acrylic plate and the model pile. Fig.3-11 shows the completed sand model ground.

Table.3-3 Physical properties of Kumamoto fine sand (K7).

Property	Value
Liquid limit, *LL* (%)	N. P
Plastic limit, *PL* (%)	N. P
Specific gravity, G_s	2.63
Fine-grained soil (%)	15.6
Unified Soil Classification System (JGS)	SM
Maximum density, ρ_{max} (g/cm^3)	1.571
Minimum density, ρ_{min} (g/cm^3)	1.197
Internal friction angle (°)	42（Dr = 80%）

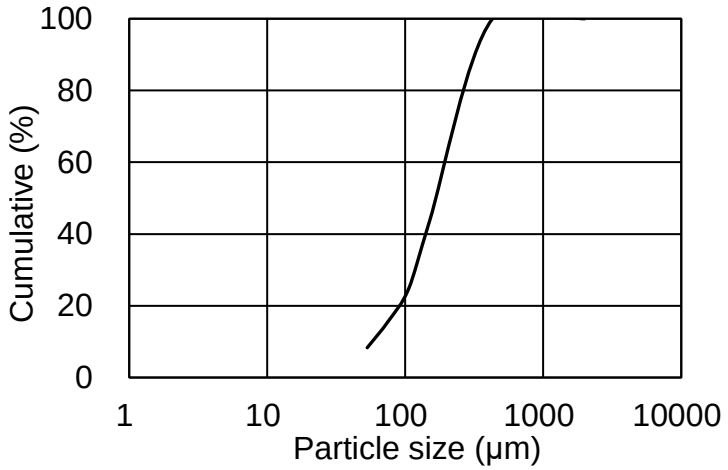

Fig.3-6 Particle size distribution curve of Kumamoto fine sand (K7).

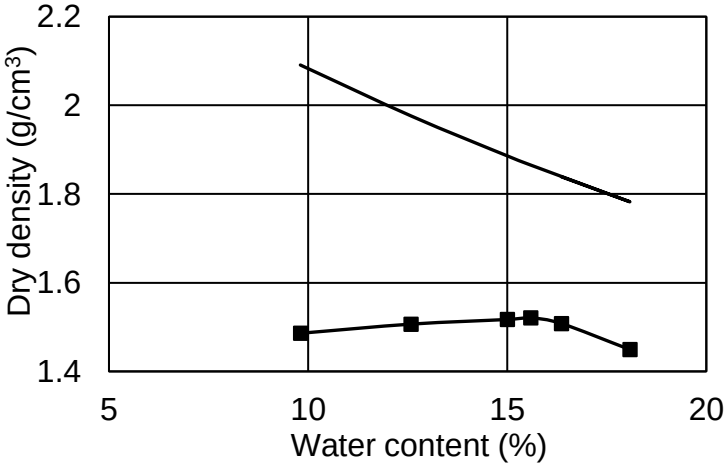

Fig.3-7 Relationship between the compaction test of Kumamoto fine sand (K7).

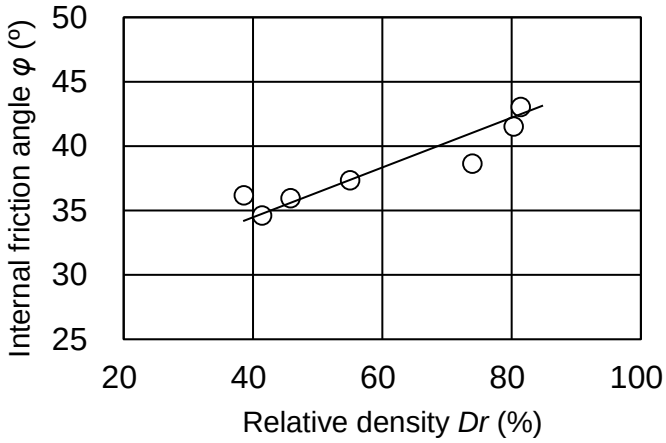

Fig.3-8 Relationship between the relative density (Dr) of sand and the internal friction angle (φ).

Fig.3-9 Experimental instrument used in the air-drop method.

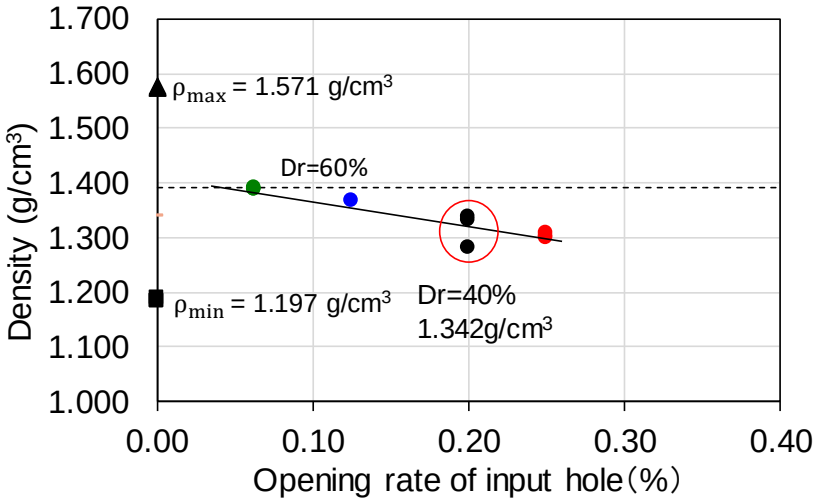

Fig.3-10 Unit weight-opening rate of inpit hole.

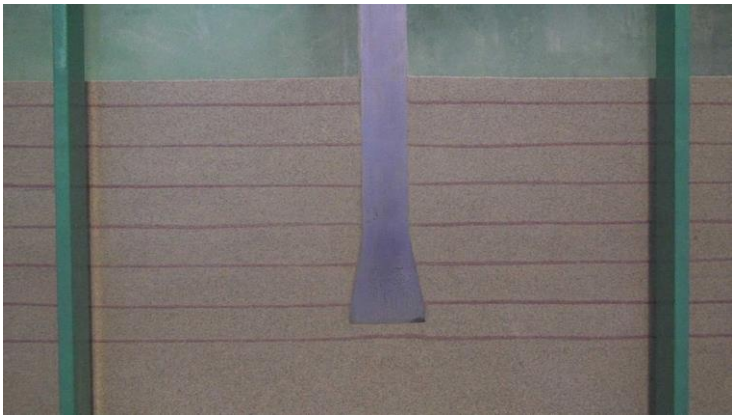

Fig.3-11 Completed sand model ground.

3.3.2 Soft-Rock Ground

(a) Material Characteristics of Soft-Rock Model Ground

Soil-cement was used to conduct model tests that assumed soft-rock ground. The material used was produced by mixing silica sand (Kumamoto silica sand. K7), rapid-cement, and water. Since the compressive strength of soft-rock ground is generally about 300~1000 kgf/cm^2, the scale of this model test is 1/50 of actual measurement. Therefore, the strength of the model ground was set to about 1000kgf/cm^2 (Uniaxial compressive strength).

Table.3-4 shows the mixing ratio of soil-cement in preliminary tests. In the mixing ratio test performed in the preliminary test, the specimens were prepared according to the mixing ratio test using 5×10cm plastic mold, and the prepared specimens were subjected to the

Table.3-4 Mixing ratio of soil-cement in preliminary experiments.

CASE	Cement content (%)	Cementwater Ratio (w/c)	Water Content (%)	CASE	Cement content (%)	Cementwater Ratio (w/c)	Water Content (%)
C1	5.0	0.30	20	C13	4.9	0.40	14
C4	6.0	0.36	20	C21	4.4	0.30	17
C5	7.0	0.42	20	C22	5.2	0.36	17
C11	3.7	0.30	14	C23	5.8	0.40	17
C12	4.1	0.33	14				

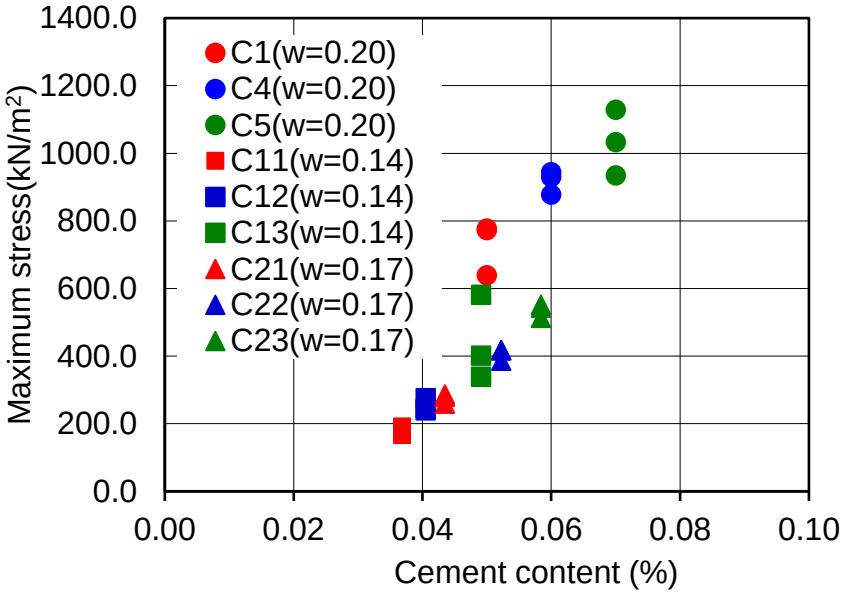

Fig.3-12 Results of uniaxial compression test according to the mixing ratio of soil-cement.

uniaxial compression test after 7 days of curing time. Fig.3-12 shows the results of the uniaxial compression test according to the mixing ratio of soil-cement.

(b) Soft-Rock Model Ground Production Method

Fig.3-13 shows the model ground construct method using the soil-cement. Soil-cement model ground was produced in 4 stages.

The soil-cement model ground production method is as follows.

1. Mix the dry sand and rapid-cement using the mixing ratio test result. At this time, the quantity of the sample is based on the 5cm height of the model chamber.

2. The mixed dry sample is stirred with water. Stirring is performed using a stirrer (Fig.3-15) and the stirring time is based on about 5 minutes.

3. Put the mixed sample into the chamber to construct the ground. At this time, compaction is performed using a compactor (Fig.3-16) to prevent air from entering the soil-cement.

4. Repeat the above three operations until the desired height is achieved.

(a) Mix the dry sand and rapid-cement.

(b) Stir sample with water.

(c) Sample insertion and compaction.

(d) Model ground curing.

Fig.3-13 Model ground construct method.

Fig.3-14 Soil-cement stirrer.

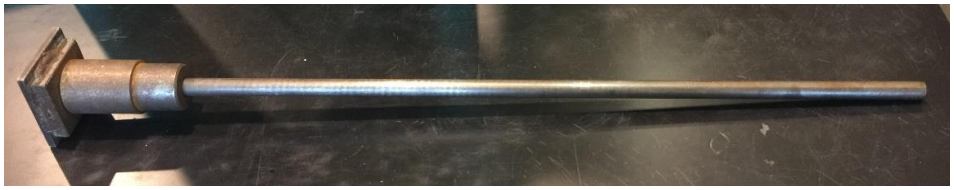

Fig.3-15 Compaction equipment.

3.4 MODEL PILE

Fig.3-16 shows the model pile. Model piles are made of steel and the surface is smooth. A total of five model piles were made, with three circular piles and two half-circular piles.

The circular model pile is a conventional pile, belled-type piles with pile tip inclination angle (θ_i) 12º and 18º. The size of the model pile is shown in Fig.3-16, the diameter of the pile (b_s) is 30mm, the diameter of the tip of the belled-type pile (b_b) is 48mm, and the total length of the pile is 370mm.

The model piles half-circular model piles were all made of belled-type piles, and the pile tip inclination angle (θ_i) were made at 12º and 30º. The half-circular model pile has a shape of a circular model pile cut in half. The pile has a diameter (b_s) of 30 mm and a tip diameter (b_b) of 48 mm. The length of the pile was made 360mm, 10mm shorter than the circular model pile, depending on the condition of the half-circular apparatus.

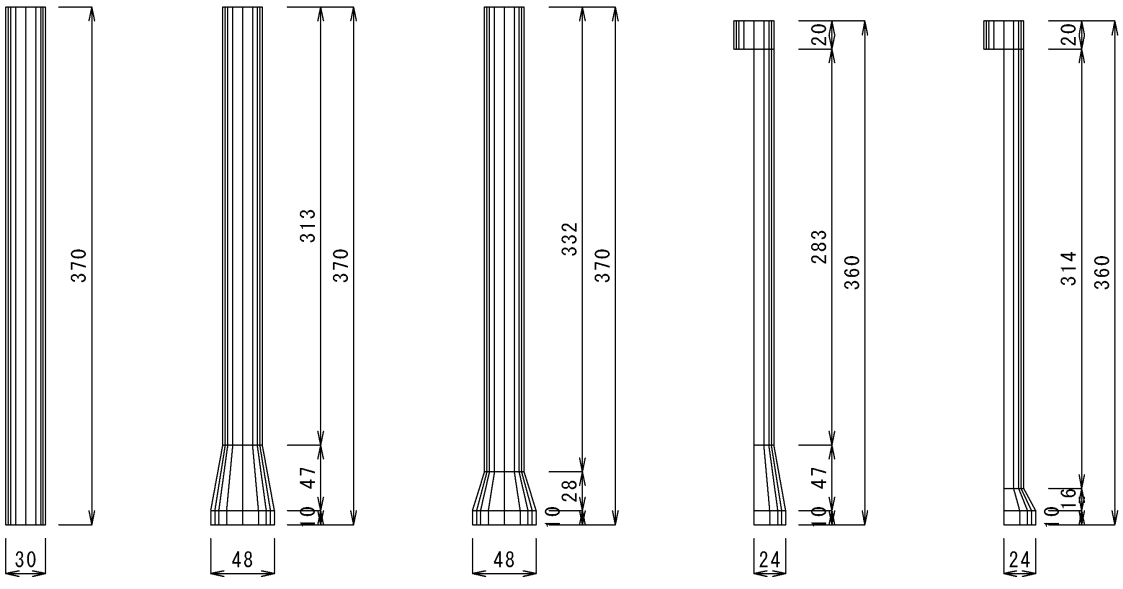

①K00 ②K12 ③K18 ④HK12 ⑤HK30

(a) Circular pile (b) Half-circular pile

Fig.3-16 Model pile.

3.5 TESTING PROCESS AND METHODOLOGY

The following steps are performed for test testing of the belled-type pile under the circular chamber and half-circular chamber:

1. Prepare a model chamber, where to prevent soil-cement from adhering to the walls of the chamber. The oil was applied to them.
2. Place the bar on top of the chamber to install the model pile and use the clamp to install the pile on the bar. At this time, the level of the pile is adjusted by using the horizontal ruler. In the half-circular test, the silicon is applied between the acrylic plate and the model pile to prevent the inflow of sand.
3. After installation of the model pile, the ground was prepared. Model ground preparation was described in reference 3.3.1(b) and 3.3.2(b).
4. Finish the test by connecting the loading device and the clamp. In addition, half-circular tests install video cameras on the front of the half-chamber.
5. Conduct an uplift model test.

3.6 SUMMARY

This chapter focuses on the development of test methods for laboratory model tests that can simulate the uplift resistance characteristic and the soil behavior of belled-type piles. The following includes laboratory tests conducted in this study. The overall method of model tests was explained, including the test apparatus, material properties of model ground and model ground production method, procedures of the test.

The summary of this chapter can be explained as follows:

1. The small model test equipment was used to evaluate the uplift resistance characteristics and soil behavior of the belled-type pile using a circular chamber, half-circular chamber, LVDT, load-cell, BF cylinder, screw-jack, and video camera.

2. Model test using conventional pile and belled-type pile can confirm the uplift resistance characteristics according to the pile shape and ground conditions. In addition, modeling is possible at high strength soft-rock model ground by using a loading apparatus that can simultaneously stress-control and strain-control.

3. Half-circular model tests have been proposed to clearly identify the properties of soil behavior. In particular, image analysis using video cameras were able to analyze the more clearly failure surface than previous studies.

REFERENCES

Japan Geotechnical Society, JGS 0560 (2009): Method for Consolidated Constant Volume Direct Box Shear Test on Soils, Tests for Mechanical Properties.

Japan Industrial Standard, JIS A 1210 (2009): Test Method for Soil Compaction Using a Rammer, Tests on Stabilized Soils.

Japan Industrial Standard, JIS A 1224 (2009): Test Method for Minimum and Maximum Densities of Sands, Tests for physical properties.

Japan Industrial Standard, JIS A 1204 (2009): Test Method for Particle Size Distribution of Soils, Tests for physical properties.

Japan Industrial Standard, JIS A 1201 (2009): Practice for Preparing Disturbed Soil Samples for Soil Testing, Sample Preparation.

Japan Industrial Standard, JIS A 1205 (2009): Test Method for Liquid Limit and Plastic Limit of Soils, Tests for physical properties.

Takano, A. and Kishida, H. (1979). Failure mechanism of soil mass under base of non-displacement pile in sand [in Japanese]. *Journal of Structural and Construction Engineering*, 285, 51-62.

Yamaguchi, H., Kimura, T., and Fujii, N. (1975). Test studies on the bearing capacity of shallow foundations by the use of a centrifuge [in Japanese]. *JSCE*, 233, 71-85.

CHAPTER IV

UPLIFT RESISTANCE AND FAILURE MECHANISM FOR BELLED-TYPE PILE IN SANDY GROUND

4.1 INTRODUCTION

This chapter evaluates the uplift resistance characteristics and the soil behavior of a belled-type pile in the sandy ground using model tests. In order to evaluate the clear behavior characteristics of the sandy ground, model tests were conducted by five different relative density (D_r).

In order to evaluate the uplift resistance characteristics of a belled-type pile in a circular model test, the pile tip inclination angle (θ_i) and penetration depth (L) were considered.

In the half-circular model test, the process was recorded with a video camera to clearly identify the failure mechanism of the ground under the same conditions as the circular model test.

4.2 UPLIFT RESISTANCE CHARACTERISTICS USING THE CIRCULAR CHAMBER MODEL

This section discusses the results of tests conducted in the circular chamber model test. This test considers two aspects of the pile tip inclination angle (θ_i) and penetration depth (L) of the belled-type pile.

4.2.1 Uplift Resistance Characteristics considering The Tip Shape of The Belled-Type Piles

(a) Model Test Result of Conventional Pile and Belled-Type Pile on Relative Density (D_r)

Fig.4-1 and Table.4-1 show the results of uplift loads on the conventional pile and belled-type piles. In Table.4-1, maximum displacement is the displacement with respect to the maximum uplift load and the residual load is the average value of the uplift loads of 20mm to 40mm (Fig.4-2).

Fig.4-1(a) shows the results of an uplift load test of a conventional pile. Based on the uplift load test, the maximum uplift load in the range of relative density D_r = 40%, 60%, 75% was found about 0.007kN, and the maximum uplift load was generated immediately after loading and reached a certain value. However, the maximum uplift load for a relative density (D_r) of 85% and 95% were found to be 0.042kN. Also, the displacements identified at this maximum uplift loads showed other characteristics. In the uplift load test with the relative density of 85%, the displacement at the maximum uplift load was confirmed at about 20mm, and for a relative density (D_r) of 95%, the displacement was about 15mm.

Fig.4-1(b) shows the results of an uplift test with a belled-type pile with the tip inclination angle (θ_i) of 12º. Based on the uplift load test, the maximum uplift load value was proportionally different according to the relative density (D_r). In the test results of relative density (D_r) 40%, the maximum uplift load was about 0.012kN and no peak was identified. However, at other relative densities, the peak of the maximum uplift load was confirmed, and the displacement of the maximum uplift load decreased as the uplift load increased. In addition, the maximum uplift load value was found to be up to 10 times larger was generated by the residual load, which was similar to the previous research.

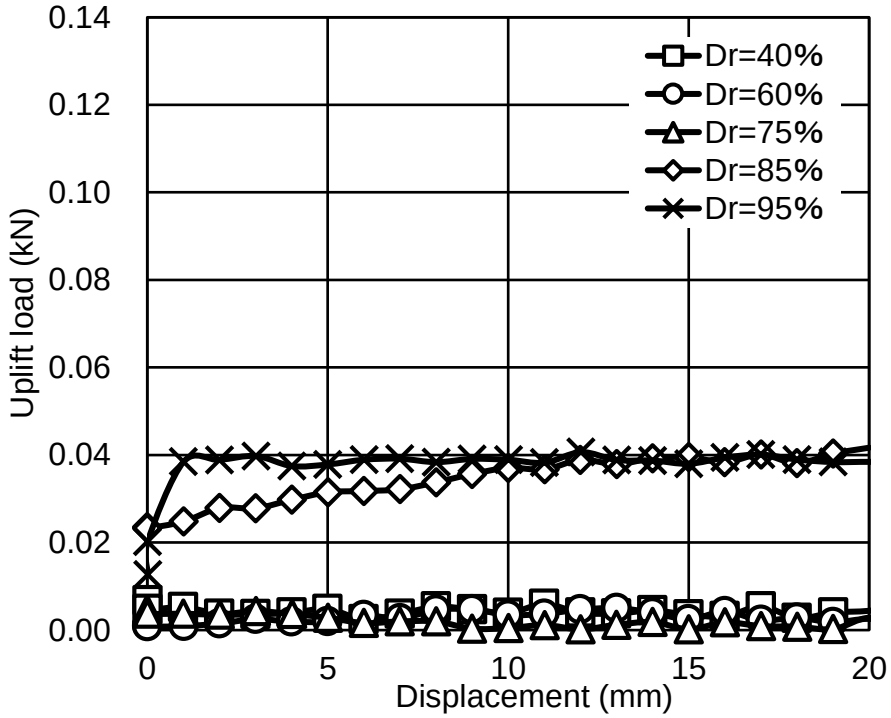

(a) θ_i = 0º

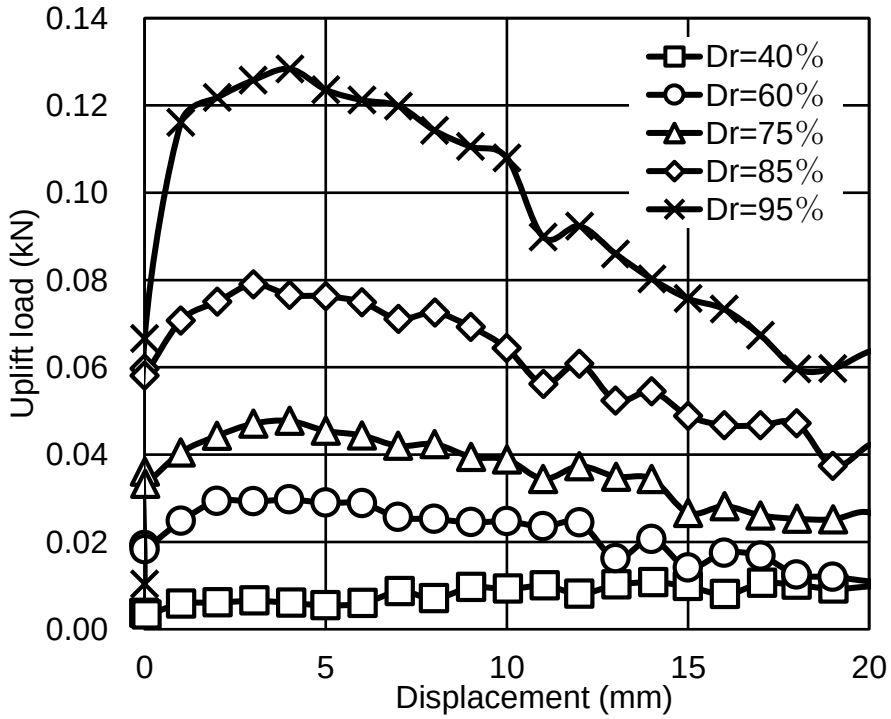

(b) θ_i= 12º

Fig.4-1 Results of an uplift load for conventional pile and belled-type piles. (L = 16cm)

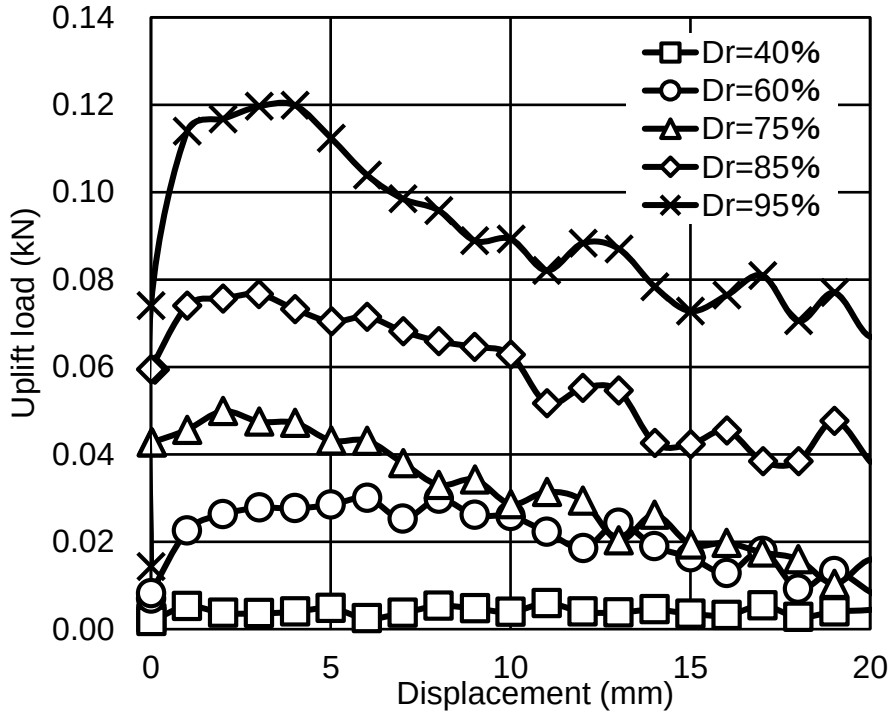

(c) θ_i = 18º

Fig.4-1 Results of an uplift load for conventional pile and belled-type piles. (L = 16cm)

Table.4-1 Results of an uplift load and residual load for conventional pile and belled-type piles. (L = 16cm)

Inclination tip angle (º)		Relative density (%)				
		40	60	75	85	95
0	Maxium uplift load (kN)	0.0071	0.0076	0.0067	0.0429	0.0422
	Maxium Displacement (mm)	0.30	12.11	0.31	20.11	15.29
	Residual load (kN)	0.0035	0.0030	0.0022	0.0412	0.0384
12	Maxium uplift load (kN)	0.0120	0.0315	0.0480	0.0812	0.1296
	Maxium Displacement (mm)	19.51	3.97	3.16	3.02	3.69
	Residual load (kN)	0.0055	0.0060	0.0153	0.0431	0.0530
18	Maxium uplift load (kN)	0.0071	0.0311	0.0359	0.0784	0.1221
	Maxium Displacement (mm)	0.30	4.49	2.07	3.17	2.07
	Residual load (kN)	0.0034	0.0051	0.0070	0.0379	0.0593

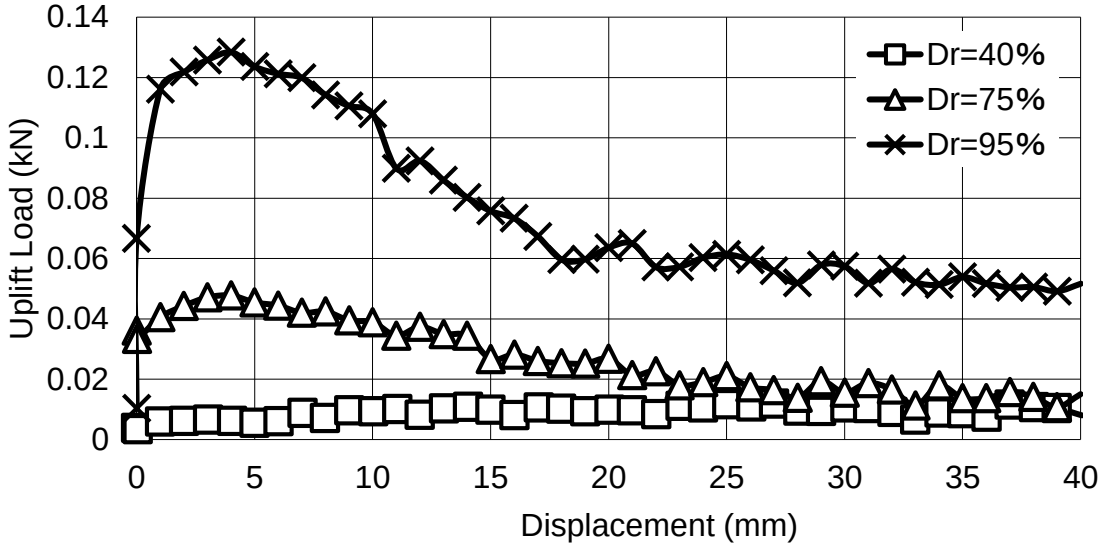

Fig.4-2 Uplift load measured up to 40 mm displacement. (θ_i = 12°, L = 16cm)

Fig.4-1(c) shows the test results of the uplift load with an inclination angle (θ_i) of 18º. The results showed the maximum uplift load value according to the higher relative density (D_r).

This tendency is similar to the belled-type pile with the tip inclination angle (θ_i) of 12º. However, the maximum uplift load was found to be slightly lower than the belled-type piles with the tip inclination angle (θ_i) of 12º.

The belled-type piles of the same pile tip diameter (b_b) have a difference in the width of the inclined surface according to the difference in the pile tip inclination angle (θ_i). Therefore, it is determined that the range to which the anchor effect can be applied is wide. Therefore, it is considered that the belled-type pile (θ_i) of 12º is more effective for the uplift load than the belled-type pile (θ_i) of 18º.

(b) Comparison of Maximum Uplift Load of Conventional Pile and Belled-Type Pile

Fig.4-3 shows the test results of the maximum uplift load on the effect of the pile tip inclination angle (θ_i). Where the influence of each relative density (D_r) is shown simultaneously.

In the conventional pile, the maximum uplift load was found to change drastically at a relative density (D_r) of 85%. This value is about 6 times higher than the relative density (D_r) of 75% and below. In the belled-type pile with a tip inclination angle (θ_i) of 12º, the increased rate of the maximum uplift load to relative density (D_r) was found to be higher under relative density (D_r) of 85% or more.

The maximum uplift load appeared to be at a relative density (D_r) of 95%. The difference was found to be about 10 times or more than the value at 40% relative density (D_r). The belled-type pile with the tip inclination angle (θ_i) of 18º was also similar to the belled-type pile with an angle (θ_i) of 12º.

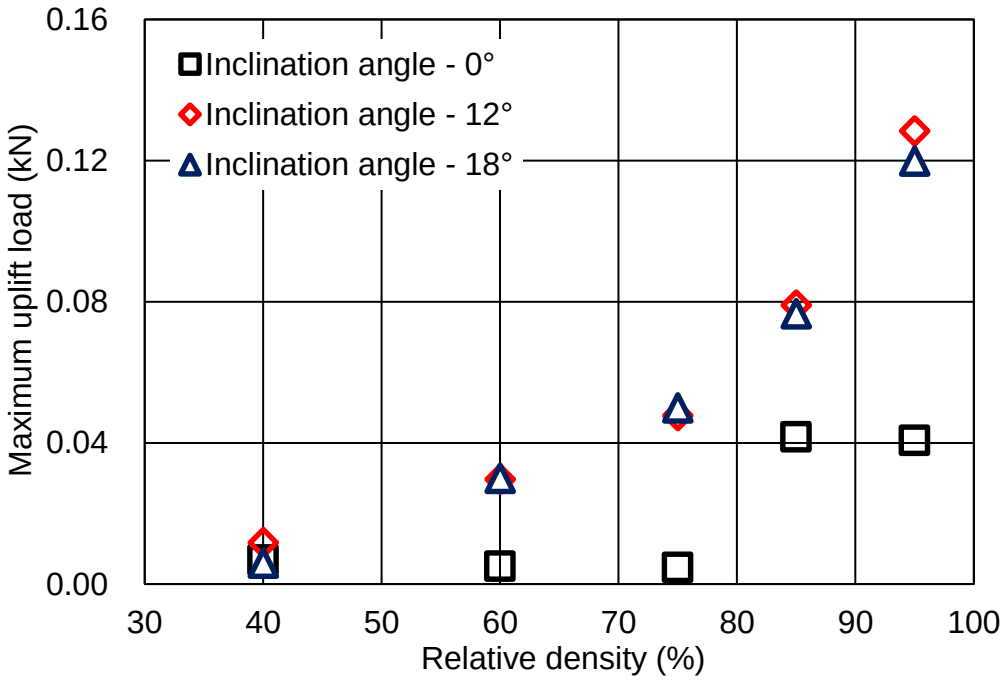

Fig.4-3 Maximum uplift load on the effect of the pile tip inclination angle (θ_i). (L = 16cm)

(c) Maximum Uplift Load and Residual Load of Conventional Pile and Belled-Type Pile

Fig.4-4 shows the comparison of the maximum uplift load and residual loads for the tip inclination angle. The maximum uplift load is the maximum value of the uplift load confirmed in the circular model test, and the residual load is the average of the uplift loads of the model test measured from 20mm to 40mm displacement.

Fig.4-4(a) shows the comparison of the maximum uplift load and the residual load of conventional piles. The maximum uplift load of the conventional pile was found to be slightly higher than the residual load at all relative densities (D_r). In addition, the maximum and residual loads were relatively high under conditions of 85% or more relative density (D_r). Based on the result, the pile-soil friction is judged to have resulted in a high result under conditions of 85% or more relative density (D_r).

Fig.4-4(b) shows the comparison of the maximum uplift load and residual load for a belled-type pile with the tip inclination angle (θ_i) of 12º. Based on the results, the relative density (D_r) of 40% showed a meaningless difference between the maximum uplift load and residual load. However, the difference between the maximum uplift load and the residual load was significant under the condition at a relative density (D_r) of 60% or more. In addition, the difference increased at a relative density (D_r) of 85% or more. The maximum uplift load was found to be higher at a relative density (D_r) of 85% or more.

Fig.4-4(c) shows the comparison of the maximum uplift load and residual load for a belled-type pile with the tip inclination angle (θ_i) of 18º. The results were similar to those of 12º. However, the maximum uplift load and residual load were slightly smaller than those with the pile tip inclination angle (θ_i) of 12º.

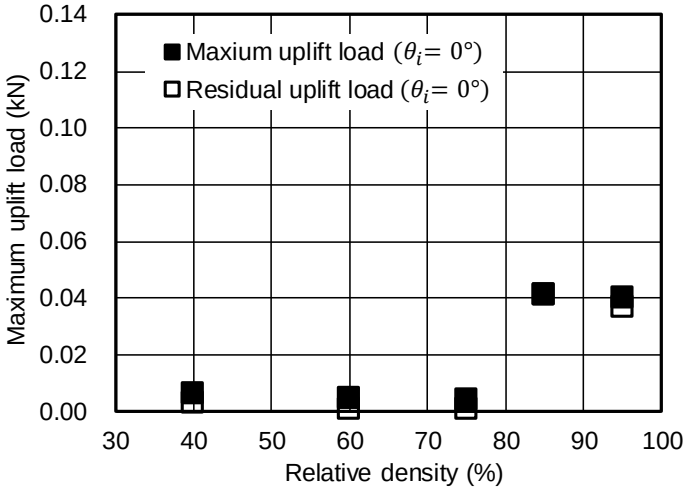

(a) θ_i = 0º

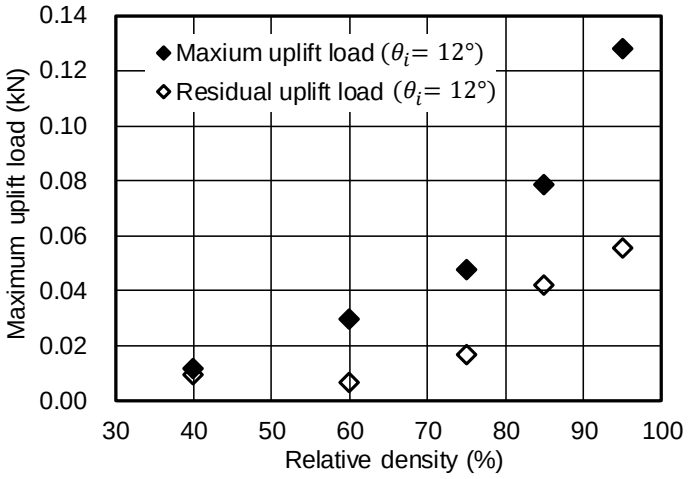

(b) θ_i = 12º

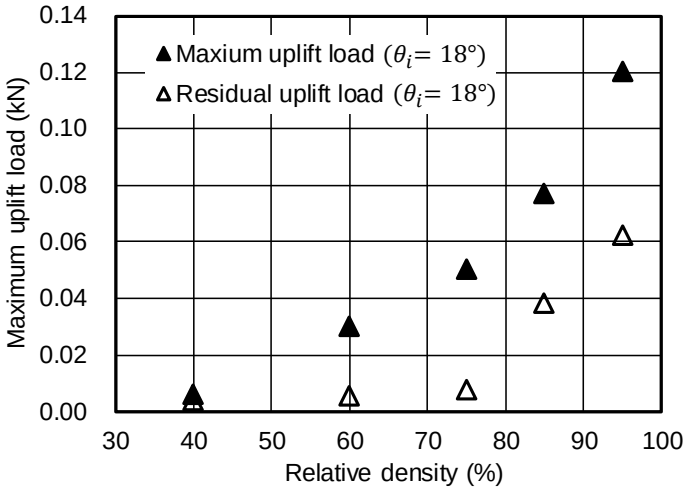

(c) θ_i = 18º

Fig.4-4 Comparison of the maximum uplift load and residual loads for the tip inclination angle. (L = 16cm)

4.2.2 Uplift Resistance Characteristics considering The Penetration Depth of The Belled-Type Piles

Fig. 4-5 and Table.4-2 show the results of an uplift load test considering the penetration depth (L) of the belled-type pile. Where the belled-type piles used in the model test had a tip inclination angle (θ_i) of 12º. The slenderness ratios (λ) were 1.6, 3.33, and 5, and the penetration depths (L) were 8 cm, 16 cm, and 24 cm.

(a) Model Test Result of Belled-Type Pile on Relative Density (D_r)

Fig.4-5(a) shows the results of an uplift test with a penetration depth (L) of 8 cm for a belled-type pile with the tip inclination angle (θ_i) of 12º. From the total results, the maximum uplift load of 0.03 ~ 0.047kN was confirmed according to the relative density (D_r). The maximum uplift load appeared immediately after loading and indicates residual load.

The belled-type pile model test with an 8cm penetration depth (L) showed a very low uplift load. Based on the result, it is confirmed through model experiments that the uplift load at low penetration depth (L) is less affected by the relative density(D_r).

Fig.4-5(b) shows the results of an uplift test with a penetration depth (L) of 24 cm for a belled-type pile with the tip inclination angle of 12º. Based on the results, the maximum uplift load of 0.03 ~ 0.188kN was confirmed according to the relative density (D_r).

The result of 40% relative density (D_r) was found to be the maximum uplift load, which showed immediately after the loading. This was similar to the model test of 40% relative density (D_r) in other cases. However, peaks were observed at a relative density (D_r) of 65% or more and higher the relative density showed to lower the difference between the maximum uplift load.

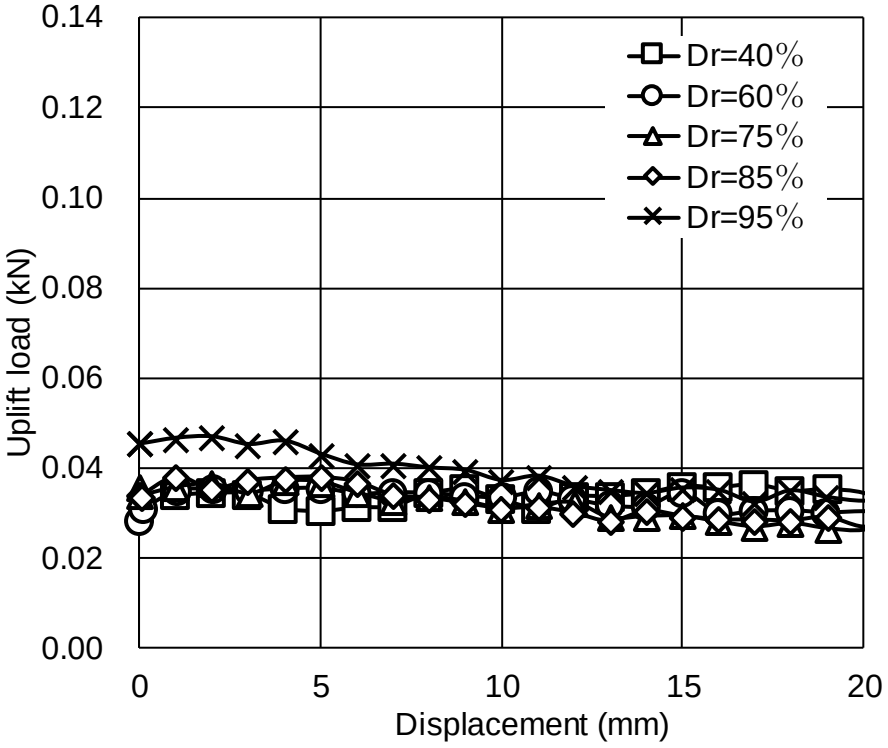

(a) L = 8cm

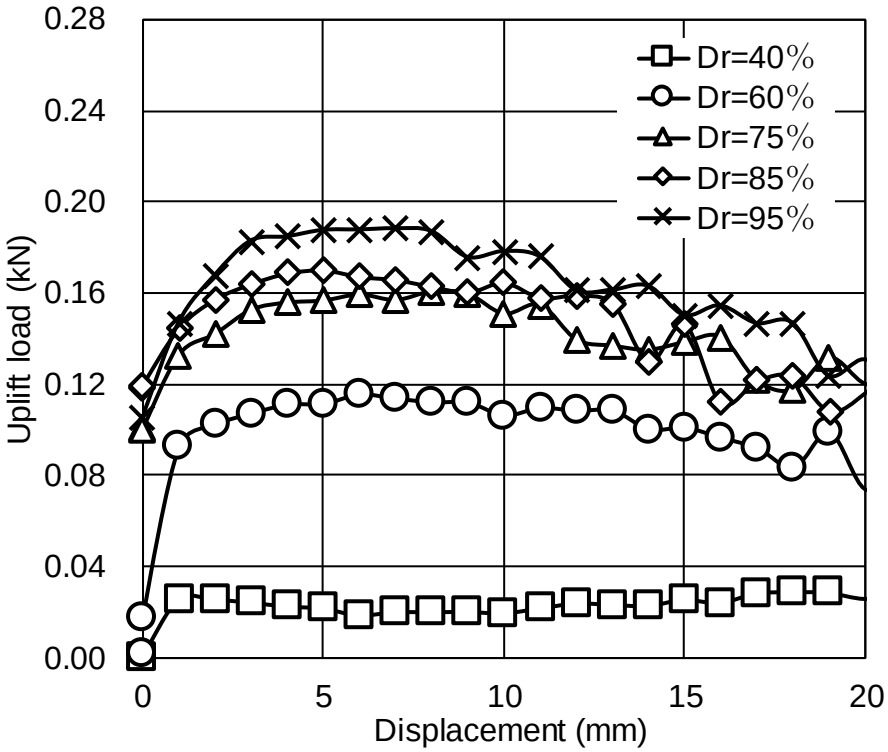

(b) L = 24cm

Fig.4-5 Results of an uplift experiment considering the penetration depth of the belled-type pile. (θ_i = 12º)

Table.4-2 Maxium uplift load and residual load results for penetration depth of belled-type piles. (θ_i = 12º)

Penetration depth (cm)		Relative density (%)				
		40	60	75	85	95
8	Maxium uplift load (kN)	0.0363	0.0355	0.0369	0.0380	0.0469
	Displacement (mm)	17.01	2.03	4.01	5.02	2.00
	Residual load (kN)	0.0350	0.0302	0.0272	0.0268	0.0322
16	Maxium uplift load (kN)	0.0120	0.0315	0.0480	0.0812	0.1296
	Displacement (mm)	19.51	3.97	3.16	3.02	3.69
	Residual load (kN)	0.0055	0.0060	0.0153	0.0431	0.0530
24	Maxium uplift load（kN）	0.0291	0.1156	0.1607	0.1703	0.1882
	Displacement (mm)	18.00	6.01	8.01	5.01	7.01
	Residual load (kN)	0.0276	0.0640	0.0933	0.0928	0.0916

(b) Comparison of Maximum Uplift Load for the Penetration Depth (L) of Belled-Type Pile

Fig.4-6 shows the test results of the maximum uplift load considering penetration depth (L). Where the influence of each relative density (D_r) is shown simultaneously.

The maximum uplift load at 8cm depth was found to increase slightly as the relative density (D_r) increased. However, the difference was found to be about 0.017 kN. Since the penetration depth (L) was not sufficiently secured in the model test, it is judged that the influence of the pile-soil friction (δ) and the failure surface presented in the previous studies did not appear.

Nevertheless, in the test of penetration depth 24cm, the maximum uplift load of 40% relative density (D_r) is similar to the maximum uplift load of other penetration depth. And maximum uplift load increased drastically up to 75% of relative density (D_r). In addition, based on the relative density (D_r) of 75%, the increase in the maximum uplift load decreases drastically.

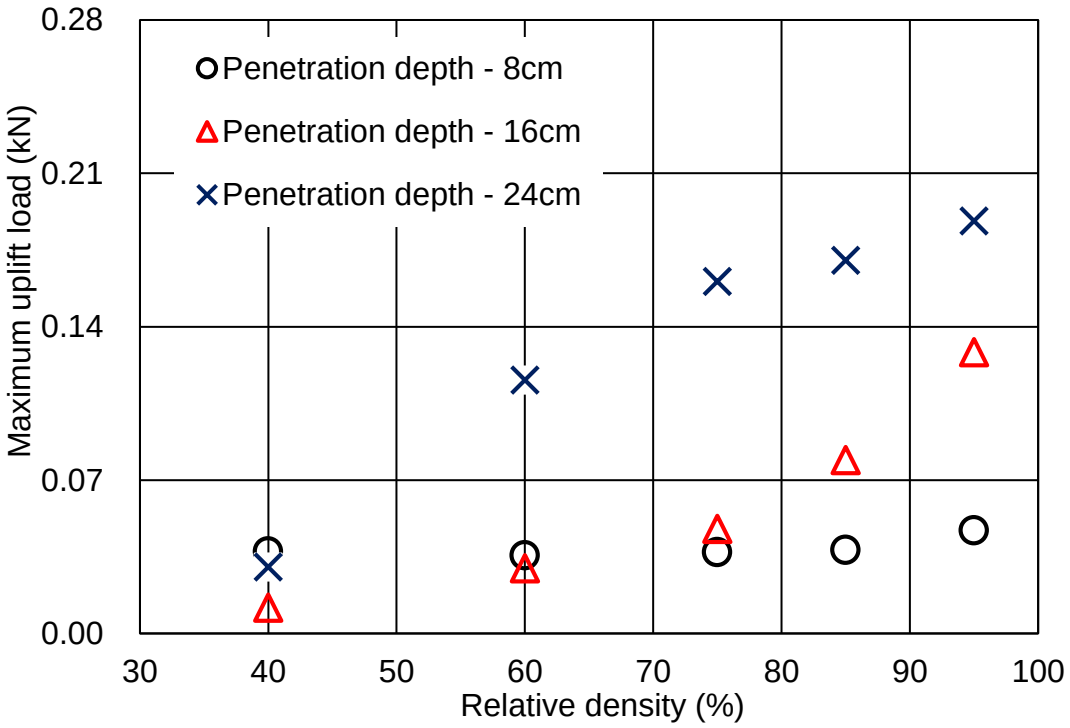

Fig.4-6 Maximum uplift load on the effect of the pile penetration depth (L). (θ_i = 12º)

In the conventional pile uplift load model studies, the change in the uplift load characteristics of piles was observed based on the relative density (D_r) of sand of 70% (Das. 1983). In addition, in the study of the uplift resistance structure system, a change in the uplift resistance mechanism with the relative density (D_r) and the penetration depth (L) of the pile was observed in the previous study (Ghalys. 1991). This trend is similar to the previous model test results.

(c) Maximum Uplift Load and Residual Load for the Penetration Depth (L) of Belled-Type Pile

Fig.4-7 shows the comparison of the maximum uplift load and residual load according to the penetration depth (L). The maximum uplift load on the pile tip inclination angle (θ_i) is the maximum value of the uplift load found in the model tests, and the residual load is the average value of the uplift loads of the model test measured from 20 mm to 40 mm.

Fig.4-7(a) shows the comparison of the maximum uplift load and the residual load of 8 cm depth. At the all relative densities, the maximum uplift load appeared to be higher than the residual load, which was similar to those of 40% relative density (D_r). However, the difference between the maximum uplift load and the residual load slightly increased at a relative density (D_r) of 60% or more.

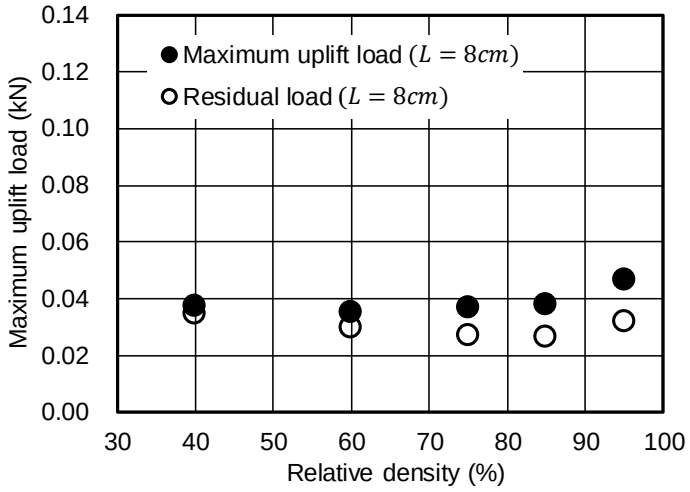

(a) L = 8cm

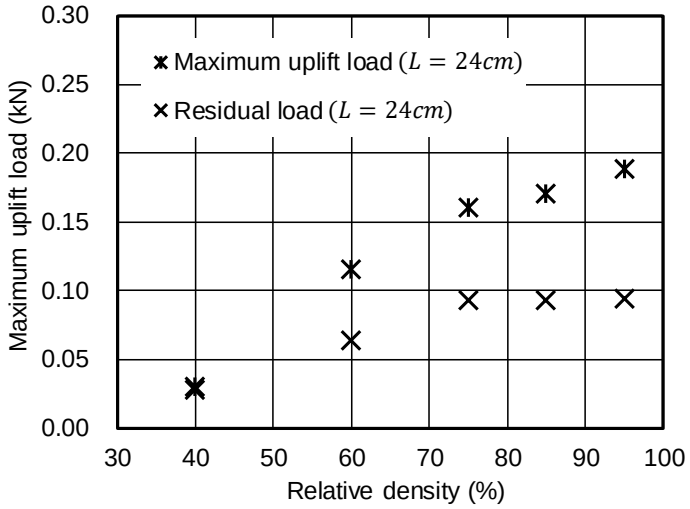

(b) L = 24cm

Fig.4-7 Comparison of the maximum uplift load and residual load according to the penetration depth. (θ_i = 12º)

Cases with a penetration depth (L) of 16 cm and pile tip inclination angle (θ_i) of 12º were reviewed in the previous section and were omitted.

Fig.4-7(b) shows a comparison of maximum uplift load and residual load at 24 cm penetration depth (L). As with the test result of 16cm penetration depth (L), there is a slight difference between the maximum uplift load and the residual load in the test results with a relative density (D_r) of 40%. Furthermore, for 40 ~ 75% relative density (D_r), the rate of increase of maximum uplift load and residual load is very high. In particular, the residual load rate at a relative density (D_r) of 75% or more is similar.

4.3 FAILURE MECHANISM USING HALF-CIRCULAR MODEL

The half-circular chamber model tests were carried out with HD cameras, and the images were analyzed. The image analysis method used images captured up to 20mm displacement and used the method of the color change of the deformed section by comparing the initial and the images were taken every minute. This section discusses the results of the tests conducted in the half-circular chamber model test. In addition, two aspects of the pile tip inclination angle (θ_i) and penetration depth (L) of the belled-type pile is considered.

4.3.1 Characteristics of Failure Mechanism for Belled-Type Pile focusing The Penetration Depth (L)

A half-circular model test was performed with a penetration depth (L) of 16cm condition to take into account the shape of the belled-type pile. In addition, two kinds of belled-type piles (θ_i = 12º, 30º) are utilized to consider the influence of the tip shape of the pile.

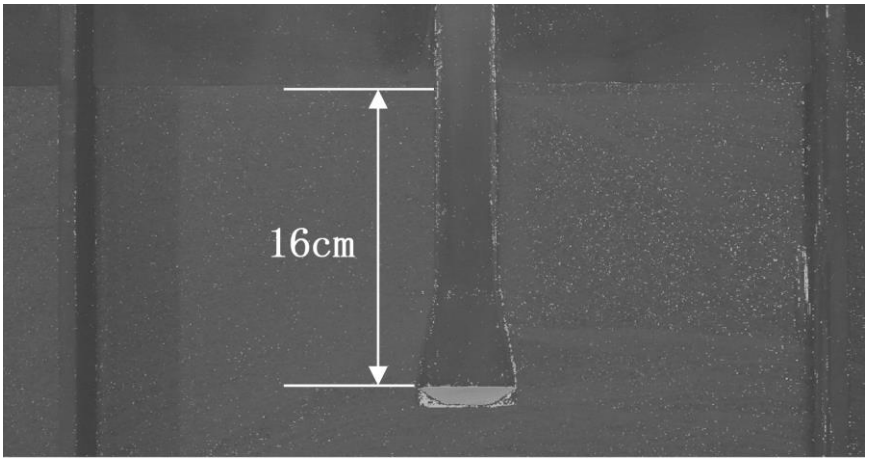

(a) D_r = 40%

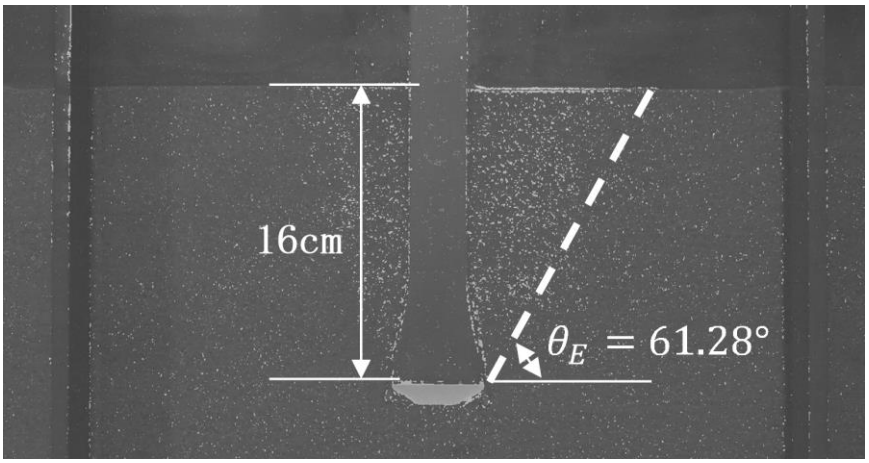

(b) D_r = 75%

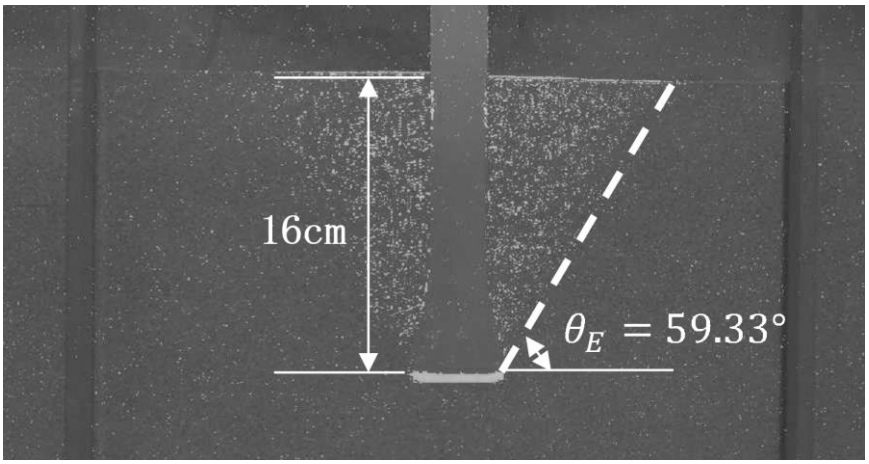

(c) D_r = 95%

Fig.4-8 Results of image analysis with θ_i = 12°. (L = 16cm)

(a) The Failure Mechanism of Belled-Type Pile by Pile Tip Inclination Angle (θ_i = 12º)

Fig.4-8 shows the results of the belled-type pile with an inclination tip angle (θ_i) of 12º. Based on the result showed that a clear failure surface was not identified for the relative density of 40%. However, the failure surface was clearly identified in the total results of the relative density (D_r) of 75% or more, and the widest failure surface was confirmed in the test result of 95% relative density (D_r).

The maximum failure surface occurred at small uplift displacement, and the shape of the failure surface was confirmed as a cone generated from the tip of the pile until the ground.

(b) The Failure Mechanism of Belled-Type Pile by Pile Tip Inclination Angle (θ_i = 30º)

Fig.4-9 shows the results of the belled-type pile with an inclination tip angle (θ_i) of 30º. Based on the results, it shows that 40% of the model ground relative density (D_r) cannot identify a failure surface. It indicates the displacement of the soil around the pile is not spread to the whole ground with low relative density (D_r) because the consolidation occurred around the pile.

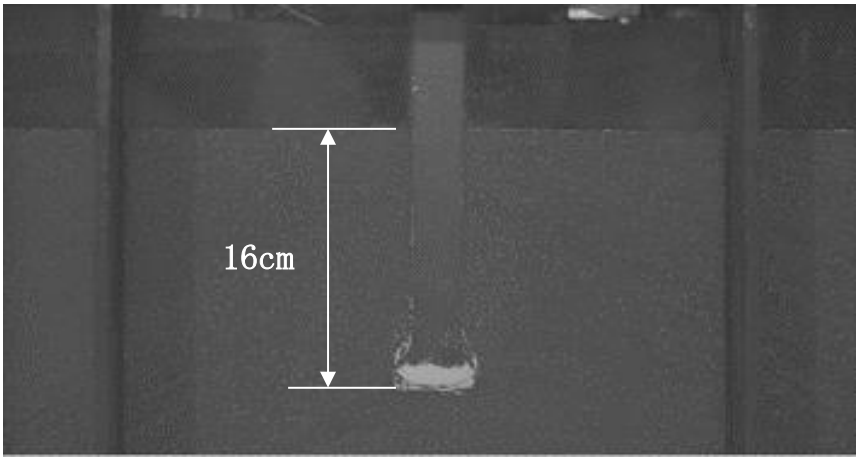

(a) D_r = 40%

Fig.4-9 Results of image analysis with θ_i = 30º. (L = 16cm)

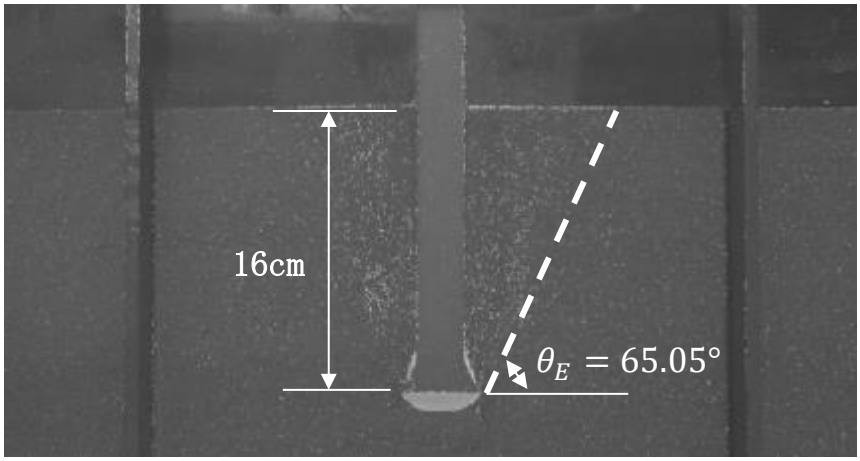

(b) D_r = 75%

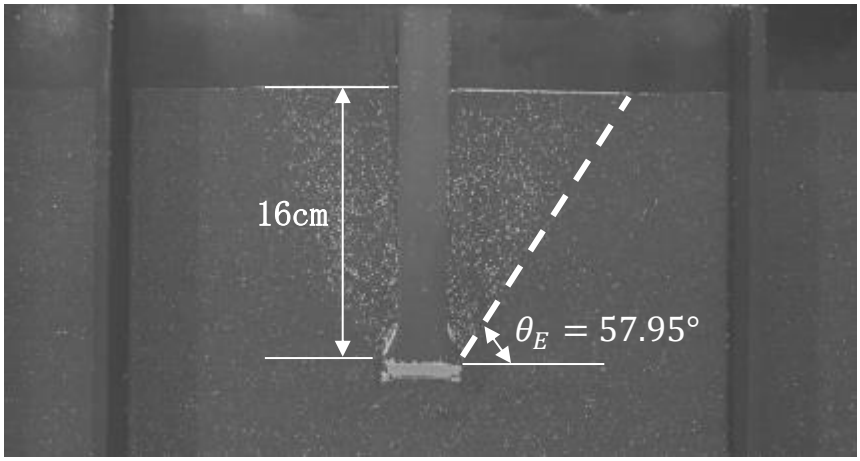

(c) D_r = 95%

Fig.4-9 Results of image analysis with θ_i = 30º. (L = 16cm)

In the case of the belled-type pile at 30º, the failure surface was generated at a relative density of more than 75%, and the shape of the failure surface was found to be cone a belled-type pile at 12º. In addition, the size of the failure angle (θ_E) is slightly larger than the pile of 12º, and the failure surface was found to be slightly smaller than the belled-type pile of 12º, but the difference is insignificant.

4.3.2 Characteristics of Failure Mechanism for Belled-Type Pile focusing The Penetration Depth (L)

Fig.4-10 shows the result of image analysis with a penetration depth (L) of 24 cm. In the figure, the failure surface was not identified for the relative density (D_r) of 40% based on the results from 16 cm in depth. The results are similar to previous studies, sand with certain relative density (D_r) does not show the effect of the tip shape of the belled-type pile. If the relative density (D_r) is 75%, the failure surface around the belled-type pile is confirmed, but not at the ground surface.

On the other hand, in the case of 95% relative density (D_r), the failure surface spreads in a straight line while maintaining a constant angle up to about 17cm from the pile tip. The failure surface is formed by the displacement of the tip.

The pile has a deep penetration depth (L), so the failure surface is formed in a circular limited shape by the horizontal earth pressure and the sand weight at the top of the failure surface. This is similar to the previous study, in which the failure surface does not appear on the earth's surface when exceeds the slenderness ratio (λ) of 4.0 (Meyerhof. 1973).

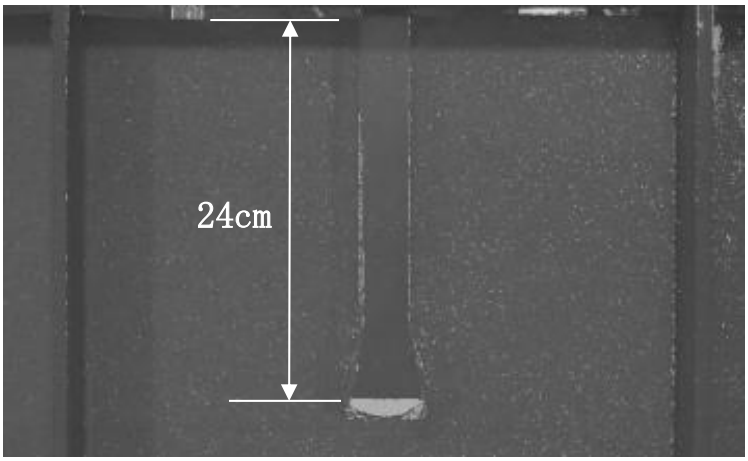

(c) D_r = 40%

Fig.4-10 Results of image analysis with θ_i = 30º. (L = 24cm)

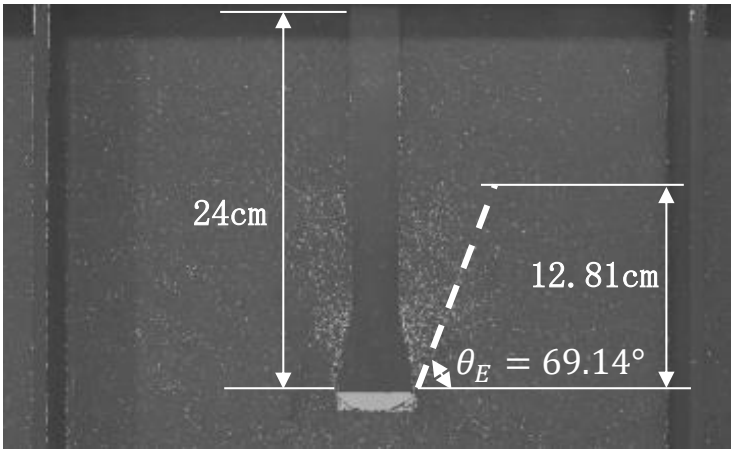

(c) D_r = 75%

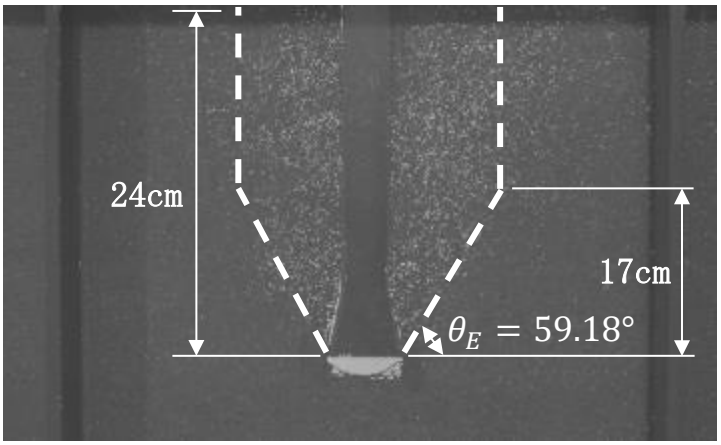

(c) D_r = 95%

Fig.4-10 Results of image analysis with θ_i = 30º. (L = 24cm)

4.4 SUMMARY

In this chapter, uplift resistance characteristics of belled-type piles and soil behavior were conducted using the laboratory test results to examine the influence on the effect of pile tip shape, relative density (D_r) of sandy ground, and penetration depth (L) of belled-type piles: (1) uplift resistance characteristics using the circular model test, (2) identification of failure mechanisms using half-circular model tests.

1. The effect of load resistance in belled-type piles was not significant in the case of ground with 40% relative density (D_r) in both piles with pile tip inclination angles (θ_i). This result was similar to the previous researches and it seems that the compaction on the pile tip area has occurred. In the result, where was not influence of pile tip shape on the uplift capacity on the low density in the ground. In addition, the uplift capacity of the belled-type pile with a pile tip inclination angle (θ_i) of 12º is slightly higher than the 18º of pile tip inclination angle (θ_i).

2. There was no clear difference in the maximum uplift loads and residual loads under all conditions with a relative density (D_r) of 40%. However, the difference was clearly seen under the conditions of relative density (D_r) 75% or more.

3. The higher the relative density (D_r), the higher the uplift load at the same penetration depth (L). In addition, under the same relative density (D_r) and penetration depth (L), the belled-type pile showed greater uplift load than the conventional pile.

4. Under a condition of 40% relative density (D_r) at the same penetration depth (L), a small upward load of about 0.04 kN was found regardless of the type of model pile. In addition, no failure surface was observed as a result of image analysis. However, under the conditions of 16cm and 24cm in penetration depth (L), a large uplift load was confirmed according to the relative density (D_r).

5. According to the relative density (D_r) and depth of penetration (L), the size and shape of the failure surface were found to be different. In particular, the failure surface shape was confirmed to be similar to the previous research results at the penetration depth (L) of 24cm.

REFERENCES

Bolton, M. D. (1986). The strength and dilatancy of sands. Geotechnique, 36(1), 65-78.

Butterfield, R., Andrawes, K. Z. (1972). On the angles of friction between sand and plane surfaces. *Journal of Terramechanics*, 8(4), 15-23.

Das, B. M., and Puri, V. K (1992). Vertical uplift load-displacement relationship of horizontal anchors in sand. *Transportation Research Record*, 36-100.

Das, B. M., and Jones, A. D. (1982). Uplift Capacity of Rectangular Foundations in Sand. *Transportation Research Board*, 54-58.

Das, B. M., Rozendal, D. B. (1992). Ultimate Uplift Capacity of Metal Piles in Sand. *International Society of Offshore and Polar Engineers*, 2(3), 40-45.

Honda, T., Hirai, Y. and Sato, E (2011). Uplift capacity of belled and multi-belled piles in dense sand. *Soils and Foundation*, 51(3), 483-496.

Subba, K., Rao, S., and Venkatesh, K. H. (1985). Uplift behaviour of short piles in uniform sand. *Soils and Foundation*, 25(4), 1-7.

White, D. J., Cheuk, C. Y. and Bolton, M. D. (2008). The uplift resistance of pipes and plate anchors buried in sand. *Geotechnique*, 50(10), 771-779.

Uesugi, M., Kishida, H. and Tsubakihara, Y. (1988). Behavior of sand particles in sand-steel friction. *Soils and Foundations*, 28(1), 107-118.

Niroumand, H., Kassim, Kh. A., and Nazir, R. (2011). Uplift response of symmetrical circular anchor plate in sand. *African Journal of Agricultural Research*, 6(28), 6057-6063.

Yamamoto, H., Li, W., Tominaga, K. and Ogura, H. (2003). Test study on effects of overburdening pressures and end shapes for point bearing capacities of pile [in Japanese]. *Journal of Structural Engineering*, B(49B), 157-162.

Hirai, Y., Walai, S. and Aoki, M. (2009). Centrifuge model tests on uplift resistance of belled pile in sand. *Journal of structural engineering*, 74(643), 1613-1619.

Japan Geotechnical Society (1995). Introduction Series 13, *Introduction to Soil Strength and Ground Destruction*, 64.

CHAPTER V

UPLIFT RESISTANCE AND FAILURE MECHANISM FOR BELLED-TYPE PILE IN SOFT-ROCK GROUND

5.1 INTRODUCTION

The model tests performed in this chapter are used as the basis for evaluating the uplift resistance characteristics and soil behavior of belled-type piles constructed in the soft-rock ground. The circular and half-circular model test was conducted to verify the uplift resistance and soil behavior of belled-type piles installed in the soft-rock.

Table.5-1 shows the uniaxial compressive strength (U_c) ranges of rocky ground. In this table, soft-rock and medium-rock have a uniaxial compressive strength (U_c) of 300 ~ 1000 kgf/cm^2 and are prescribed by the Japan Geotechnical Society. The model grounds performed in this study are assumed to be soft-rock and medium-rock. Therefore, the strength of model ground assuming soft-rock and medium-rock is set to 1000kgf/cm^2.

Table.5-1 Test results of uniaxial compressive strength of rock.

Type	Extremely Hard-rock	Hard-rock	Medium-rock	Swelling Hard-rock
Uniaxial compressive strength (kgf/cm^2)	1000 or more	500~1000	100~599	100~500
Type	Anisotropic medium-rock	Sandy soft-rock	clayey soft-rock	Swelling hard-rock
Uniaxial compressive strength (kgf/cm^2)	100~500 Anisotropic rock (Gneiss etc.)	10~100 Soft sand (included by weathered rock)	10~100 Clayey rock	10~100 Bentonite

※ Write with reference to JGS: 3811-2004.

In order to consider the strength characteristics of the soft-rock model ground was constructed using soil-cement, and two mixing ratios were used according to the strength characteristics. On the other hand, the analysis method of the model test was performed in the same way as sand ground. Where it is assumed that the pile is made of steel and no deformation occurs because it is a study on the uplift resistance mechanism of the pile.

5.2 UPLIFT RESISTANCE CHARACTERISTICS USING THE CIRCULAR CHAMBER MODEL

Table.5-2 shows the total conditions and uniaxial compressive test (U_c) results. In the circular chamber model test, the inclination angle (θ_i), penetration depth (L) and ground strength characteristics of the belled-type pile were considered. In addition, stress control tests (BF cylinder) were carried out under the conditions of circular soft-rock ground, and uniaxial compression tests were performed using samples by examining the compressive strength characteristics of model grounds.

5.2.1 Uplift Resistance Characteristics focusing The Tip Shape on Belled-Type Piles

Fig.5-1 shows the results of an uplift test on the effect of the tip of model piles on soft-rock ground.

Table.5-2 Test conditions and uniaxial compression test (U_c) results.

Test ID	Inclination angle (θ_i)	Penetration depth		Support layer thickness	Total thickness	Uniaxial compressive strength (U_c)
		Soil cement	Sand			
	(°)	(mm)	(mm)	(mm)	(mm)	(kN/m^2)
K00H16C	0	160.0	-	200.0	360.0	615
K12H16C	12	160.0	-	200.0	360.0	737
K12H08C	12	87.0	-	200.0	287.0	1001

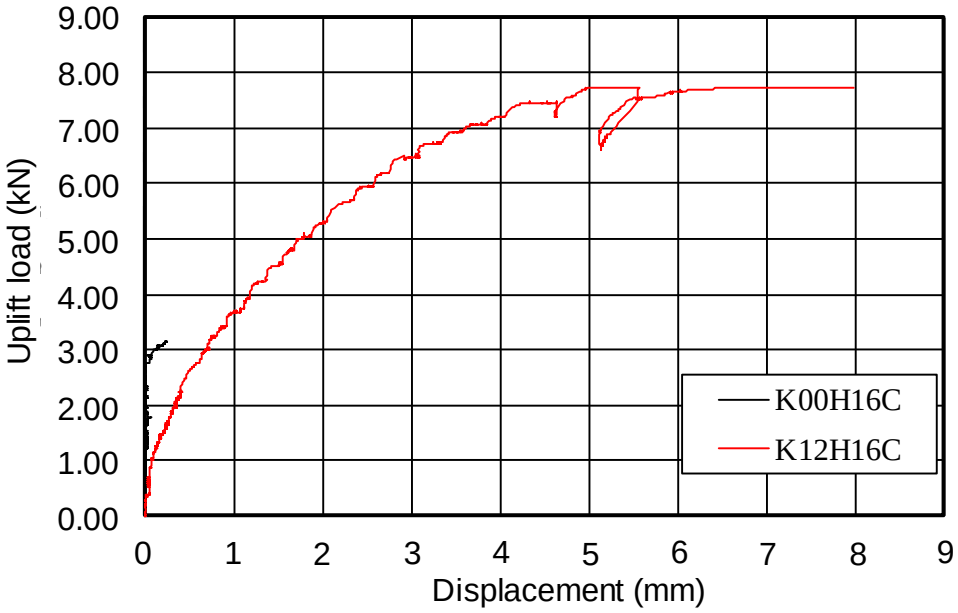

Fig.5-1 Results of an uplift test on the effect of the tip of model piles on soft-rock ground.

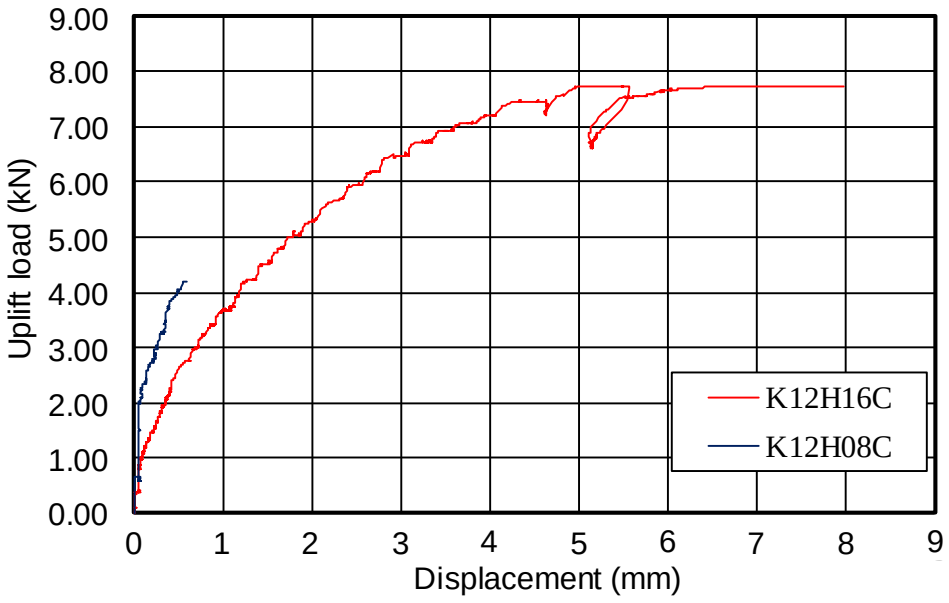

Fig.5-2 Results of an uplift experiment considering the penetration depth of the belled-type pile on the soft-rock ground.

Based on the result, the conventional pile (K00H16C) increased the uplift load to 2.7kN without changing the displacement. After that, the displacement increased and a maximum uplift load of 3.2 kN was observed at about 2.5mm displacement.

In the belled-type pile (K12H16C) test results, the displacement load starts to increase with increasing load at about 0.6kN. The uplift load of 7.73 kN no longer increases, only displacement increases, and shearing occurs.

The obtained test result of the belled-type piles showed that the maximum uplift load about 2.8 times higher than the conventional piles. The uplift load of the model pile applied to the soil-cement model ground is dependent on the adhesion between the molde pile and the soft-rock ground.

The belled-type pile applied to the model ground with the same penetration depth (L) has 13% higher surface area contact with the ground than the conventional pile, but the uplift load shows about 2.8 times higher.

5.2.2 Uplift Resistance Characteristics of Penetration Depth of Belled-Type Piles

Fig.5-2 shows the results of an uplift test considering the penetration depth (L) of the belled-type pile. Where the belled-type piles used in the model test had a pile tip inclination angle (θ_i) of 12º. The slenderness ratios (λ) were 1.6, 3.33 and the penetration depth (L) were 8 cm, 16 cm.

The test results of K12H16C and K12H08C are used to examine the uplift resistance characteristics of belled-type piles depend on the penetration depth (L) of piles. Based on the result of K12H08C, the displacement began to increase with increasing load at 2.0kN. At an uplift load of 4.19 kN, the ground failure occurred, and the displacement was found to

be about 0.56 mm. At this time, the failure surface form of soil-cement was identified as an inverted truncated cone model.

5.3 UPLIFT RESISTANCE CHARACTERISTICS USING THE HALF-CIRCULAR CHAMBER MODEL TEST

Half-circular model tests of soft-rock ground were performed under stress-strain conditions. Two half-circular model piles were used in the test conditions, and the model test was conducted at two ground strengths by adjusting the water-cement ratio.

Table.5-3 Shows the conditions for a half-circular model test. Additionally, the penetration depth (L) of the model pile is set to 8cm. Since soft-rock (soil-cement) ground has more uplift capacity than sand and clay ground, model tests were conducted on shallow foundations ($L/b_b < 3$).

Table.5-3 Experimental conditions for circular chamber on the soft-rock ground.

Test ID	Inclination angle (θ_i)	Penetration layer		Support layer thickness	Total thickness	Uniaxial Compression Strenth (U_c)
		Soil cement	Sand			
	(°)	(mm)	(mm)	(mm)	(mm)	(kN/m^2)
HK12H88C_①	12	80	83	210.0	373.0	787
HK12H88C_②	12	80	84	210.0	374.0	286
HK30H88C_①	30	75	84	210.0	368.0	656

Table.5-4 Mixing ratio of the two type soil-cement strength.

Mixing ratio ID	Fine sand (K7) conten (%)	Rapid-cement content (%)	Water content (%)	W/C
①	77	7	17	2.33
②	80	4	16	4

In order to observe the shape of the failure surface against the strength of the soft-lock model ground, the mixing ratio was composed of two types. Table.5-4 shows the mixing ratio of the two types of soil-cement strength.

5.3.1 Characteristics of Failure Mechanism of Belled-Type Pile focusing on The Pile Tip

Fig. 5-3 shows the result of the half-circular test according to the soil-cement strength. In this test, the K12H88C_① model ground has about 2.7 times higher ground strength than the HK12H88C_② model ground. Model piles used in both tests were belled-type piles with a tip angle (θ_i) of 12º.

Based on the result, the maximum uplift load of 1.3kN was confirmed for HK12H88C_① with high rapid-cement content. In addition, a maximum uplift load of displacement of less than 2 mm was confirmed. HK12H88C_②, which has a relatively low cement content, had a maximum uplift load of 0.59 kN and the displacement was 3.76 mm. HK12H88C_①, which has a high rapid-cement content, has a maximum uplift load of about 2.2 times higher than HK12H88C_②. This value is slightly lower than about 2.7 times compared with the uniaxial compressive test (U_c) result using the same mixing ratio. In addition, in the test of HK12H88C_②, it is determined that the cohesive force between the pile and the ground is reduced due to the problem between the pile and the acrylic plate. Therefore, the maximum uplift load is considered to have decreased.

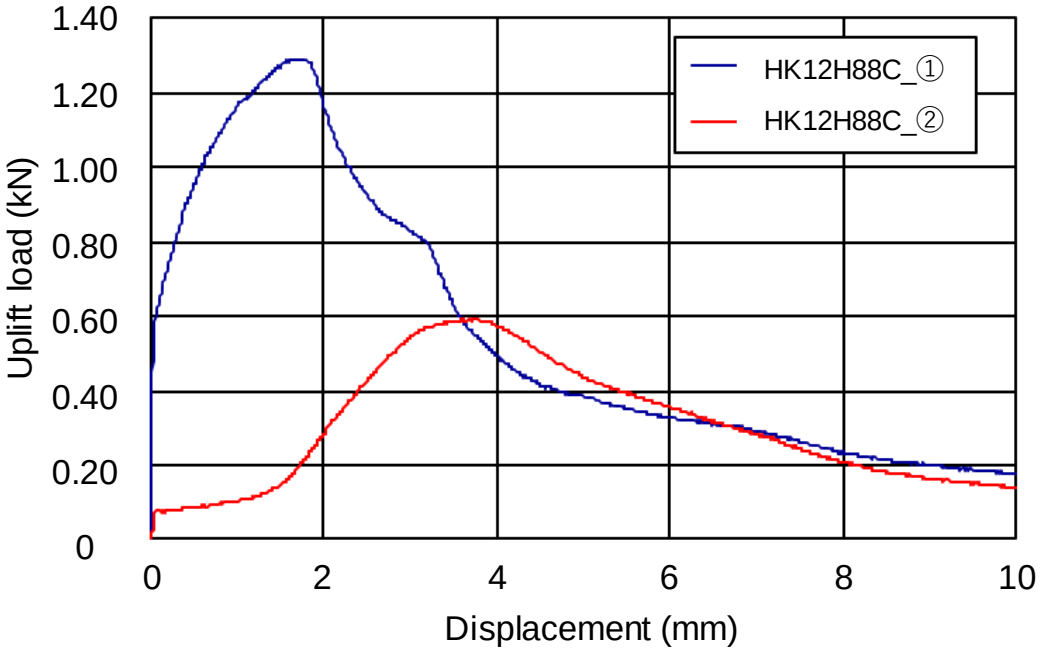

Fig.5-3 Result of half-circular test according to the soil-cement strength.

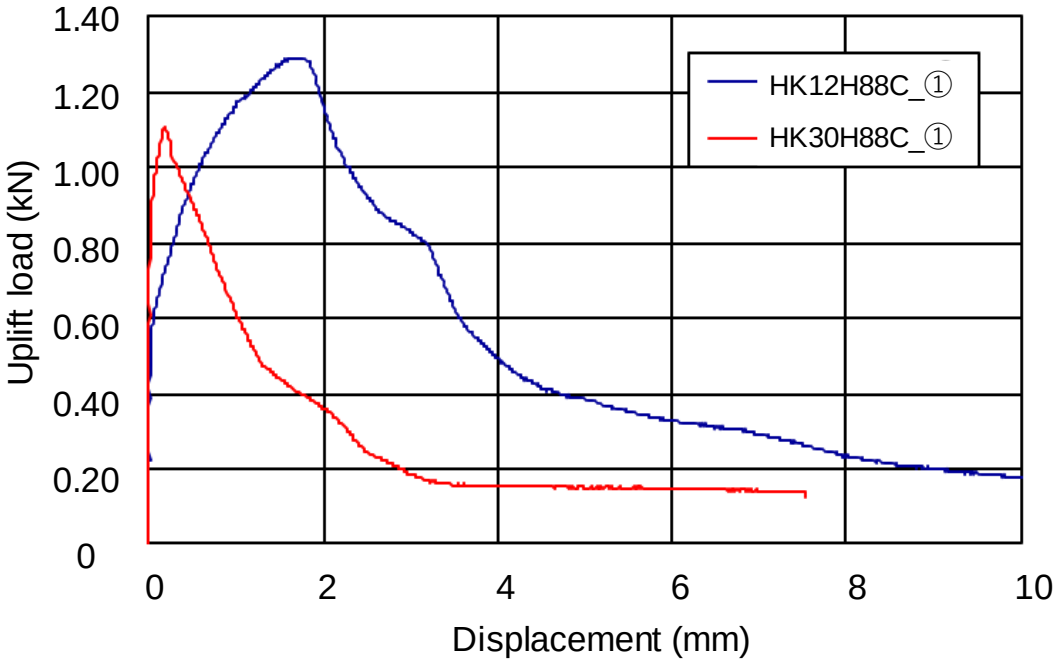

Fig.5-4 Result of half-circular test according to the pile tip inclination angle (θ_i).

5.3.2 Characteristics of Failure Mechanism of Belled-Type Pile focusing on The Soil-Cement Strength

Fig. 5-4 shows the result of the half-circular test according to the pile tip inclination angle (θ_i). The model ground was produced using the same mixing ratio. Model piles were half-circular model piles and model piles were modeled at 12º and 30º depending on the pile tip inclination angle (θ_i). Based on the result of comparing the uplift load of the model pile, the maximum uplift load of HK12H88C_① was 1.29kN at the uplift displacement of 1.62mm. In HK30H88C_①, the maximum uplift load of 1.10kN was generated at the uplift displacement of 0.19mm. In both tests, peak was identified and an inflection point occurred at the stage of softening. Based on the result of comparing the maximum uplift loads of the two models, the maximum uplift load of HK30H88C_① was found to be about 17% higher than that of the HK12H88C_①.

5.3.3 Failure Mechanism Analysis of Half-circular Model Tests

In this section, the test process was monitored using a video camera to analyze the failure mechanism of belled-type piles installed in the soft-rock ground. In addition, image analysis allowed us to observe the monitoring results more specifically than previous studies.

Fig.5-5 to Fig.5-7 show the failure surface analysis results performed in the half-circular test. Based on the result, the comparing failure surface of HK12H88C_① and HK30H88C_①, the shape of the failure surface is similar because the soil-cement has the same strength. However, since HK12H88C_② has a relatively low ground strength, the failure surface is relatively smaller than HK12H88C_① and HK30H88C_①.

Fig.5-8 and Table.5-5 shows the failure surface measurement methods and a list of the measured failure surface. The range of the failure surface is the distance from the pile center to the top of the model ground. The failure angle shows the value calculated from the average value of the shear distance and the value calculated from the minimum distance. Where the () value of the failure angle shown in Table.5-5 shows the calculated minimum distance.

In all cases, the failure angle was highest under the condition of HK12H88C_①, and the lowest failure angle was found in the case of HK12H88C_②. Based on the result, the ground strength was high, and it was confirmed that the widest failure angle was formed under the condition of the pile tip inclination angle of 12º.

Fig.5-5 (b), Fig.5-6 (b), and Fig.5-7 (b) show the result of image analysis. Based on the image analysis, the failure surface of the soil-cement ground was clearly identified, and the behavioral characteristics of the sand ground formed on the soil-cement ground were confirmed.

The failure surface shape of soil-cement was confirmed by the invert truncated model, and the failure surface was linear. In addition, the failure surface was widely confirmed depending on the strength. Basically, the Soil-cement has a brittle failure characteristic, and it is considered that the failure surface caused linearly due to the high strength of the ground.

Soil-cement ground failure by uplift load generates the behavior of upper sand ground. The failure surface shape of the sand ground caused by the behavior was found to be a cylindrical failure surface in all cases. Thus, under model ground conditions assuming soft-rock layers and sand layers, if the rupture of the soft-rock layers is caused by the uplift load of the bottom pile, the effect of the upper sand ground on the uplift resistance is considered the corresponding sand weight.

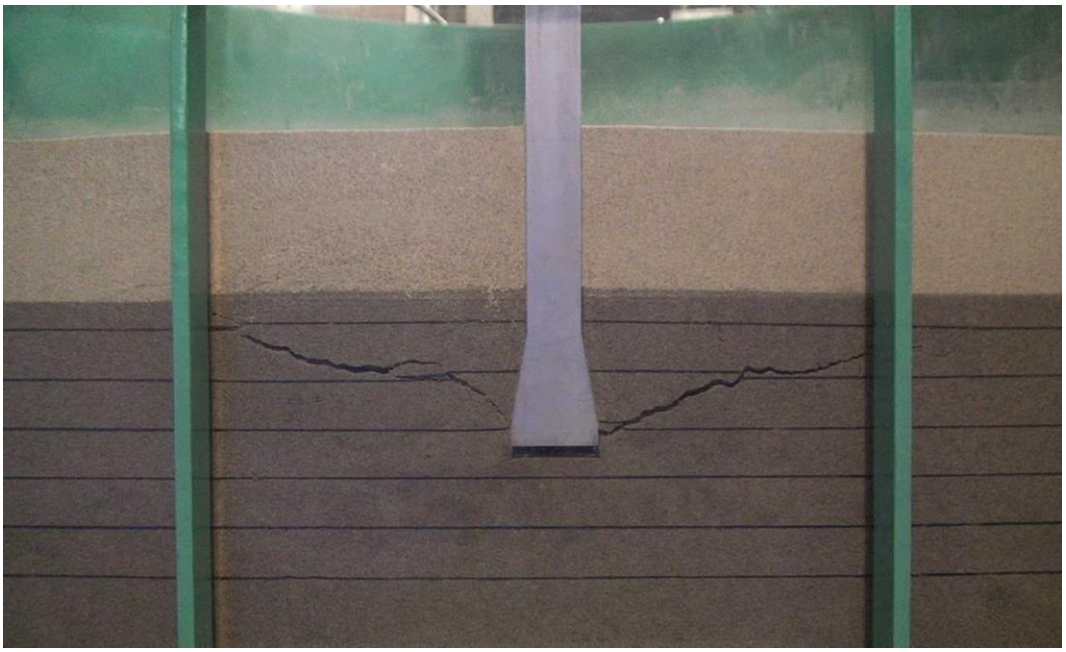

(a) The failure surface due to uplift load.

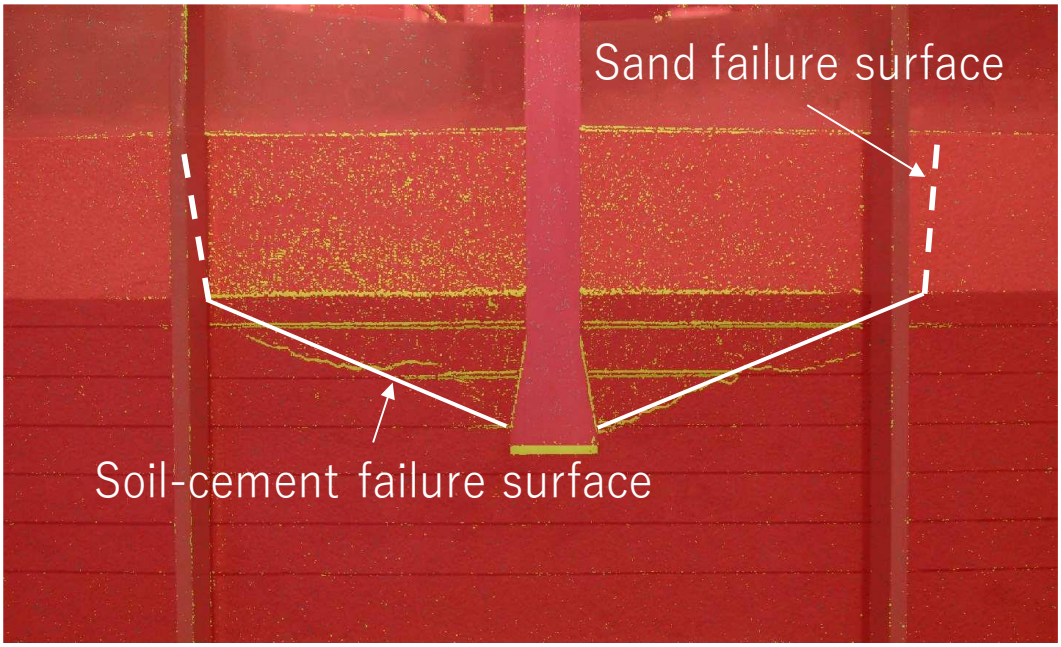

(b) The failure surface identification by image analysis.

Fig.5-5 Soil-cement ground failure status. (HK12H88C_①)

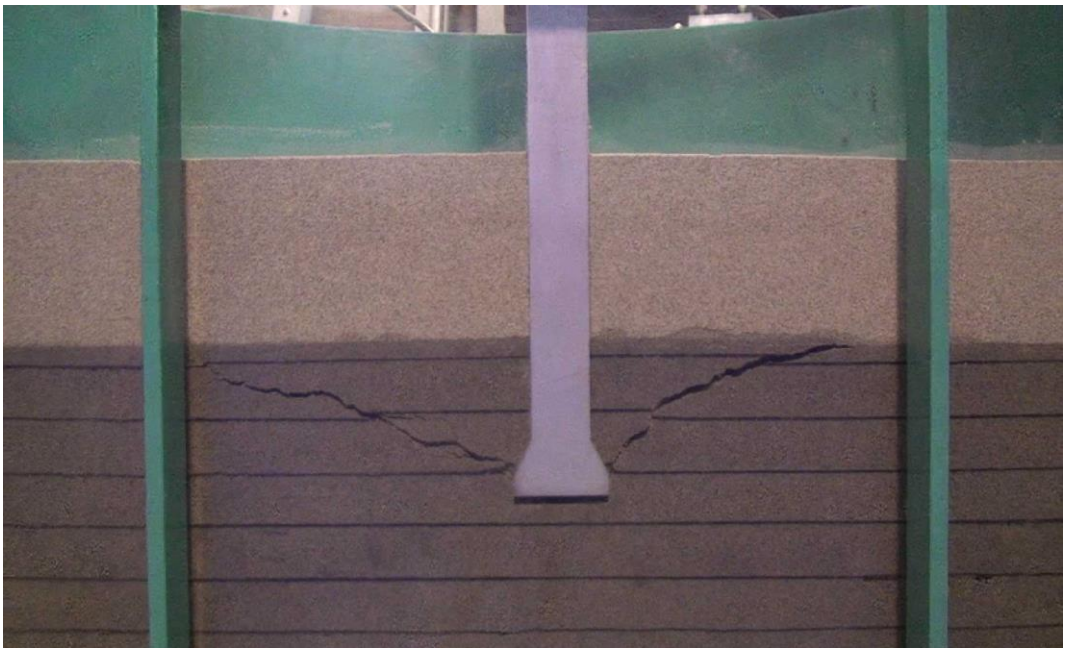

(a) The failure surface due to uplift load

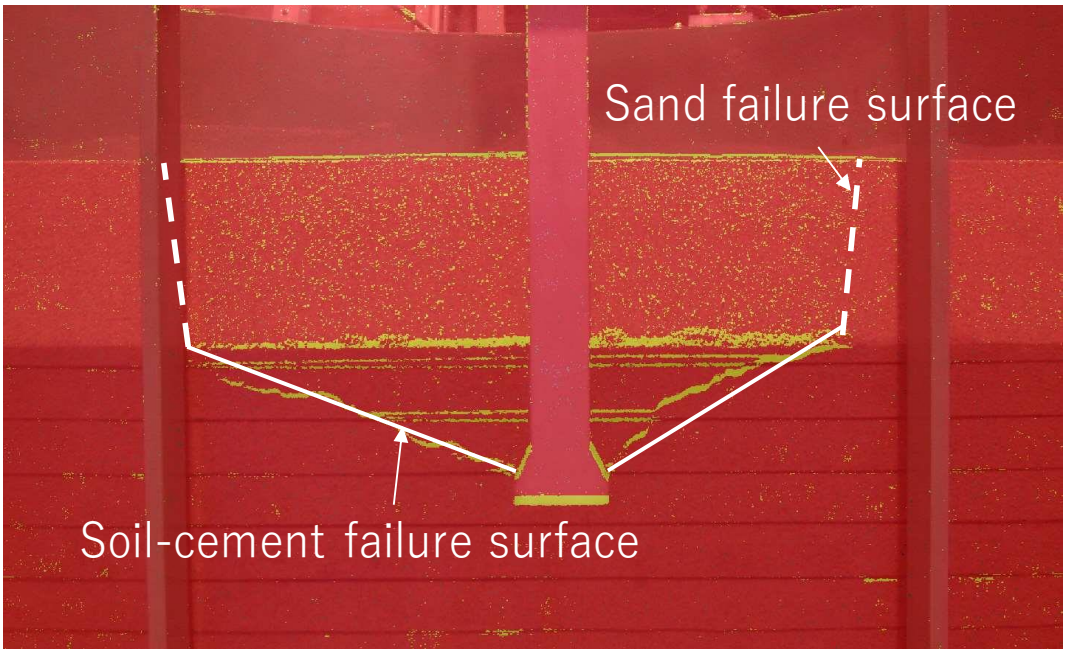

(b) The failure surface identification by image analysis

Fig.5-6 Soil-cement ground failure status (HK30H88C_①)

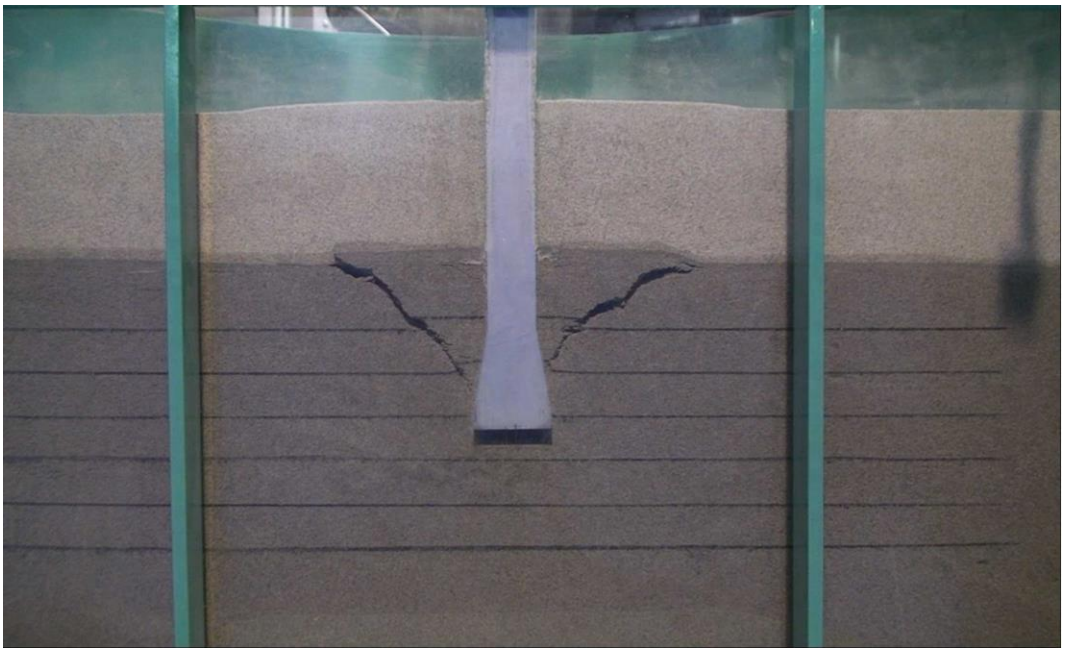

(a) The failure surface due to uplift load.

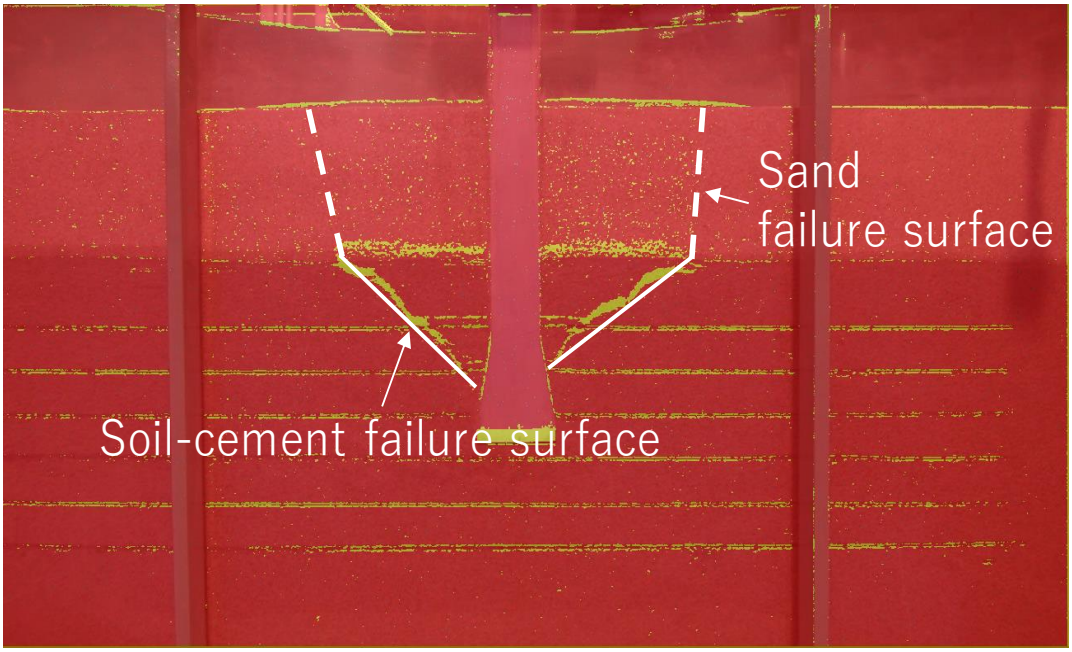

(b) The failure surface identification by image analysis.

Fig.5-7 Soil-cement ground failure status. (HK12H88C_②)

Table.5-5 Measured failure surface and failure angle (θ_E).

Experiment ID	Distance from the failure surface to the center				Failure angle (θ_E)
	Right (L_{f2})	Lift (L_{f3})	Back side (L_{f1})	Average (L_{fa})	
	(mm)	(mm)	(mm)	(mm)	(°)
HK12H88C _①	200	245	145	197	22.1 (28.9)
HK12H88C _②	125	120	120	122	30.9 (33.7)
HK30H88C _①	200	145	125	157	27.0 (31.3)

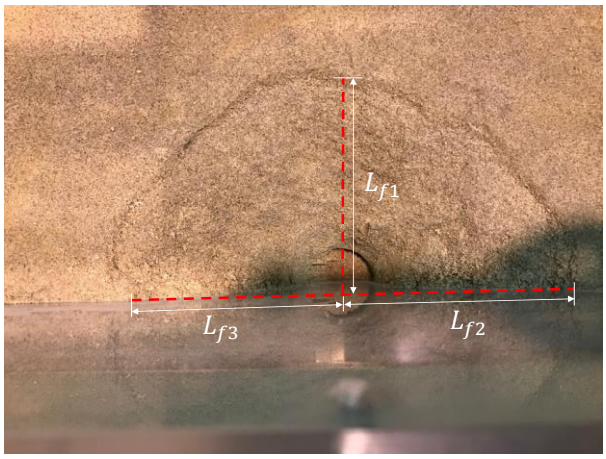

Fig.5-8 Measurement of failure surface and failure angle.

5.4 SUMMARY

In this chapter, model tests were performed on various effects of belled-type piles on the soil-cement assuming soft-rock ground. In the model test, the model test was carried out on the effect of the pile shape, the strength of the ground, and the pile penetration depth (L), and the uplift resistance characteristics and the soil behavior were confirmed: (1) uplift resistance characteristics using the circular model test, (2) identification of failure mechanisms using half-circular model tests

1. In the circular model test, longitudinal piles and conventional piles were identified with a maximum uplift load of up to 2.8 times under the same ground strength and penetration depth (L). In addition, the deeper penetrating depth (L) increased the

maximum uplift load, and the displacement increased until the maximum uplift load appeared.

2. In the stress-strain results of the half-circular model test, the belled-type piles with a pile tip inclination angle (θ_i) of 12º showed a maximum uplift load difference of up to 2.2 times depending on the ground strength. In addition, the maximum uplift load of the belled-type pile at pile tip inclination angle (θ_i) of 12º was about 17% higher than the result of 18º under the same soil-cement strength.

3. The range of failure angle calculated in the half-circular test was found to be 60º ~ 70º and the belled-type pile with the pile tip inclination angle (θ_i) of 12º was found to have the widest failure surface in the ground of the same strength. In addition, the failure surface of the sandy ground on the soil-cement ground was identified as circular. Therefore, the effect of sandy ground on the uplift load can be thought of only as of the weight of sand.

REFERENCES

Benmokrane, B., Chennouf, A and Mitri, H. S, (1995). Laboratory evaluation of cement-based grouts and grouted rock anchors. *International Journal of Rock Mechanics and Mining Sciences & Geomechanics*, 32(7), 633-642.

Serrano, A. and Olalla, C. (1999). Tensile resistance of rock anchors. *International Journal of Rock Mechanics and Mining Sciences*, 36(4), 449-474

Chae, D. H., Cho, W. j. and Na, H. Y. (2012). Uplift capacity of belled pile in weathered sandstones. *International Journal of Offshore and Polar Engineering,* 22(4), 297-305.

Wu, X., Feng, Z., Tian, T. and Wang, W. (2013). Improved technology of cast-in-site concrete pile on soft soil foundation. *Electronic Journal of Geotechnical Engineering*, 18, 4343-4352.

Sego, D. C., Biggar, K. W. and Wong, G. (2003). Enlarged Base (Belled) Piles for Use in Ice or Ice-Rich Permafrost. *Journal of Cold Regions Engineering*, 17(2), 68-88.

Suzuki, N., Chatani, F., Nishiyama, T. and Seki, T. (2010). Vertical load-deflection behavior and evaluating the resistance of under-reamed bored pile. *Journal of Structural Engineering*, 75(656), 1847-1856.

Yamazaki, M., Nagaoka, H. and Nakamura, T. (1995). Effect of under-reamed end shapes on the structural strength of cast-in-place concrete pile ends. *Journal of Structural Engineering*, 470, 95-103.

CHAPTER VI

PREDICTION OF UPLIFT CAPACITY BY BELLED-TYPE PILE IN SANDY GROUND AND SOFT-ROCK GROUND

6.1 INTRODUCTION

This chapter proposes a model to predict the penetration depth (L) of belled-type piles, unit weight of sand, and uplift resistance in the soft-rock ground. The proposed model utilizes the internal friction angle (φ), the dilatancy angle (ψ) and the adhesion of the soil-cement proposed in the geotechnical parameter.

The newly proposed model utilizes the limit equilibrium equations proposed in the previous conventional piles and considers the effect of the pile tip shape using the results of model tests.

6.2 UPLIFT RESISTANCE PREDICTION MODEL FOR SHALLOW SANDY GROUND ($L/b_b < 3$)

Uplift resistance of the shallow ground ($L/b_b < 3$) to study the current predictive models have been carried out a study based on the belled-type pile and uplift resistance structure system. In the previous studies, the tip shape of the belled-type pile and the pile-skin friction (δ) cannot be considered at the same time.

In this study, an effective uplift resistance model considering the tip shape and pile-skin friction (δ) of the bell pile by using the limit equilibrium equation model proposed.

6.2.1 Prediction Model for Failure Surface and Failure Angle

Fig.6-1 shows the results of the image analysis of the belled-type piles performed on the shallow ground of the belled-type piles in this study. It is difficult to clearly determine the difference between the linear and nonlinear failure surface of the ground obtained from the model test results. Therefore, in this research, in order to simplify the calculation, the failure surface was assumed to be the linear line.

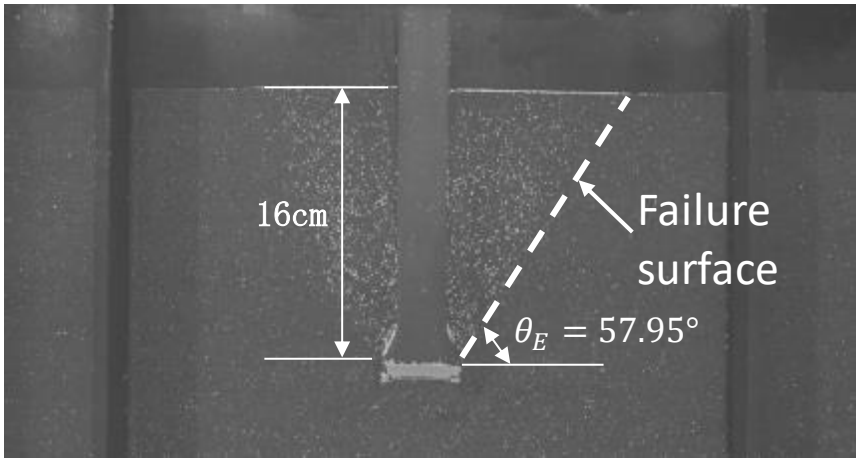

Fig.6-1 Results of the image analysis of the bell piles performed on the shallow ground of the belled-type piles in this study.

$$\theta_{\mathrm{E}} = \left(90° - \frac{\psi}{2} - \theta_i\right) \times \kappa \tag{6.1}$$

$$\kappa = (1 - \frac{Dr}{100} + 0.7) \tag{6.2}$$

Where, κ: coefficient of unit weight, Dr: relative density (%), ψ: dilatancy angle (º), φ: internal friction angle(º), θ_{E}: failure angle (º), θ_i : pile tip inclination angle (º)

In the previous research of uplift loading on the conventional pile, the value of the failure angle, $\theta_E = \varphi/4$º (Shanker *et al*. 2007), which has similar value with the test results. In addition, Eq.6.2 is proposed with reference to previous studies. In previous model tests, the

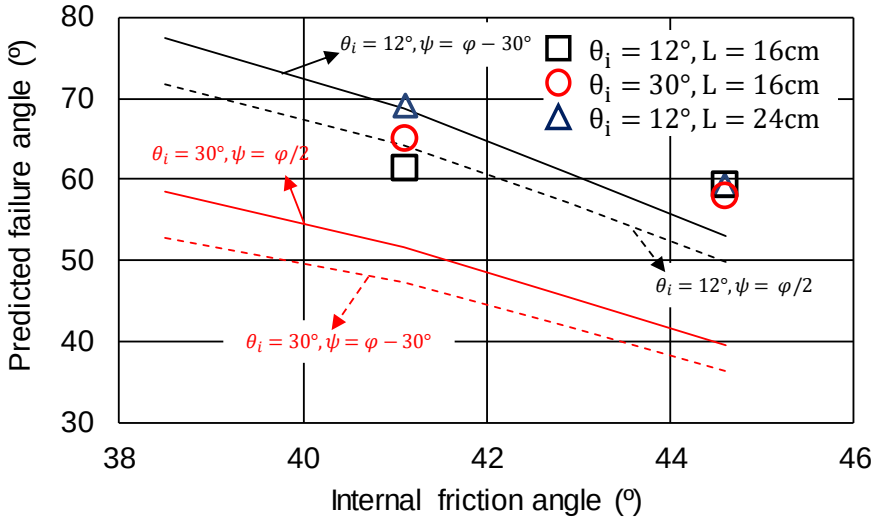

Fig.6-2 Relationship between calculated value and measured value of failure angle (θ_E).

results showed that the uplift resistance decreased at 70% of the relative density (D_r) of sand (Das. 1983).

According to the results, the density coefficient was proposed (κ). This coefficient was determined based on test results. The following failure angles were estimated based on the results of the above two studies and the pile tip inclination angle (θ_i) as following Eq.6.1.

Fig.6-2 shows the failure angles calculated using Eq.6.1 and the failure angles measured in the image analysis. The failure angle calculation uses the internal friction angle (φ), and the dilatancy angle (ψ) uses two representative empirical equations proposed in previous studies (Das. 1983, JGS.1995). In addition, the relationship between the relative density (D_r) and internal friction angle (φ) was referred to Fig.3.8.

Based on the result, the higher the internal friction angle (φ), the higher the experimental value was than the calculated value in all cases.

6.2.2 Evaluate of Uplift Resistance Capacity Model

Fig.6-3 shows the definition sketch and free body diagram of the resultant shear failure surface of the belled-type pile by shallow ground ($L/b_b < 3$).

The proposed model was analyzed based on the limit equilibrium equations of Chattopadhyay and Pise (1986). Chattopadhyay and Pise (1986) conducted a model test on the uplift load in the conventional pile and the model was presented using the limit equilibrium method. In addition, this study has compared the results of the model test with the proposed models. In the research by Chattopadhyay and Pise (1986), the failure surfaces were evaluated by considering the pile tip inclination angle (θ_i) to simplify the failure surface, assuming the failure surface is the linear line. In the proposed model of the failure surface, the pile tip inclination angle (θ_i) was considered. Which was not considered in the previous researches. The proposed model assumes the following three assumptions.

(1) The failure surface intersects linearly with the surface of the ground.

(2) For a belled type pile with $\delta \geq 0$, the angle between the failure surface and the surface is assumed to approach $\left(90° - \frac{\psi}{2} - \theta_i\right) \times \kappa$ based on the previous researches. κ means the coefficient assumed in the previous researches.

(3) For piles with $\delta \geq 0$, subject to ultimate uplift force Pu, the failure surface starts tangentially to the ground surface.

Fig.6-2(b) shows the equilibrium of forces at the failure surface which assumes the failure surface starts at the coordinates of the end of the pile tip ($b_b/2, 0$), which slope was expressed failure surface was assumed as the linear line.

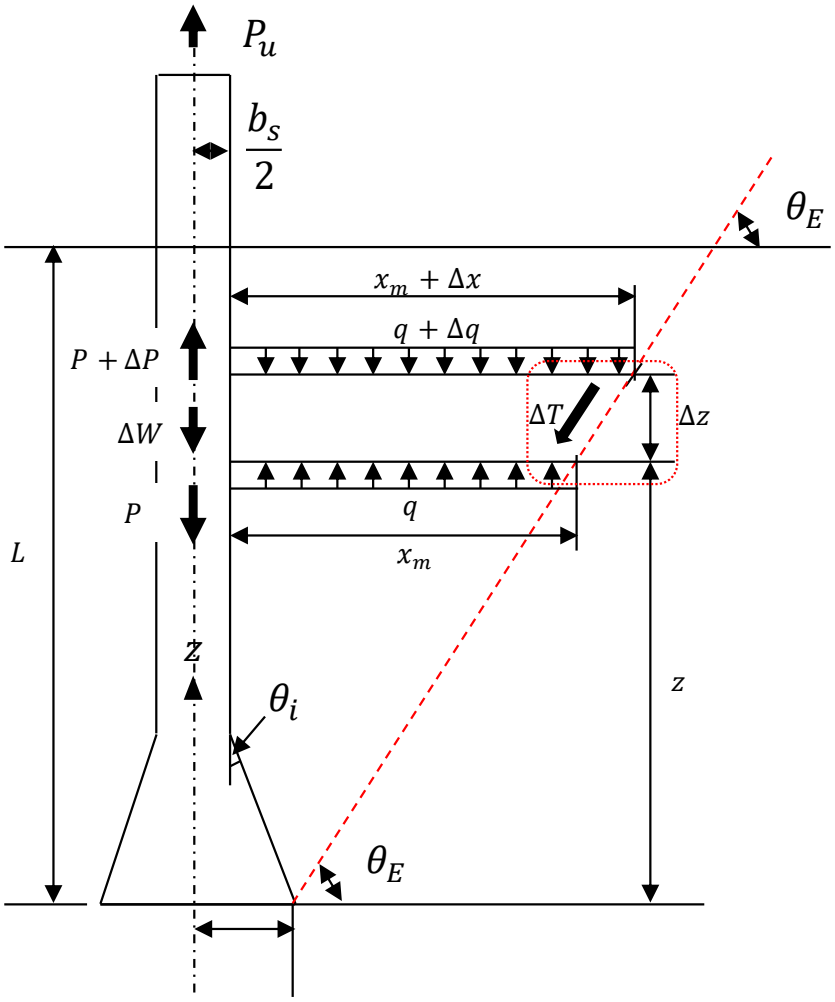

(a) Definition sketch of the resultant shear failure surface.

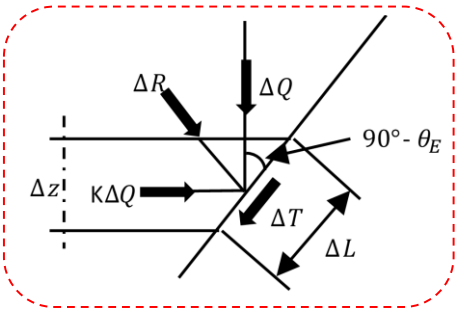

(b) Free body diagram of the resultant shear failure surface.

Fig.6-3 Definition sketch and free body diagram of the resultant shear failure surface of the belled-type pile by shallow ground. ($L/b_b < 3$).

Shear resistance (ΔT) along the failure surface length (ΔL) can be calculated by the following equation.

thus

$$\Delta R = \Delta Q(\cos\theta_E + K_0 sin\theta_E) \tag{6.3}$$

Here

$$K = K_0 = (1\text{-}\sin\varphi) \tag{6.4}$$

In Fig.6-3(a), ΔQ can be expressed as follows.

$$\Delta Q = \gamma_d(L - z - \Delta z/2)\Delta L \tag{6.5}$$

$$\Delta L = \frac{\Delta z}{sin\theta_E} \tag{6.6}$$

where

$$\Delta R = \gamma_d\left(L - z - \frac{\Delta z}{2}\right)(cos\theta_E + K_0 sin\theta_E)\frac{\Delta z}{sin\theta_E} \tag{6.7}$$

and

$$\Delta T = \gamma_d\left(L - z - \frac{\Delta z}{2}\right)(cos\theta_E + K_0 sin\theta_E)\frac{\Delta z}{sin\theta_E} tan\varphi \tag{6.8}$$

Considering the vertical equilibrium of the circular wedge and assuming that the weight of the pile of length dz equals the weight of the pile to the volume occupied by the pile.

$$(P + \Delta P) - P + q\pi x_m^2 - (q + \Delta q)\pi(x_m^2 + \Delta x)^2 - \Delta W - 2\pi\left(x_m^2 + \frac{\Delta x}{2}\right)\Delta T sin\theta_E = 0 \quad (6.9)$$

Eq.6-9 replaces and simplifies the ΔT value from Eq.6-10.

$$\frac{\Delta P}{\Delta z} = \pi q \frac{\Delta x}{\Delta z}(2x_m + \Delta x) + \pi \frac{\Delta q}{\Delta z}(x_m + \Delta x)^2 + \pi \frac{\Delta q}{\Delta z}(x_m + \Delta x)^2 + \pi(x_m + \Delta x)^2\gamma_d +$$
$$2\pi\left(x_m + \frac{\Delta x}{x}\right)\gamma_d\left(L - z - \frac{\Delta z}{2}\right)(cos\theta_E + K_0 sin\theta_E)tan\varphi \quad (6.10)$$

At the limit, to replace q in Eq.6-10 with $q = \gamma_d$(L - z).

$$\frac{dP}{dz} = 2\pi\left(\frac{z}{tan\theta_E} + \frac{b_b}{2}\right)\gamma_d(L - z)\frac{1}{tan\theta_E} + 2\pi\left(\frac{z}{tan\theta_E} + \frac{b_b}{2}\right)\gamma_d(L - z)(cos\theta_E +$$
$$K_0 sin\theta_E)tan\varphi \quad (6.11)$$

Eq.6-11 as an integral, it was organized as Eq.6-12.

$$\therefore P_u = \int_0^L 2\pi\left(\frac{z}{tan\theta_E} + \frac{b_b}{2}\right)\gamma_d(L - z)\left[\frac{1}{tan\theta_E} + (cos\theta_E + K_0 sin\theta_E)tan\varphi\right]dz \quad (6.12)$$

If except for the pile weight, it can be expressed as follows. Herein, the shape of the pile is assumed to be a conventional pile for simple calculation.

$$\therefore P_{u(net)} = P_u - \frac{\pi {b_b}^2}{4} \times L \times \gamma_d \quad (6.13)$$

6.2.3 Validation of The Develop Model

The representative uplift load models in previous researches and test results in this research were compared. In the selection of representative models in the previous researches, typical models using conventional piles, belled-type piles, and anchor plates were selected. The selection of representative models, which are similar to parameter characteristics such as internal friction angle (φ) and relative density (Dr) was selected, respectively. Moreover, in order to compare quantitatively the calculated results of the previous models with the proposed model results, the percentage of error (ε) was evaluated.

Eq.6.14 represents the difference between the calculation result the model test result as an absolute value in percentage.

$$\varepsilon\,(\%) = \left|\frac{(P_u)_{predicted} - (P_u)_{experiment}}{(P_u)_{experiment}}\right| \times 100 \qquad (6.14)$$

(a) Compare with the Previous Model

Fig.6-4 and Table.6-1 show the calculation results of the previous models and the test results of the model tests. The dilatancy angle (ψ) and the pile-soil friction angle (δ) used in the model calculations were provided in the reference ($\delta = \psi = \varphi/2^{o}$). In addition, since the tip diameters (b_b = 0.048 m) of the belled type piles used in this research were the same, the calculation results of the two types of belled-type piles (θ_i = 12º, 18º) were the same.

In the case of the conventional pile (θ_i= 0º), the standard model (Eq.2.1) has shown a difference of uplift loading of up to 17 times (Dr = 95%) depending on the relative density (Dr). Based on the result of the comparison of the truncated cone model, a difference of up to 3 times was confirmed depending on the relative density (D_r) of 85%. For the truncated

cone model, the results of highly reliable tests were confirmed under the conditions of the relative density (Dr) of 75% or less.

It can be concluded that the reliability of the proposed model is higher than the conventional pile model (θ_i = 0º). The models of Meyerhof's (1973), Downs and Chieurzzi (1966) have shown relatively good corresponding. Comparing to Meyerhof's model (1973), Downs and Chieurzzi's (1966) and Ovesen (1981), the reliability of the model test results of the belled-type pile was higher than the other models. In the other models, the percentage of error (ε) was more than 100%.

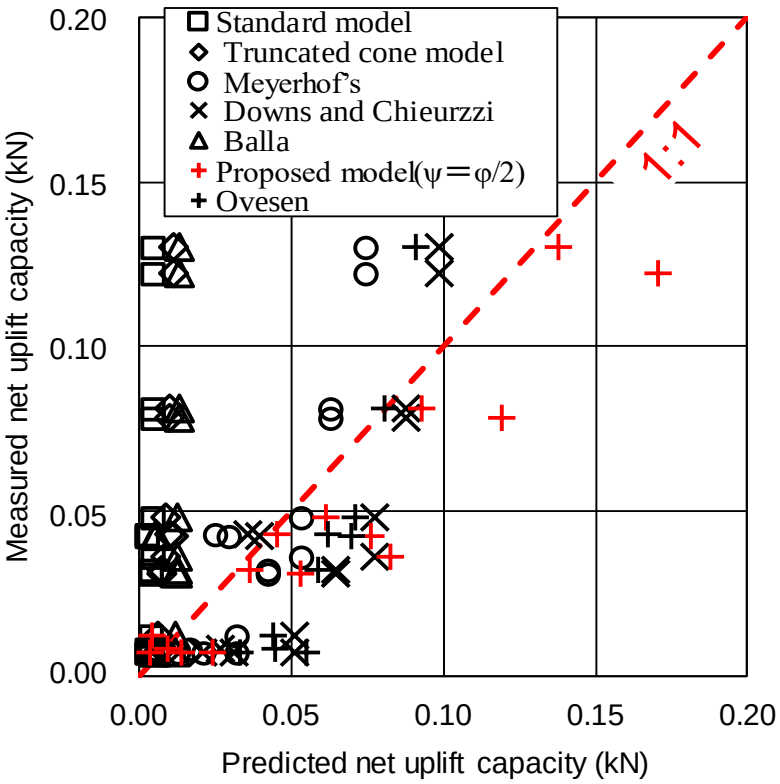

Fig.6-4 Calculation results of the previous models and the experimental results of the model experiments.

Table.6-1 The calculation results of the previous models and the experimental results of the model experiments.

Inclination angle	D_r	γ_d	Internal friction angle	Standard model		Truncated cone model		Meyerhof's model		Downs and Chieurzzi		Ovesen		Balla		Experiment
θ_i(°)	(%)	(kN/m^3)	φ (°)	Pu (kN)	ε (%)	Pu (kN)	ε (%)	Pu (kN)	ε (%)	Pu (kN)	ε (%)	Pu (kN)	ε (%)	Pu (kN)	ε (%)	Pu (kN)
0	40	13.13	35.0	0.002	228.7	0.006	25.0	0.012	42.8	0.021	66.2	0.033	78.9	0.004	57.6	0.007
	65	13.88	38.5	0.002	262.5	0.007	10.2	0.016	51.2	0.026	69.4	0.045	82.1	0.005	69.8	0.008
	75	14.44	41.1	0.002	213.0	0.009	19.7	0.021	66.2	0.031	77.6	0.054	87.1	0.005	43.3	0.007
	85	14.81	42.9	0.002	1817.7	0.010	339.0	0.024	76.6	0.035	22.5	0.062	30.4	0.005	761.9	0.043
	95	15.19	44.6	0.002	1777.6	0.011	282.9	0.029	45.9	0.040	6.3	0.070	39.8	0.005	726.8	0.042
12	40	13.13	35.0	0.003	252.2	0.006	114.3	0.031	61.7	0.051	76.3	0.044	72.6	0.011	5.6	0.012
	65	13.88	38.5	0.004	806.3	0.007	340.8	0.042	23.8	0.065	50.4	0.058	45.2	0.012	165.3	0.032
	75	14.44	41.1	0.004	1241.4	0.009	450.8	0.053	9.4	0.077	37.9	0.071	32.4	0.013	283.7	0.048
	85	14.81	42.9	0.004	2157.7	0.010	727.0	0.062	30.0	0.087	7.2	0.080	0.8	0.013	534.2	0.081
	95	15.19	44.6	0.004	3532.3	0.011	1085.1	0.074	76.4	0.098	32.0	0.090	43.7	0.013	899.7	0.13
18	40	13.13	35.0	0.003	105.4	0.006	25.0	0.031	77.7	0.051	86.2	0.044	84.0	0.011	38.4	0.007
	65	13.88	38.5	0.004	777.9	0.007	327.1	0.042	26.2	0.065	52.0	0.058	46.9	0.012	157.0	0.031
	75	14.44	41.1	0.004	906.0	0.009	313.1	0.053	32.1	0.077	53.5	0.071	49.3	0.013	187.8	0.036
	85	14.81	42.9	0.004	2074.1	0.010	696.3	0.062	25.2	0.087	10.6	0.080	2.9	0.013	510.7	0.078
	95	15.19	44.6	0.004	3308.8	0.011	1012.1	0.074	65.5	0.098	23.9	0.090	34.9	0.013	838.2	0.122

(b) Influence of Dilatancy Angle (ψ) on The Proposed Model

Generally, the dilatancy angle (ψ) relates to the volumetric deformation rate of the ground, therefore a complex test is required. Previous researchers have studied the relationship between internal friction angle and dilatancy angle (ψ) using model tests (Das.1983, JGS.1995) and are currently using the results extensively.

In this research, the dilatancy angle (ψ) was used as an important parameter to determine the failure angle (θ_E). Therefore, the proposed model was compared using two different dilatancy angles ($\psi = \varphi/2°$, $\psi = \varphi$ - 30º). Fig.6-5 and Table.6-2 show the comparison between the calculated values of the proposed model for two dilatancy angles and the uplift loading of model tests. The calculated values with the dilatancy angle of $\psi = \varphi/2°$ were

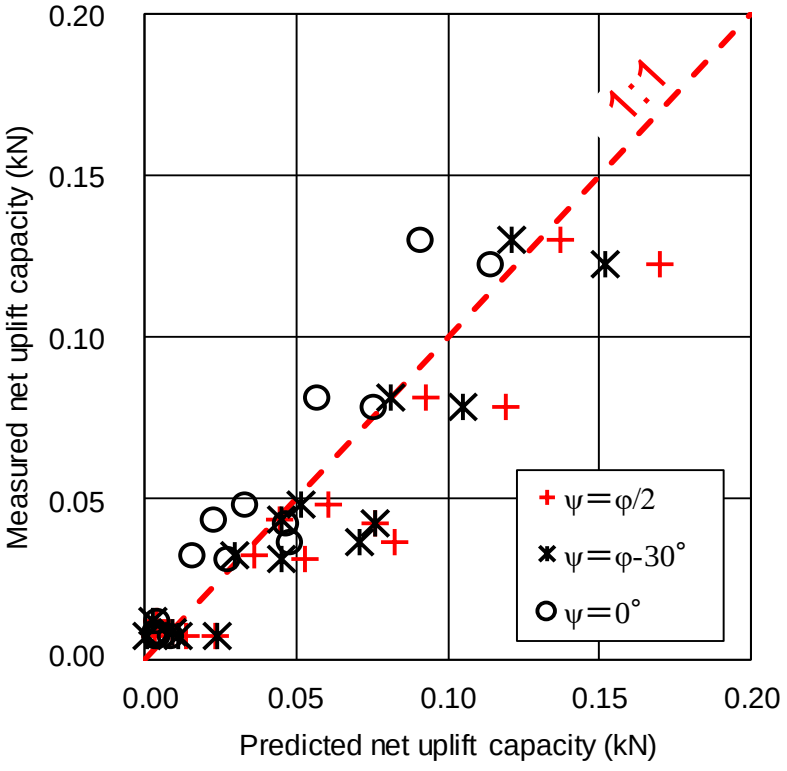

Fig.6-5 Comparison between the calculated values of the proposed model for two dilatancy angles and the uplift loading of model tests.

about 16% higher than the test values. In addition, in Table.6-2, the error (ε) was found 50% or less in most cases excluding the case with a relative density (D_r) of 40%.

In the predicted result with dilatancy angle (ψ) of $\psi = \varphi$ - 30º, an error was smaller than the result with dilatancy of $\psi = \varphi/2$º. Particularly, in the case of the belled-type pile with a pile tip inclination angle (θ_i) of 12º, the error (ε) was less than 10% excluding the case with a relative density (D_r) of 40% and the reliability was found very high. However, the calculation results with the dilatancy angle (ψ) of $\psi = \varphi$ - 30º of 40% of relative density, the pile tip inclination angle (θ_i) of 0º and 12º were calculated much lower than the test value.

Table.6-2 Calculation and comparison of the proposed models for dilatancy angle (ψ).

Inclination angle	D_r	γ_d	Internal friction angle	Experiment	Proposed model		
					$\psi=0^o$	$\psi=\varphi/2^o$	$\psi=\varphi$ - 30^o
θ_i(°)	(%)	(kN/m^3)	φ (°)	(kN)			
0	40	13.13	35.0	0.007	0.0032	0.003	0.001
	65	13.88	38.5	0.008	0.0035	0.009	0.009
	75	14.44	41.1	0.007	0.0083	0.024	0.024
	85	14.81	42.9	0.043	0.0230	0.045	0.045
	95	15.19	44.6	0.042	0.0465	0.076	0.076
12	40	13.13	35.0	0.012	0.0038	0.004	0.003
	65	13.88	38.5	0.032	0.0154	0.036	0.03
	75	14.44	41.1	0.048	0.0328	0.061	0.052
	85	14.81	42.9	0.081	0.0569	0.093	0.081
	95	15.19	44.6	0.13	0.0911	0.137	0.121
18	40	13.13	35.0	0.007	0.0038	0.014	0.011
	65	13.88	38.5	0.031	0.0273	0.053	0.045
	75	14.44	41.1	0.036	0.0480	0.082	0.071
	85	14.81	42.9	0.078	0.0755	0.119	0.105
	95	15.19	44.6	0.122	0.1140	0.170	0.152

6.3 UPLIFT RESISTANCE PREDICTION MODEL FOR DEEP SANDY GROUND ($L/b_b > 3$)

The uplift resistance model proposed in the previous section was carried out on the shallow ground. Until now, most of the uplift resistance structure systems and belled-type piles have been carried out on shallow grounds, so there is a lack of research on the failure mechanism and uplift resistance prediction model for deep foundations ($L/b_b > 3$).

Therefore, this section proposes an uplift resistance model of a belled-type pile that is conducted on deep foundations using model tests and previous studies.

6.3.1 Prediction Model for Failure Surface and Failure Angle

(a) Failure Angle

The failure angle of the deep foundation is also proposed in consideration of the relative density of sand ground and the inclination angle of the pile tip. This method is presented in the same way as the shallow foundation failure angle (θ_{E}).

$$\theta_{\mathrm{E}} = \kappa\left(90° - \frac{\psi}{2} - \theta_i\right) \tag{6.1}$$

$$\kappa = (1 - \frac{\mathrm{Dr}}{100} + 0.7) \tag{6.2}$$

Where, κ: coefficient of unit weight, D_r: relative density (%), ψ: dilatancy angle (º), φ: internal friction angle (º), θ_{E}: failure angle (º), θ_i : pile tip inclination angle (º)

(b) Failure Surface

Fig.6-6 shows the Weibull-curve failure surface applied to the image analysis performed on the deep foundation ($L/b_b > 3$). In the previous section, failure surfaces due to belled-type piles during uplift loads were known as invert truncated models in the shallow

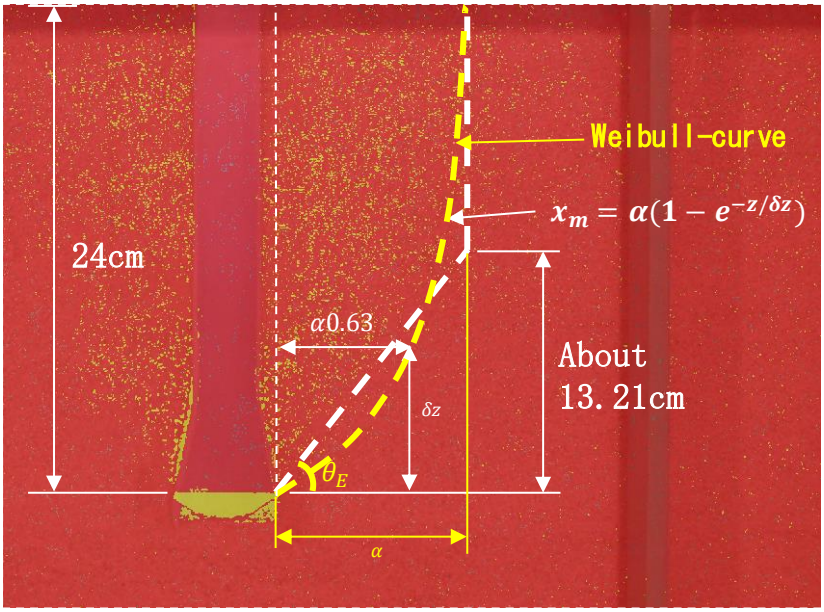

Fig.6-6 Weibull-curve failure surface applied to the image analysis performed on the deep foundation. ($L/b_b > 3$)

foundation. However, in model tests and previous studies by deep foundations, the shape of the failure surface was observed differently from the shallow foundation ($L/b_b < 3$) surface under the slenderness ratio ($\lambda = L/b_b$) of about 3 ~ 4. Therefore, the Weibull-curve, which is a non-linear curve, is applied to analyze the failure surface of the deep foundation ($L/b_b > 3$) effectively.

The increase in the uplift resistance of the belled-type pile is thought to be due to the increase in confine pressure around the belled-type pile tip and the lateral earth pressure close to the passive pressure state as the displacement increase. Therefore, considering that the tip slope height affects the depth of the failure surface shape, δ_z introduced λ which is determined based on the slope height.

Therefore, the Weibull-curve is shown in Fig.6-7 was applied as an estimation equation for the failure line considering the effect of the penetration depth (L).

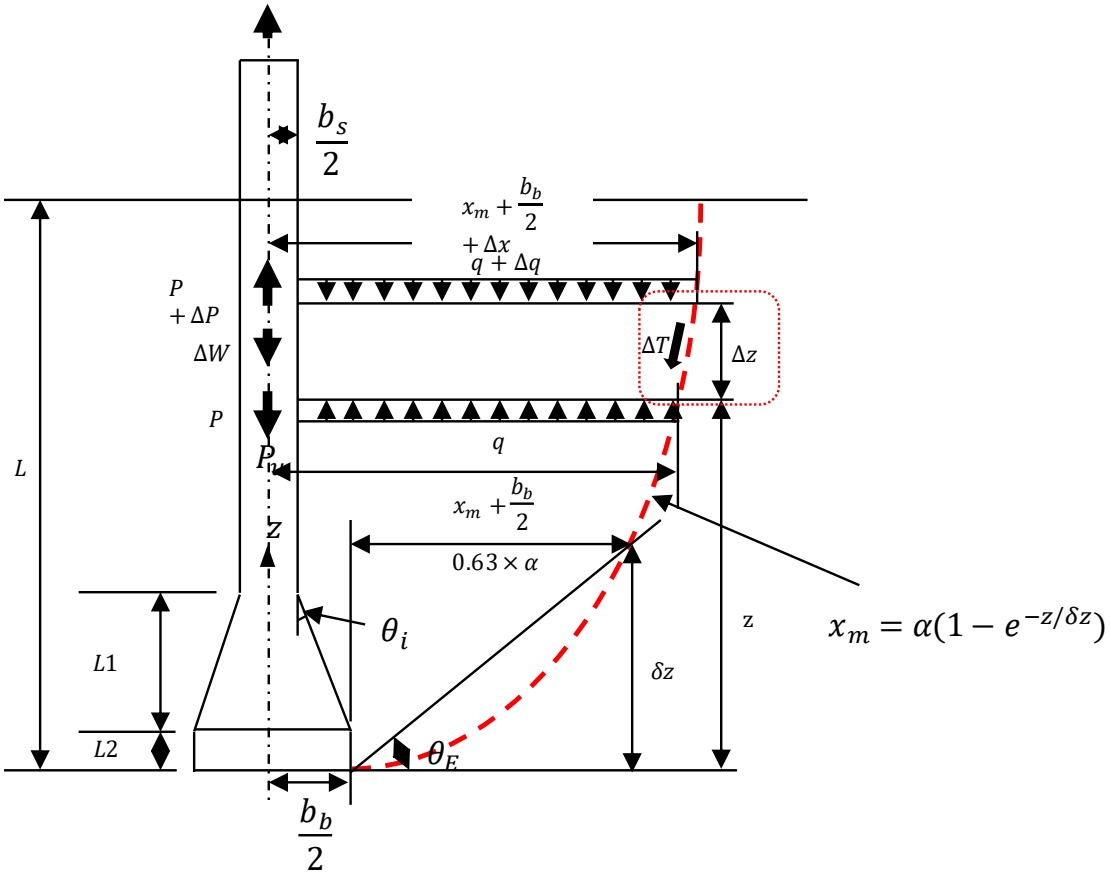

(a) Definition sketch of the resultant shear failure surface.

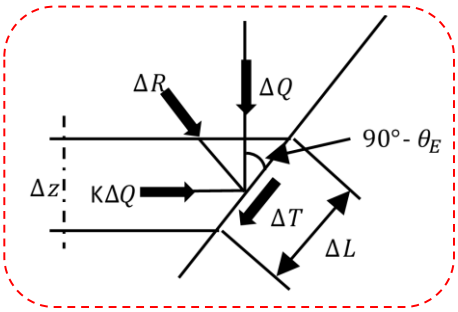

(b) Free body diagram of the resultant shear failure surface.

Fig.6-7 Definition sketch and free body diagram of the resultant shear failure surface of the belled-type pile by deep ground. ($L/b_b > 3$)

This curve has a fixed point of x_m= 0.63·α when z = δ_z and has a characteristic α as an asymptote. Therefore, it is possible to uniquely determine failure lines with different penetration lengths with limited parameters.

$$x_m = \alpha\left(1 - e^{-z/\delta_z}\right) \tag{6.15}$$

$$\alpha = \frac{\delta_z}{0.63 \cdot tan(\theta_E)} \tag{6.16}$$

$$\delta_z = \eta \cdot L1 + L2 \tag{6.17}$$

Where, x_m: the horizontal position of the failure surface at depth z (m), z: the depth from the pile tip (m), $L1$: the height of the slope at the bottom (m), $L2$: the height at which the bottom is raised (m), η: depth factor of failure surface shape.

α and δ_z is defined by Eq.6-16 and Eq.6-17, respectively. Note that α is determined using the failure angle (θ_E) and δ_z in Eq.6-15. Therefore, considering that the tip slope height affects the depth of the failure surface shape, δ_z introduced η which is determined based on the slope height.

Fig.6-8 is an example of applying depth factor (η) from 1 to 5. The Weibull-curve is a probability distribution curve useful in statistics. In this study, it was used to control the properties of failure surface alignment. The failure surface using the Weibull-curve can control the shape of the failure surface by using the depth factor (η).

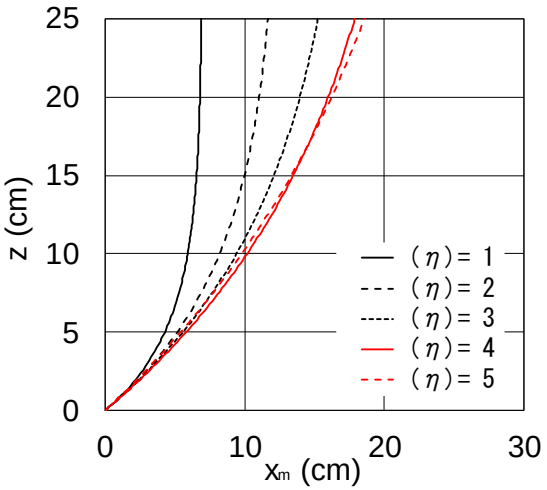

Fig.6-8 Shape of failure surface for depth factor (η).

6.3.2 Evaluate of Uplift Resistance Capacity Model

The proposed model for deep foundations ($L/b_b > 3$) uses the limit equilibrium equations of Chattopadhyay and Pise (1986), and the calculation method is the same as for shallow foundations ($L/b_b < 3$). However, the following assumptions are applied because the failure surface has a Weibull curve.

(1) The failure surface intersects linearly with the surface of the ground.

(2) For a belled type pile with $\delta \geq 0$, the angle between the failure surface and the surface is assumed to approach $\left(90° - \frac{\psi}{2} - \theta_i\right) \times \kappa$ based on the previous researches. Where κ means the coefficient of unit weight.

(3) For piles with $\delta \geq 0$, subject to ultimate uplift force P_u, the failure surface starts tangentially to the ground surface.

(4) The failure surface for the unit height is assumed to be linear.

Fig.6-2(b) shows the equilibrium of forces at the failure surface which assumes the failure surface starts at the coordinates of the end of the pile tip ($b_b/2, 0$), which slope was expressed failure surface was assumed as the linear line.

Shear resistance (ΔT) along the failure surface length (ΔL) can be calculated by the following equation.

Thus

$$\Delta R = \gamma_d \left(L - z - \frac{\Delta z}{2}\right)(cos\theta + K_0 sin\theta)\frac{\Delta z}{sin\theta} \qquad (6.18)$$

Here

$$K = K_0 = (1\text{-}\sin\varphi) \tag{6.19}$$

$$\Delta T = \gamma_d \left(L - \mathrm{z} - \frac{\Delta z}{2}\right)(cos\theta + K_0 sin\theta)(\Delta z tan\varphi)/sin\theta \tag{6.20}$$

Considering the vertical equilibrium of the circular wedge and assuming that the weight of the pile of length dz equals the weight of the pile to the volume occupied by the pile.

$$(P + \Delta P) - P + q\pi\left(x_m + \frac{b_b}{2}\right)^2 - (q + \Delta q)\pi\left(x_m + \frac{b_b}{2} + \Delta x\right)^2 - 2\pi\left(x_m + \frac{b_b}{2} + \frac{\Delta x}{2}\right)\Delta T sin\theta = 0 \tag{6.21}$$

Eq.6.21 replaces and simplifies the ΔT value from Eq.6.22.

$$dP = 2\gamma_d \pi\left(x_m + \frac{b_b}{2}\right)(L - z)[\cot\theta + (cos\theta + K_0 sin\theta)tan\varphi]dz \tag{6.22}$$

Eq.6.22 replaces and simplifies the ΔT value from Eq.6-23.

$$\frac{\Delta P}{\Delta z} = \pi q \frac{\Delta x}{\Delta z}(2x_m + \Delta x) + \pi \frac{\Delta q}{\Delta z}(x_m + \Delta x)^2 + \pi \frac{\Delta q}{\Delta z}(x_m + \Delta x)^2 + \pi(x_m + \Delta x)^2 \gamma_d + 2\pi\left(x_m + \frac{\Delta x}{x}\right)\gamma_d \left(L - z - \frac{\Delta z}{2}\right)(cos\theta_E + K_0 sin\theta_E)tan\varphi \tag{6.23}$$

At the limit, to replace q in Eq.6.23 with $q = \gamma_d(L - z)$.

$$\frac{dP}{dz} = 2\pi\left(\frac{z}{tan\theta_E} + \frac{b_b}{2}\right)\gamma_d(L - z)\frac{1}{tan\theta_E} + 2\pi\left(\frac{z}{tan\theta_E} + \frac{b_b}{2}\right)\gamma_d(L - z)(cos\theta_E + K_0 sin\theta_E)tan\varphi \tag{6.24}$$

Eq.6-24 as an integral, it was organized as Eq.6.25.

$$\therefore P_u = \int_0^L 2\gamma_d(x_m + \frac{b_b}{2})(L - z)\,[\cot\theta + (cos\theta + K_0 sin\theta)tan\varphi]dz \tag{6.25}$$

$$\therefore P_{u(net)} = P_u - W_{pile} \tag{6.26}$$

6.3.3 Validation of The Develop Model

In this section, the model test results, and comparative analysis were conducted to examine the proposed uplift resistance model of the belled-type piles for deep foundations ($L/b_b > 3$).

At present, the uplift resistance mechanism and the proposed model for the deep foundation ($L/b_b > 3$) of the belled-type pile are limited, and the models available in the design are still insufficient. Therefore, two important parameters were used to examine the reliability of the belled-type pile model for the deep foundation proposed in this study.

In selecting the parameters, the dilatancy angle (ψ) was used to study the effects of the two dilatancy angle (ψ), which were studied in the same way as the deep and shallow foundations. In addition, the pile tip inclination height was analyzed in five steps from 1 to 5 because it is a depth factor (η) that determines the shape of the failure surface that is important in the deep foundation ($L/b_b > 3$) uplift resistance model.

Table.6-3 shows the parameters used in the calculation. The parameters used in Table.6-3 are calculated values using the internal friction angle (φ) according to the unit weight. In addition, the dilatancy angle (ψ) used two expansion angles ($\psi = \varphi/2°$, $\psi = \varphi$ - 30°), which is the same as the shallow ground ($L/b_b < 3$).

Table.6-3 Parameters of Kumamoto fine sand (K7) used in the calculation.

Dr	γ_d	φ	$\psi = \varphi/2°$	$\psi = \varphi$ - 30°
(%)	(kN/m^3)	(°)	(°)	(°)
40	12.9	35.0	17.5	5.0
65	13.7	38.5	19.3	8.5
75	14.3	41.1	20.6	11.3
85	14.7	42.9	21.5	12.9
95	15.2	44.6	22.3	14.6

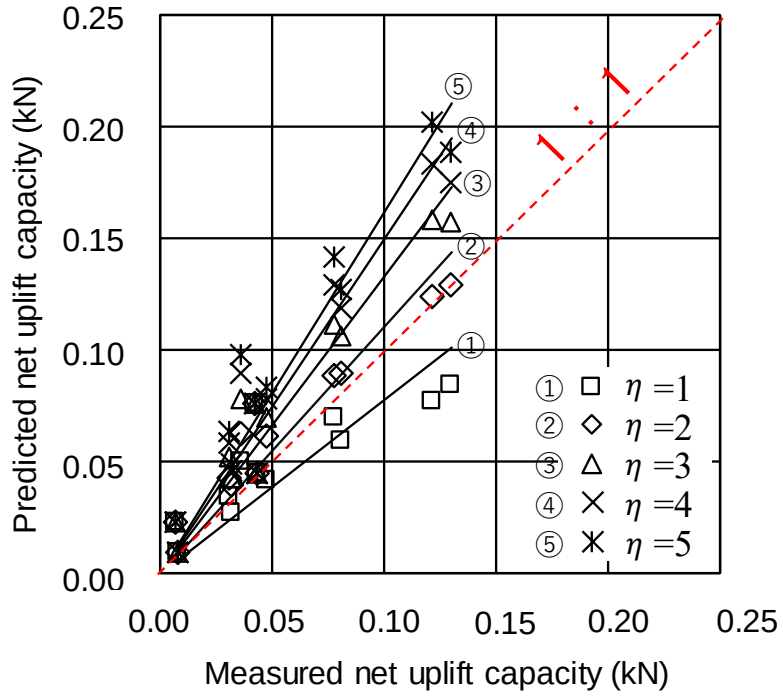

(a) $\psi = \varphi/2^{o}$

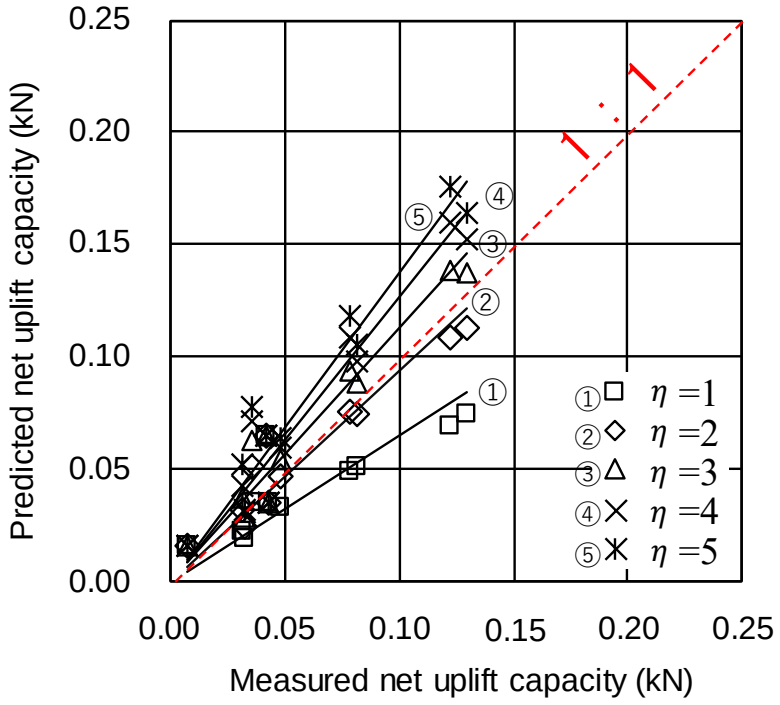

(b) $\psi = \varphi$ - 30°

Fig.6-9 Results of comparing the calculated values and experimental values of the deep foundation model for the pile tip inclination angle (θ_i).

(a) Comparison of Model Test Results and Estimated Values for Pile Tip Inclination Angle (L) = 16cm

Fig.6-9 shows the results of comparing the calculated values and test values of the deep foundation ($L/b_b > 3$) model for the tip shape. In the calculation, the penetration depth (L) of the pile was 16cm, and the model pile was used in three kinds (θ_i = 0º, 12º, 18º) according to the pile tip angle.

Fig.6-9(a) shows the result of the $\psi = \varphi/2$º. Based on the result of the pile tip inclination higher, the higher the calculated value. In particular, the predicted values were calculated higher than the test results in the cases except η = 1. In addition, the calculation results of η = 2 were calculated most similarly to the test value and the predicted value.

Fig. 6-9(b) shows the calculation result of $\psi = \varphi$ - 30º. A trend similar to the $\psi = \varphi/2$º was found in the result of $\psi = \varphi$ - 30º. In particular, the calculated value and the test value were found to be the most similar η = 2. The result was found to be closer to the calculated value than the $\psi = \varphi/2$º.

(b) Comparison of Model Test Results and Estimated Values for Penetration Depth (θ_i) = 12º

Fig.6-10 shows the results of comparing the calculated values and test values of the deep foundation ($L/b_b > 3$) model for penetration depth (L). In the calculation, the penetration depths of 8cm, 16cm and 24cm were adopted for a belled-type pile with 12º of tip inclination angle (θ_i).

Fig.6-10 (a) shows the results of the $\psi = \varphi/2$º. The comparison shows that the difference between the test value and the calculated value is the highest at η = 5, and the calculated

value is about 2.5 times larger than the test value. In addition, the good agreement between the test values and calculated values was found at η = 2.

Fig. 6-10 (b) shows the calculation result of $\psi = \varphi$ - 30º. In comparison, the test and calculated values were calculated most similarly in η = 2, and the results were found to be the same in all cases performed on the deep foundation ($L/b_b > 3$) model. In addition, the test results and the calculated values were found to be similar at $\psi = \varphi$ - 30º rather than $\psi = \varphi/2$º.

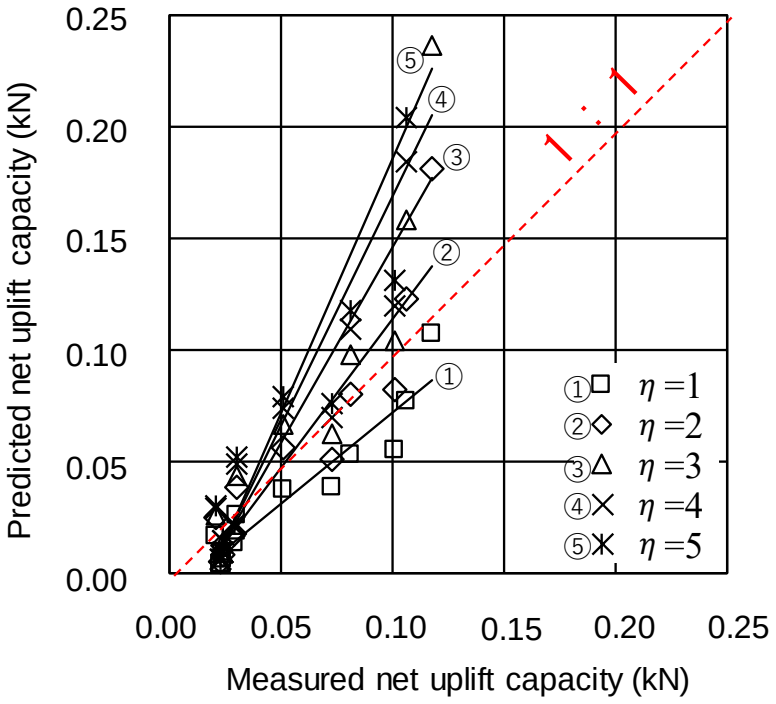

(a) $\psi = \varphi/2^{\circ}$

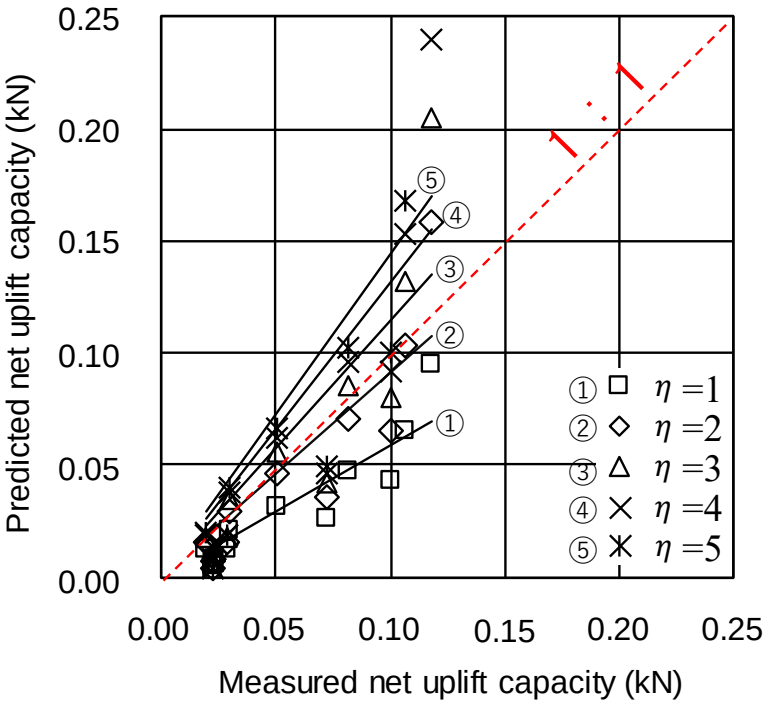

(b) $\psi = \varphi$ - 30°

Fig.6-10 Results of comparing the calculated values and experimental values of the deep foundation model for penetration depth (L).

6.4 UPLIFT RESISTANCE PREDICTION MODEL FOR SANDY GROUND

The belled-type piles have been generally studied for clay and sand ground. However, with the recent development of construction technology, it can be applied to soft-rock grounds with N=50 or more. Therefore, research on the belled-type piles for the soft-rock ground is necessary.

In this section, the failure mechanism and soil behavior of the belled-type pile in the soft-rock ground were examined using the model test results. The model and the laboratory test results were used to propose an uplift resistance model of the belled-type pile applicable to the soft-rock ground.

6.4.1 Prediction Model for Failure Surface and Failure Angle

(a) Failure Mechanism of Belled-type Piles applied in Soft-Rock Ground

Fig.6-11 shows the failure mechanism for the uplift load of soil-cement ground. This result is a preliminary test, a test was performed using a screw-jack provided that the pile tip inclination angle (θ_i) was 12º and penetration depth (L) 16 cm. Based on the result, three patterns of failure were confirmed.

Fig.6-11(a) shows the static condition of the pile. In this state, there is only adhesion between the pile and the soil, and the shape of the failure surface is not observed. However, in Fig.6-1(b), the displacement causes compression and compaction on the soil around the slope of the belled-type pile tip.

In the final step of Fig.4-11(c), not only the compression and crushing around the belled-type pile tip, but also the stress propagation throughout the soil causes the failure surface to be formed.

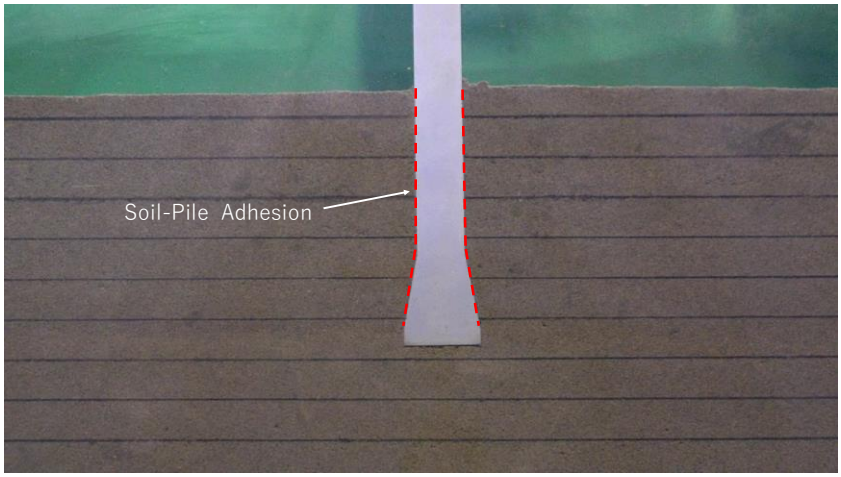

(a) Static.

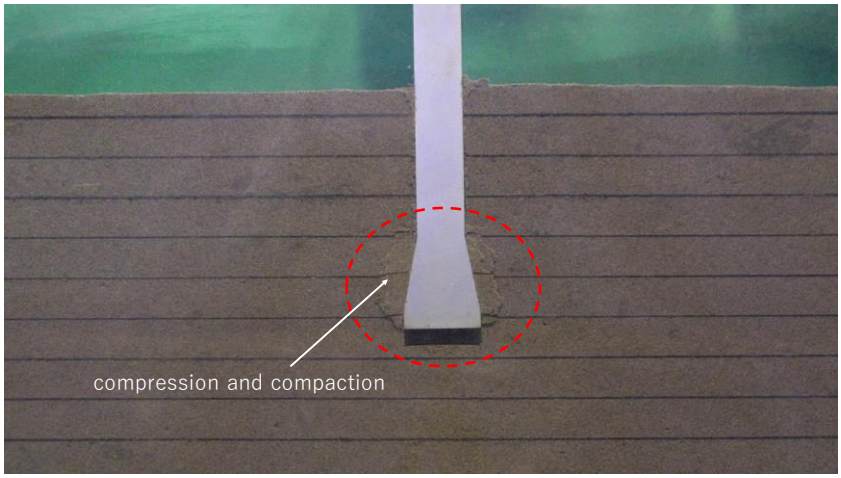

(b) Consolidation and Compression.

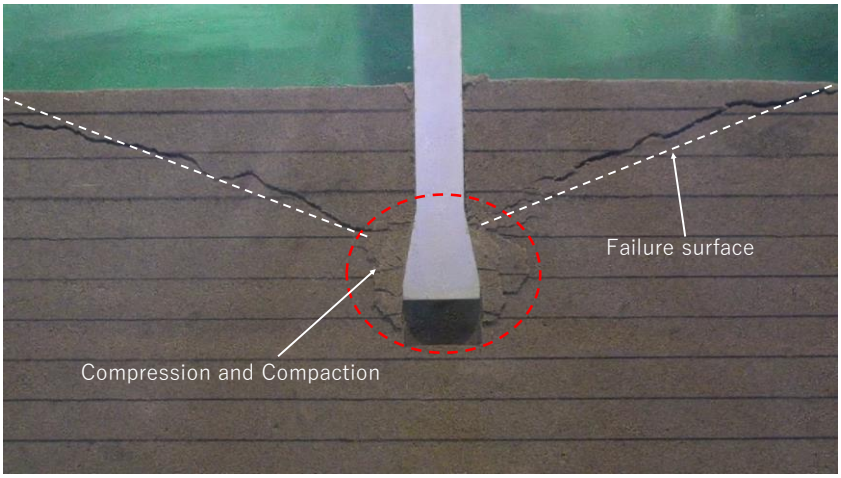

(c) Failure surface formation state.

Fig.6-11 Failure mechanism for the uplift load of soil-cement ground.

Based on the result of the three-stage failure mechanism identified in the preliminary tests, the failure mechanism of the belled-type piles applied on the soft-rock ground is clearly different from the conventional piles. Therefore, a different analytical approach is required than the model and method proposed for the sandy and clay grounds suggested by the previous researchers.

Fig.6-12 shows a sketch of the conventional pile and belled-type pile with failure surface formation. It is concluded that the conventional piles constructed on the soft-rock ground only act on the adhesion between the piles and the soil. However, Fig.6-12(b) shows the failure mechanism of the belled-type pile. The belled-type piles applied to the soft-rock ground were found to have maximum uplift loads at displacements of about 2 to 5 mm. Therefore, it is considered that there is no cohesion between pile and soil due to the initial displacement, and the failure mechanism of the belled-type pile is considered to be due to the influence of pile tip soil compression and failure surface.

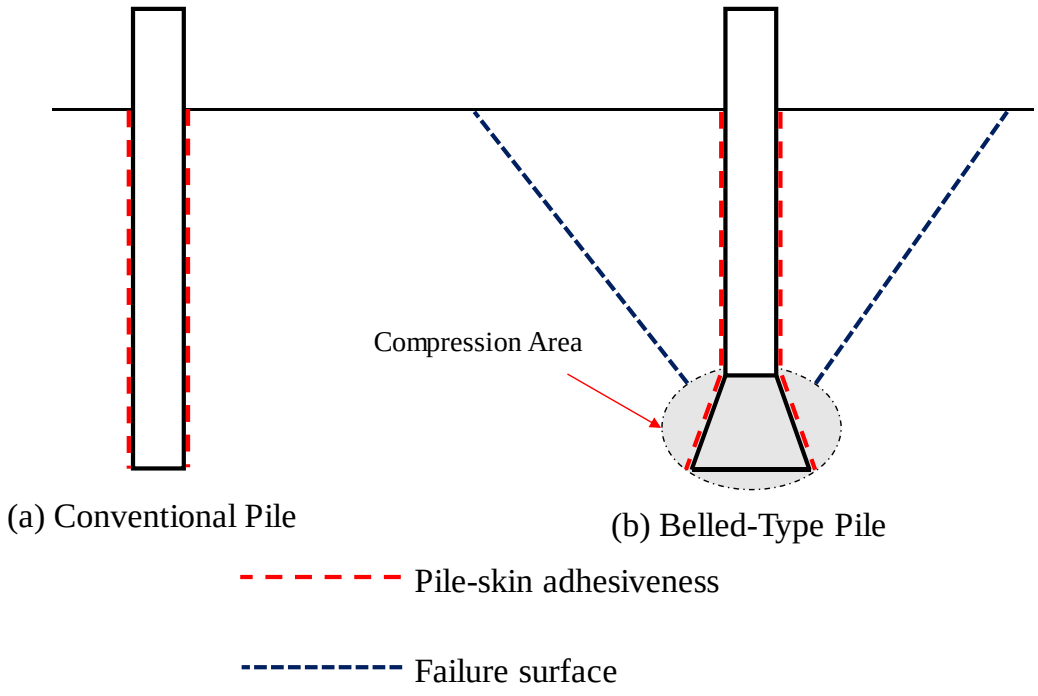

Fig.6-12 A sketch of a conventional pile and a belled-type pile with a failure surface formation state.

(b) Failure Angle and Failure Surface

Fig.6-13 shows the results of the image analysis of the preliminary test. The image analysis showed that a failure surface was created in the compressed area, and the failure surface was observed nonlinearly. However, a non-linearly observed failure surface is difficult to identify with clear patterns. Therefore, the failure surface is assumed to be linear in this study to simplify the calculation.

Table.6-4 shows the results of the uniaxial compression test (U_c) and tensile test of specimens prepared with the same mixing ratio as the model ground strength. And the Mohr-circle was used to determine adhesion and internal friction angle (φ_{sc}).

The internal friction angles identified in Table.6-4 were found to be similar to the failure angles identified in the chapter 5 model tests. Therefore, the failure angle (θ_{E}) utilizes the internal friction angle (φ_{sc}) of the specimen. Eq.6.27 shows the failure angle.

$$\theta_E(U_c) = \varphi_{sc} = \tan^{-1}\left(\frac{\sigma_c - \sigma_t}{\sigma_c + \sigma_t}\right) \tag{6.27}$$

Where, σ_c : compressive stress. σ_t: tensile stress. φ_{sc}: soil-cement internal friction Angle (°)

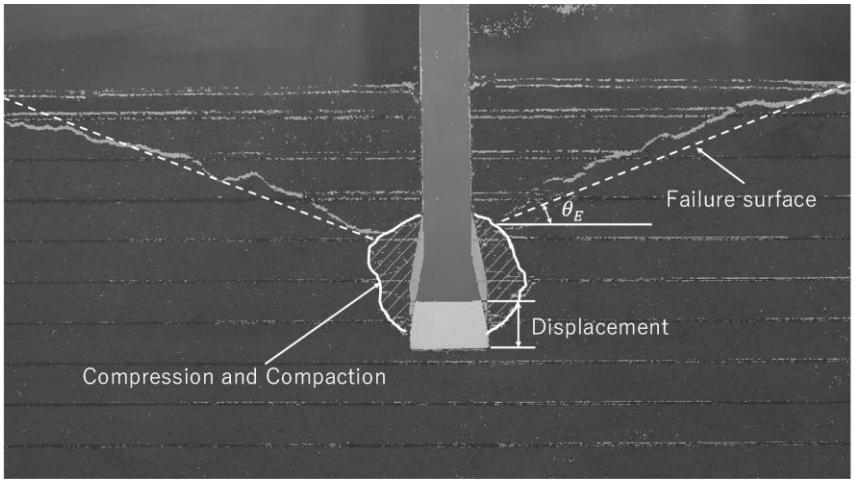

Fig.6-13 Results of image analysis of the preliminary experiment.

Table.6-4 Internal friction angle (φ_{sc}) and shear stress (τ_{sc}) of model ground by mixing ratio.

Table.6-4 (a) Mixing ration ID - ①.

Compressive stress	Tensile stress	Internal friction angle	Shear stress
σ_c	σ_t	φ_{sc}	τ_{sc}
(kN/m^2)	(kN/m^2)	(^{o})	(kN/m^2)
795.58	69.44	60.0	105.6
757.92	44.43		
809.55	55.88		

Table 6-4 (b) Mixing ration ID - ②.

Compressive stress	Tensile stress	Internal friction angle	Shear stress
σ_c	σ_t	φ_{sc}	τ_{sc}
(kN/m^2)	(kN/m^2)	(^{o})	(kN/m^2)
261.63	31.49	54.2	46.1
298.05	23.70		
297.48	33.99		

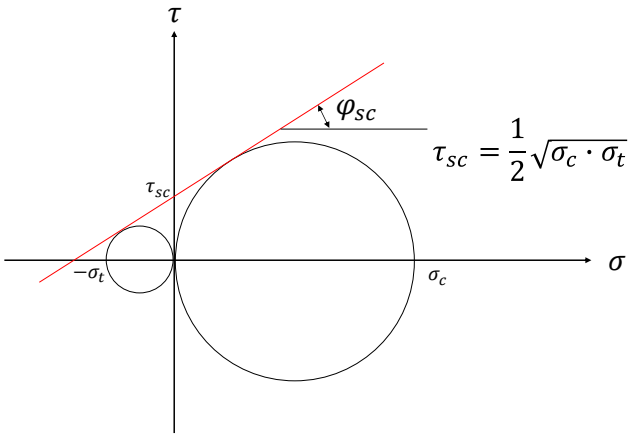

Fig.6-14 Determination of internal friction angle and shear stress.

6.4.2 Evaluate of Uplift Resistance Capacity Model

Fig.6-15 shows the definition sketch and free body diagram of the resultant shear failure surface of the belled-type pile by soft-rock ground.

The uplift resistance model of soft-rock ground is calculated by the shearing stress of the failure surface and the weight of soil inside the failure surface using the failure mechanism identified in the model test. Therefore, taking into account the shape of the failure surface, the failure surface caused by belled-type piles during the uplift load is composed of the truncated cone model, and the failure surface can be constructed as shown in Eq.6.28.

$$\therefore P_{u(net)} = \sum S_f + \sum W_s \tag{6.28}$$

where it is assumed that the start of the failure surface occurs at the center of the inclined surface.

$$\sum S_f = \left[\pi(b_{ct} + b_{cb})\sqrt{(b_{ct} - b_{cb})^2 + L_c^2}\right] \times \tau_{sc} \tag{6.29}$$

$$\sum W_s = \left[\frac{1}{3}\pi L_c(b_{ct}^2 + b_{ct}b_{cb} + b_{cb}^2)\right] \times \gamma_s \tag{6.30}$$

$$b_{ct} = \frac{L_c}{\tan(\theta_E)} + b_{ct} \tag{6.30}$$

$$L_c = L - (\frac{L1}{2} + L2) \tag{6.31}$$

$$b_{cb} = \frac{b_b}{2} - \left(\frac{\frac{b_b}{2}}{2} - b_s\right) / \tan(\theta_E) \tag{6.32}$$

Where, S_f: shear stress on failure surface, W_s: the weight of soil inside the failure surface,

γ_c: Unit weight of Soil-Cement.

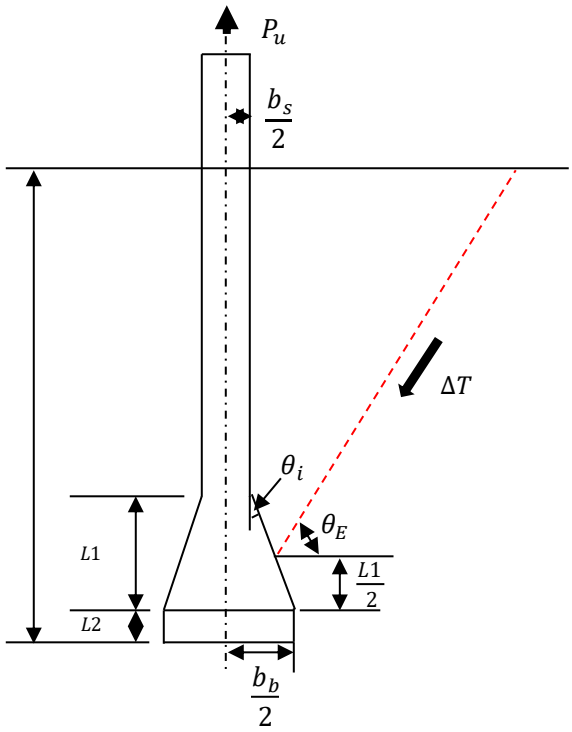

(a) Definition sketch of the resultant shear failure surface

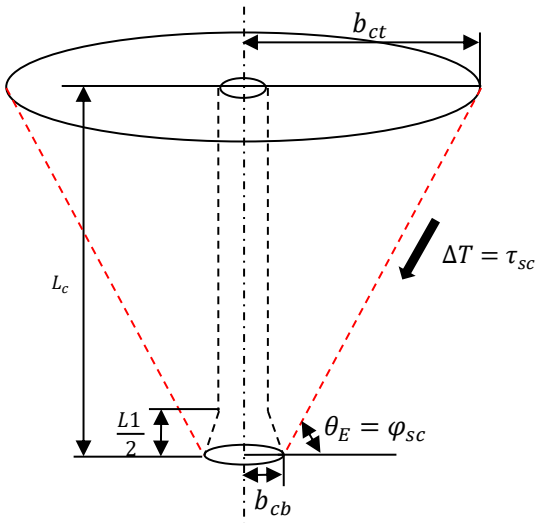

(b) Calculation element of soft-lock ground

Fig.6-15 Definition sketch and free body diagram of the resultant shear failure surface of the belled-type pile by soft-rock ground.

6.4.3 Validation of The Develop Model

In this section, the model test results and comparative analyses were conducted to examine the reliability of the proposed uplift resistance model of the belled-type pile for soft-rock. In the reliability verification, the test values (Table.6-4) and the failure angle equation proposed in the sand ground were modified and applied.

The modified angle of failure angle equation is as follows.

$$\theta_{\mathrm{E}}(\varphi) = \left(90° - \frac{\varphi}{2} - \theta_i\right) \tag{6.33}$$

$$\theta_{\mathrm{E}}(\psi) = \left(90° - \frac{\psi}{2} - \theta_i\right) \tag{6.34}$$

Where, D_r: relative density (%), ψ: dilatancy angle (º), φ: internal friction angle (º), θ_{E}: failure angle (º), θ_i: pile tip inclination angle (º).

The modified failure angle equation excludes the coefficient of unit weight (κ) applied to the sand ground and takes into account the internal friction angle, dilatancy angle, and the pile tip inclination angle (θ_i).

Table.6-5 and Table.6-6 shows the calculation results for the proposed model. In the penetration depth of 16 cm, the failure angle using the results of the uniaxial compression test (U_c) was found to be close to the model test, and at 8 cm penetration depth (L), the value of $\theta_{\mathrm{E}}(\varphi)$ was calculated to be the most similar to the model test. In addition, to compare the test results and the calculated results in detail, the difference between the test value and the calculated value was compared using Eq.6-14. Based on the results, the failure angle (θ_{E}) with the closest test value and the calculated value was identified as the soil-cement internal

friction angle (φ_{sc}) of uniaxial compression test ($\theta_{\mathrm{E}}(U_c)$), and the difference between the calculated value and the test value was found to be the highest at $\theta_{\mathrm{E}}(\varphi)$.

Fig.6-16 shows the comparison of test and calculated values. Based on the result, it was found that the correlation was relatively high at low uplift load, but the higher the load, the higher the difference between the calculated value and the test value.

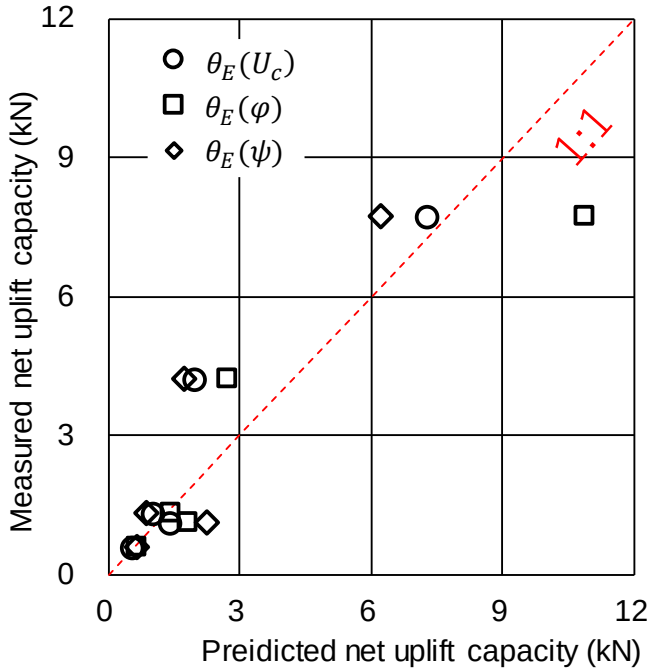

Fig.6-16 Results of comparing the calculated values and experimental values of the soft-rock ground.

Table.6-5 Calculation results for the proposed model.

Experiment ID	Inclination angle	Penertration depth	Uniaxial compressive strength			Experiment result	Proposed model		
			c	φ	strength		$\theta_E(U_c)$	$\theta_E(\varphi)$	$\theta_E(\psi)$
	θ_i(°)	(m)	(kN/m^2)	(°)	(kN/m^2)	(kN)			
K12H16C	12	0.1365	105	59	737	7.73	6.8638	10.2067	5.9162
K12H08C	12	0.0565	105	59	1001	4.20	1.7857	2.4454	1.5999
HK12H88C_①	12	0.0565	105	59	787	1.30	0.8995	1.2541	0.8051
HK12H88C_②	12	0.0565	46	54	286	0.59	0.4602	0.5574	0.5872
HK30H88C_①	18	0.0720	105	59	656	1.10	1.2766	1.6426	2.0205

Table.6-6 Predicted and measured uplift load capacity of laboratory and maximum uplift load used in the comparison study along with average error percentage for all methods.

Experiment ID	Inclination angle	Penertration depth	Experiment result	$\theta_E(U_c)$		$\theta_E(\varphi)$		$\theta_E(\psi)$	
	θ_i(°)	(m)	(kN)	P_u (kN)	ε (%)	P_u (kN)	ε (%)	P_u (kN)	ε (%)
K12H16C	12	0.1365	7.73	6.8638	11.2	10.2067	32.0	5.9162	23.5
K12H08C	12	0.0565	4.20	1.7857	57.5	2.4454	41.8	1.5999	61.9
HK12H88C_①	12	0.0565	1.30	0.8995	30.8	1.2541	3.5	0.8051	38.1
HK12H88C_②	12	0.0565	0.59	0.4602	22.0	0.5574	5.5	0.5872	0.5
HK30H88C_①	18	0.0720	1.10	1.2766	16.1	1.6426	49.3	2.0205	83.7

6.5 SUMMARY

In this chapter, a new uplift resistance model is proposed for sandy ground and soft-rock ground. The proposed model is presented for shallow sand, deep sand, and soft-rock. In addition, the results of model tests were compared with the calculated values to examine the reliability of each model.

Based on the result of the following results were confirmed.

1. The proposed model for shallow sandy grounds was constructed using the limit equilibrium equation proposed in the previous studies, and the pile tip inclination angle (θ_i) was considered. Based on the result, a higher correlation was confirmed than the models proposed in previous studies. However, the comparison results of the unit density of 40% were confirmed that the reliability is very poor.

2. The deep sandy ground model suggested a Depth coefficient (λ) that can take into account the depth at which the failure surface is formed. In addition, in order to confirm the reliability of the proposed model, it was found that the closest result to the test value was obtained at the depth coefficient (λ) 2 as a result of comparing the model test value with the calculated value.

3. The proposed model for the soft-rock ground is suggested as an effective model by analyzing the mechanism of the soft-rock ground using the test results. The parameters used in the proposed model are based on the data obtained from the ground survey.

In order to evaluate the reliability of the proposed model, the calculated values of the proposed model are compared with the test results. As a result of the comparison, the

calculation results of the parameter obtained using the specimen test was found to be the most similar to the model test result.

REFERENCES

Bui, D. T., Moayedi. H., Abdullahi, M. M., A Rashid, A. S. and Nguyen, H. (2019). Prediction of pullout behavior of belled piles through various machine learning modeling techniques. *Sensors (Basel)*, 19(17), 3678.

Chaudhary, A. Goswami, P., Sahu, A. K. S. (2016). Effect of skin resistance and enlarged base on pull out capacity of modeled piles. *Electronic Journal of Geotechnical Engineering*, 21(23),7503-7516

Das, B. M. (1978). Model tests for uplift capacity of foundations in clay. *Soils and Foundations*, 18(2), 17-24.

Dickin, E. A. (1988). Uplift Behavior of Horizontal Anchor Plates in Sand. *Journal of Geotechnical Engineering*, 114(11), 1300-1317.

Dickin, E. A., and Leung, C. F. (1992). The influence of foundation geometry on the uplift behaviour of piles with enlarged bases. *Canadian Geotechnical Journal*, 29(3), 498-505.

Dickin, E. A. (1994). Uplift resistance of buried pipelines in sand. *Soils and Foundations*, 34(2), 41-48.

Dickin, E, A., and Laman, M. (2007). Uplift response of strip anchors in cohesionlesssoil. *Advances in Engineering Software*, 38(3-9), 618-625.

Gaaver, K. E. (2013). Uplift capacity of single piles and pile groups embedded in cohesionless soil. *Alexandria Engineering Journal*, 52(3), 365-372.

Goel, S. and Patra, N. R. (2007). Prediction of load displacement response of single piles under uplift load. Geotechnical and Geological Engineering, 25, 57-64.

Hirai, Y., Wakai, S. and Aoki, M. (2016). In-situ pull-out tests of cast-in-place concrete piles with belled enlargements. *The 15th Asian Regional Conference on Soil Mechanics and Geotechnical Engineering*, 2(41), 1478-1481.

Hong, W. P., and Neatha, C**.** (2015). Prediction of uplift capacity of a micropile embedded in soil. *KSCE Journal of Civil Engineering*, 19(1), 116-126.

Hsu, S. T., and Liao, H. J. (1998). Uplift behaviour of cylindrical anchors in sand.*Canadian Geotechnical Journal*, 35(1), 70-80,

Liu, J., Liu, M. and Zhu, Z. (2012). Sand deformation around an uplift plate anchor. *Journal of Geotechnical and Geoenvironmental Engineering*, 138(6), 728-737.

MATSUO, M. (1967). Study on the uplift resistance of footing (1), *Soils and Foundations*, 7(4), 1-37.

MATSUO, M. (1968). Study on the uplift resistance of footing (2), *Soils and Foundations*, 8(1), 18-48.

Meyerhof, G. G. (1973). Uplift resistance of inclined anchors and piles. *Proceedings 8th International Conference on SMFE*, Moscow. 2, 167-173.

Murray, E. J. (1987). Uplift of Anchor Plates in Sand. *Journal of geotechnical engineering*, 113(3), 202-215.

Niroumand, H., Kassim, K. A., and Nazir, R (2011)**.** Uplift capacity of anchor plates in two layered cohesive-frictional soils. Journal of Applied Sciences, 11(3), 589-591.

Shanker, K., Basudhar, P. K. and Patra, N. R. (2007). Uplift capacity of single piles: predictions and performance. *Geotechnical and Geological Engineering*, 25 (2), 151-161.

Shelke, A. and Patra, N. R. (2008). Effect of arching on uplift capacity of pile groups in sand. *International Journal of Geomechanics*, 8(6), 347-354.

Shelke, A. and Patra, N. R. (2008). Effect of Compressive load on uplift capacity of single piles. *Geotechnical and Geological Engineering*, 27, 365-377.

Shelke, A. and Patra, N. R. (2009). Effect of arching on uplift capacity of single piles. *Geotechnical and Geological Engineering*, 27, 365.

Terada, M., Ebisu, S., Nishiyama, T., Kusuda, H. and Kawakami, Y. (2004). Visualization and observation on fracturing of rock anchors using fluorescent resins [Japanese]. *Journal of Japan Society Engineering*, 45(2), 83-89.

Tatsuoka, F., Molenkamp, F., Torii, T. and Hino, T. (1984). Behavior of lubrication layers of platens in element tests. *Soils and Foundations*, 24(1), 113-128

Yasufuku, N., Ochiai, H. and Maeda, Y. (1999). Geotechnical analysis of skin friction of cast-in-place piles related to critical state friction angle [in Japanese]. *JSCE*, 617, 89-100.

CHAPTER VII

CONCLUSIONS AND FUTURE WORKS

7.1 CONCLUSIONS

The main objective of this dissertation is to investigate the mechanism of uplift resistance of applied belled-type piles in the sand ground and soft-rock ground and to propose a new model. In this study, both test and theoretical approaches were carried out to understand the failure mechanism of belled-type piles.

The conclusion of this research can be summarized as follows:

<Shallow Sand Foundation>

1. The effect of load resistance in belled-type piles was not significant in the case of ground with 40% of relative density (D_r) in both piles with pile tip inclination angles (θ_i). This result was similar to the previous researches and it seems that the compaction on the pile tip area has occurred. In the result, where was not influence of pile tip shape on the uplift capacity on the low density in the ground. In addition, the uplift capacity of the belled-type pile with the pile inclination angle (θ_i) of 12º is slightly higher than the 18º of the pile tip inclination angle (θ_i).

2. The standard model and the truncated cone model generate the higher difference value of predicted uplift capacity compared to the test results. It was indicated about 33 times the difference between test and predicted model. The proposed model corresponding better accuracy than the previous models to predict the uplift capacity of the conventional pile embedded into different relative density (D_r).

3. A new equation model considering the characteristics of belled-type piles was proposed by using the limit equilibrium method. The dilatancy angle (ψ) of the ground was considered as a key parameter to predict the uplift capacity of the belled-type pile. The dilatancy angle value of $\psi = \varphi$ - 30º provides the lowest average error to predict the uplift capacity. The result has been shown that the maximum error (ε) of the proposed model in the belled-type pile was less than 50%, excluding the case with a relative density (D_r) of 40%.

<Deep Sand Foundation>

1. This increase of uplift load values is higher in the high relative density (D_r). In the same conditions of the relative density (D_r) and penetration depth (L), a belled-type pile has been identified as a higher increase in the uplift load than a conventional pile.

2. The uplift load of the belled-type pile was found to be about 0.04 kN in 8cm penetration depth (L) regardless of the relative density (D_r). However, under the conditions of 16cm and 24cm in penetration depth (L), a large uplift load was confirmed according to the relative density (D_r).

3. In the half-circular test, no failure surface was observed under the condition of 40% relative density (D_r), and the failure surface was observed under the condition of 75% or more, irrespective of the penetration depth (L). In particular, the shape of the failure surface at the penetration depth (L) of 16 cm and 24 cm was similar to the shape of the failure surface shown in the previous research.

4. In this study, the evaluation model was proposed using the limit equilibrium equation for the pile tip inclination angle (θ_i) of the belled-type pile, the image analysis result,

and the uplift load of the conventional pile. Furthermore, the coefficient to be determined based on the parameters at the tip inclination height to determine the failure surface shape λ proposed, using linear regression analysis of the calculated values by model tests with new evaluation equation was investigated the optimal value of λ. Based on the result, it was confirmed that $\lambda = 2$ was the closest to the test value.

<Soft-Rock Foundation>

1. High uplift loads were found under the high shear stress of the model ground, and the conventional pile had the maximum uplift loads at lower displacements than the belled-type piles. Further, the belled-type pile is about 2.8 times higher than the conventional pile was observed in the same model test conditions.

2. The uplift load of a belled-type pile is determined by the shear stress of the failure surface and the weight of the soil inside the failure surface.

3. Based on the result of estimating the uplift load using the proposed model, the predicted values using the parameters obtained from the test specimens were calculated to be the most similar to the model test results.

7.2 FUTURE WORK

Although the objectives of this dissertation have been successfully achieved, the three proposed models scope further research to extend their practice. Some of the scopes and issues that require more investigation are listed as follow:

1. The ground of site condition is mostly composed of multi-layer ground. Therefore, it is necessary to expand the evaluation model considering the characteristics of the composite ground.

2. In this study, the mechanism of belled-type piles applied to sand and soft-rock ground was identified by using laboratory model tests. The results were summarized and suggested as a new model. In the future, the study plans the reliability of the evaluation model using case analysis applied to the actual ground and the large scale of 1/50 or more.